Master of Science Thesis

Predicting residual strength of composites after cyclic loading

A numerical, progressive damage analysis based approach

Alexandros Michaïl Mitrousias

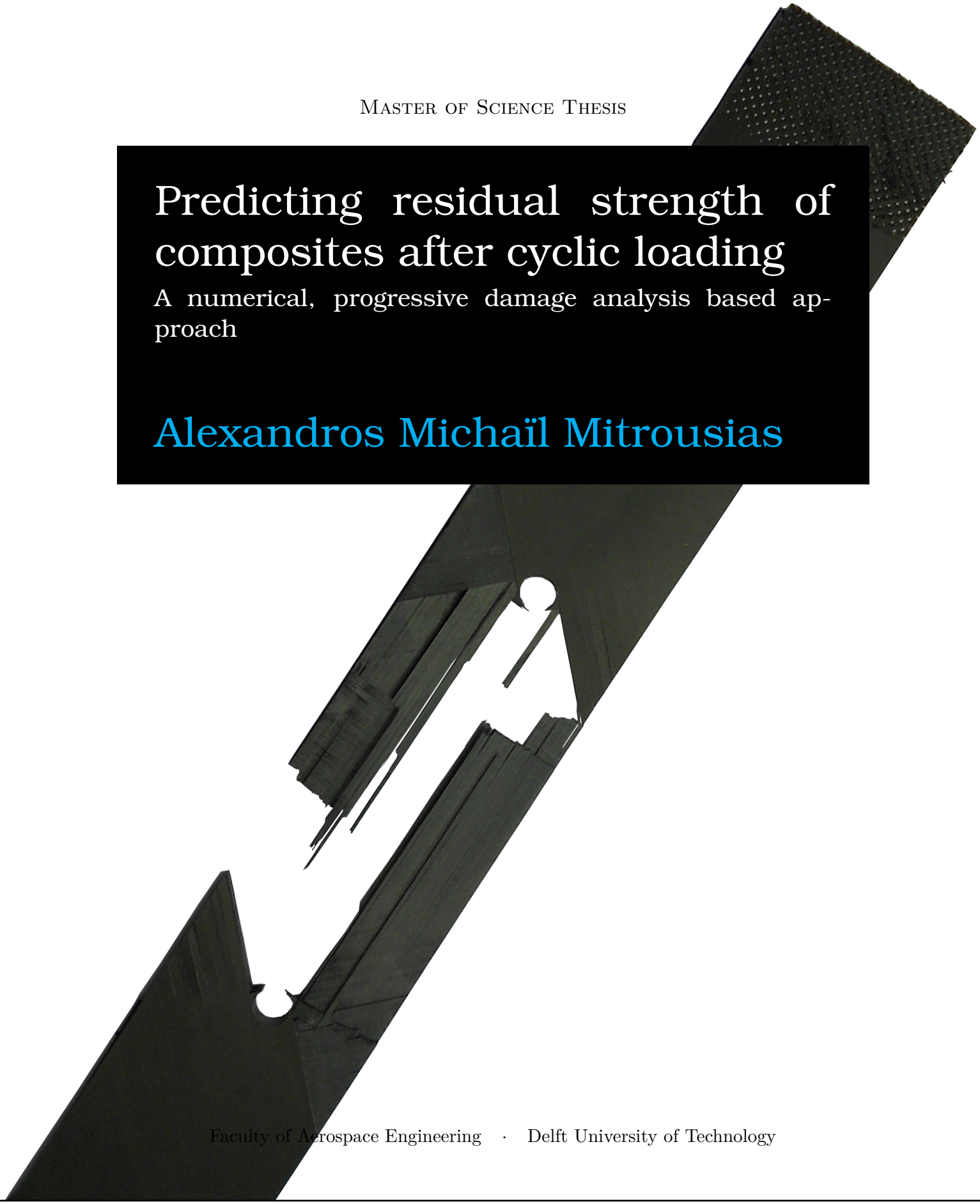

Faculty of Aerospace Engineering · Delft University of Technology

TU Delft Delft University of Technology

Predicting residual strength of composites after cyclic loading

A numerical, progressive damage analysis based approach

Master of Science Thesis

For obtaining the degree of Master of Science in Aerospace Engineering
at Delft University of Technology

Alexandros Michaïl Mitrousias

13-07-2017

Faculty of Aerospace Engineering · Delft University of Technology

Delft University of Technology
Faculty of Aerospace Engineering
Department of Aerospace Structures and Materials

GRADUATION COMMITTEE

Dated: 13-07-2017

Chair holder:

Prof.dr.ir. R. Benedictus

Committee members:

Dr.ir. J.J.E Teuwen

Dr.ir. D. Zarouchas

Dr.ir. J.M.J.F van Campen

mr. N. Eleftheroglou

Abstract

As the demand on new lightweight materials increases due to economic and environmental reasons, fiber reinforced plastics seem an interesting solution. In order to maximize their potential, ways have to be found to introduce damage tolerant designs. To this end, in the present exercise, the damage caused by cyclic loading is investigated.

Cyclic loading causes loss of stiffness and strength of composite structures. In the present work a progressive damage analysis model has been built. Damage is tracked by a macroscopic failure criterion. Failure occurring at levels below the macroscopic level are captured by a degradation theory which requires S-N curves as input. An attempt is made to use S-N curves derived from static tests only. Stress solutions are obtained using a finite element package. In order to bring the macroscopic damage, degradation and stress solution parts together, a cycle jumping algorithm has been developed which minimizes the amount of FEM stress solutions required and the required amount of function evaluations.

In its current form, the model is able to properly predict the trend of stiffness and strength behavior. Showing that a model like this has potential. For the proper predictions of magnitudes, additional failure modes should be modeled and the usage of S-N curves obtained from large specimens for applying on smaller geometries (elements) should be reconsidered.

Table of Contents

List of Figures

List of Tables

Glossary

1D 1 dimensional. 4, 8

2D 2 dimensional. 5, 17, 21

3D 3 dimensional. 4, 6, 13, 16, 17, 21, 22

ASTM American Society for Testing Materials. 10, 18, 19, 28, 31, 39, 43, 49, 62, 76

BC boundary condition. xiii, 15, 19, 20, 31

CA Constant amplitude. 45, 53, 61, 67

CDF cumulative density function. 8, 62

CFRP carbon-fiber reinforced plastic. 1, 4, 22, 24, 74

CV coefficient of variation. 33, 44

DIC digital image correlation. xiv, 18, 34, 35, 37, 42, 43

E Longitudinal stiffness, plane of action is denoted by subscript. Numbers denote ply oriented axis system, letters denote load oriented axis system (x=parallel to load). 22, 26

EC engineering constant. 5, 7, 26, 57, 59

FE finite elements. 4, 10, 13, 15, 16, 26, 34, 35, 76

FEA finite element analysis. 18, 26, 35, 43

FEM finite element method. xiii, 3, 16, 34, 35, 54, 55, 57, 60, 73

FF fiber failure. 60

FI failure index. x, 21, 24, 26, 55, 57, 58

G Shear stiffness, plane of action is denoted by subscript. Numbers denote ply oriented axis system, letters denote load oriented axis system (x=parallel to load). 18, 26, 33

γ Engineering shear strain, plane of action is denoted by subscript. Numbers are in a fiber oriented axis (1 parallel to fiber). Letter are in a load oriented axis (x parallel to fiber). 18

MPa Mega Pascal. SI unit of pressure. 30, 31, 33, 34, 43, 44, 45

MD multi-directional. 6, 39, 40, 77

MF matrix failure. 60

ν Poisson's ratio. Relation between strains in action direction to another direction. First subscript is action direction. Second subscript is other direction.. 22, 33

OHT open-hole tensile specimen. xiii, xiv, 10, 16, 20, 21, 31, 33, 39, 49, 68, 71

OSL observed significance level. 45, 44, 45

PD progressive damage. 16

PDA progressive damage analysis. 2, 5, 10, 13, 16, 27, 29, 76

PDAM progressive damage analysis model. 3, 4, 5, 7, 8, 9

PID proportional-integral-derivative. 43

QSPDA Quasi-static progressive damage analysis. 27, 30, 53, 55, 59

R Ratio between $\frac{\sigma_{max}}{\sigma_{max}}$. x, xv, 4, 8, 45, 53, 61, 62, 63, 64

S-N curve Applied stress versus maximum number of cycles before failure. x, xiv, 2, 8, 9, 49, 54, 61, 62, 64, 65, 66, 68, 71, 73, 74, 77

σ_{max} Maximum stress of cycle. 5, 9, 10, 45, 53, 55, 68, 70

σ_{ult} Ultimate static strength. 9, 42, 45, 62

σ_{min} Minimum stress of cycle. 9

σ Normal stress, plane of action is denoted by subscript. Numbers denote ply oriented axis system, letters denote load oriented axis system (x=parallel to load). 22, 23

S Fracture resistance against shear. Plane is denoted by subscript. 24

σ_{res} Remaining strength after cyclic loading. 45

SOHT Specimen open-hole tensile. 39, 45

τ Shear stress, plane of action is denoted by subscript. Numbers are in a fiber oriented axis (1 parallel to fiber). Letter are in a load oriented axis (x parallel to fiber). 18, 19, 22, 23, 24

u displacement. 21

θ_{fp} Failure plane angle. Plane is parallel to fibers and angle is defined to be zero when in-plane stress is perpendicular to plane.. 22, 24, 25, 26

UD unidirectional. 4, 6, 28, 33, 39, 74

VA variable amplitude. 61, 67

WWFE world-wide failure exercise. 5, 6, 21, 22

X Fracture resistance parallel to fibers. Superscript denotes tensile (T) or compression (C) strength.. 22

Y Fracture resistance transverse to fibers. Superscript denotes tensile (T) or compression (C) strength.. 24

Acknowledgments

Now that I have have completed my MSc thesis after nine months of work, I want thank the people that have helped me all along.

First I want to thank Dimitri, for his belief in me and my ideas. He has been a great supervisor, giving me a lot of freedom in my research and being able to guide me whatever road I choose to go. Working together with him has been both a pleasure and great learning experience for me.

Special thanks also go to Nick. I am grateful of his help and especially his patience he had with me. No matter how many times a day I passed along his office to discuss a concern of mine he always smiled when I came in. I always left his room enlightened from my concern.

I want to thank Pelle whom was able to proof read my thesis and joined me in the library when I was finishing my work.

Finally, I want to express how grateful I am that I had the opportunity to work on such a project. The amount of knowledge I have gained can not be described by words.

Delft, University of Technology
13-07-2017

Alexandros Michaïl Mitrousias

´α
— *ÎŞÎžÎśá£ęÎžÎ£ÏĆ*

Chapter 1

Introduction

1.1 Background

The aviation industry is in an era where it is continuously growing. Associated with this growth is the increased use of energy. Not only for manufacturing the aircraft, but especially in the form of fuel for keeping the aircraft in the air. Fuel usage can be associated with 12% of the total operating costs of an aircraft according to Swan and Adler [1]. They also state that fuel consumption is linearly related to the weight of the aircraft. Moreover, it is known that fossil fuels (currently the fuel of choice for most modern aircraft) negatively impact the environment. Hence, it seems logical to reduce fuel consumption or to explore alternative types of fuel, for example electricity. A quick look at the the specific energy (in Wh/Kg) of jet fuel versus a lithium battery finds values of 11889 and 500 respectively. The direct effect of this difference is a reduction in the payload carrying capacity of the airliner, for the case of using a lithium battery as fuel. Concluding, a reduction of aircraft weight will reduce the energy required and allow for reduction in fuel consumption or increase the feasibility of alternative fuels. Reduction of aircraft weight may thus be a requirement for the continued growth of the aerospace industry.

To this end, composites are becoming increasingly popular, due to their high stiffness/strength to weight ratio [2] and are currently being applied in significant parts in commercial and military applications, [3]. As of today, the most notable usage of composites in commercial aviation industry might well be the Airbus A350 and the Boeing 787 where more than 50% of the structural parts are made of carbon-fiber reinforced plastic (CFRP), [4]. Composite usage is not exclusive to the aviation industry. Other industries in which the usage of composites might not be neglected are the wind energy sector (wind turbine blades), civil engineering (bridges) and the automotive industry, [3]. The way in which composites are used throughout all these industries varies. In general however, all the composite parts are subjected to cyclic loads. These cyclic loads may range from 1E5 cycles for fuselage parts, [5], up to 1E9 cycles for wind turbine blades, [3]. For parts subjected to the lower range of cycles, static designs might govern the design, but as the amount of cycles increase, so does the dependency on a fatigue (cyclic loading) governed design increase.

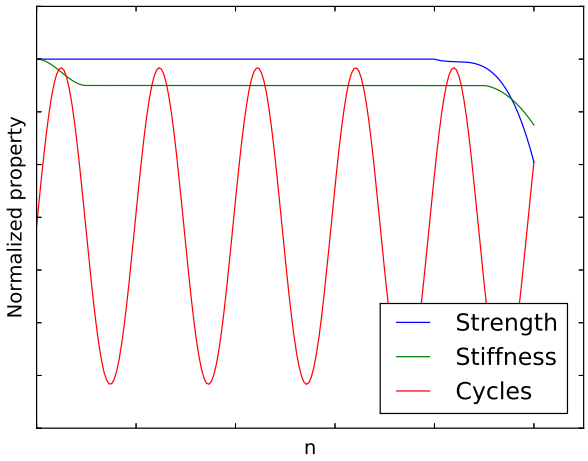

Figure 1.1: General behavior of strength and stiffness as a function of cycles (n)

With the introduction of composites, new design methodologies have to be introduced. One of the reasons for this is the anisotropic properties of CFRPs compared to the isotropic behavior of conventional design materials (aluminum). Moreover, complex damage mechanisms occur in composites, which at the macro-meso level can be roughly divided into three categories; delaminations, fiber failures and matrix failures, [6]. One source of damage is the previously mentioned cyclic loading (fatigue). Currently, the effect of cyclic loading is assessed by costly full-scale models [7] and hence, knockdown factors are applied early in the design process such that large changes are not required at this stage (testing-stage) [8]. This design philosophy may lead to inefficient designs and does negatively contribute to the reduction of weight. An improvement in the knowledge of fatigue behavior of composites could improve the design capabilities such that the effects of fatigue can be considered in preliminary design stages. Moreover, better understanding of fatigue in composites might reduce maintenance costs by increasing the reliability of damage predictions. This is favorable since maintenance is another 13% of the operational costs of aircraft, Swan and Adler [1].

In the present work, a model is to be built that can be used as an assessment tool for parameters influenced by fatigue, in order to reduce the usage of knockdown factors and to increase the efficiency of the design. To do such, deeper understanding is required of the effects of fatigue. In general, the effect of fatigue on the mechanical properties of a composite part is the reduction of stiffness and strength. These effects are shown on figure 1.1. This is just a general trend-line. For example, for high amplitudes, the strength degradation will tend to be more sudden, whereas for low amplitudes it might be more of a wear-out behavior, [3]. The reduction of strength and stiffness is the result of damage which is accumulated during cycling. This damage may occur as early as the first cycle and may for instance be driven by manufacturing flaws, [5]. The way in which these defects evolve during fatigue will be a complex process involving multiple types of damages which will probably interact to introduce even more complexity. Another factor which has to be considered is the previously mentioned anisotropy of composites, which will lead to different S-N curves for different fiber orientations, whereas for metals only one S-N curve is sufficient due to their isotropic behavior.

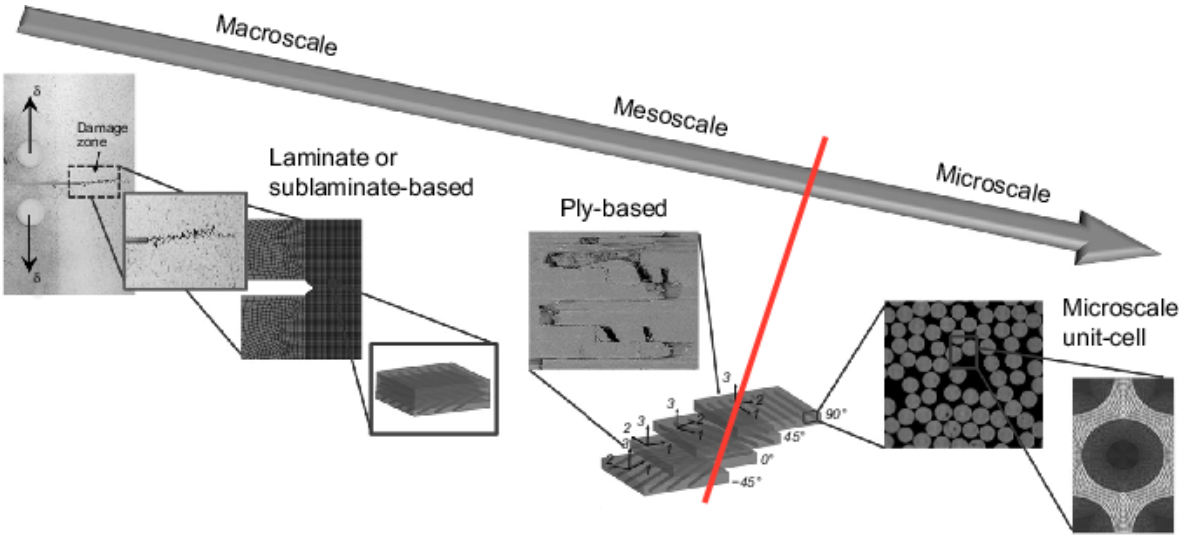

Figure 1.2: Modeling scales, source: Forghani et. al. 2015

It is thought that in order to make a generalized model, which could be applied on different cases, the use of progressive damage analysis (PDA) might be a possible solution. PDA is one of the three methods of performing fatigue analysis according to Degrieck and Paepegem [9]. By additionally applying discretization to the model, the resolution and accuracy of such a PDA can be increased. In general, discretization is done by using finite elements. The modeling of damage can then be performed on the element level. Kassapoglou [6] suggests an approach to model fatigue damage, which will be adopted in the present work. In the approach, it is suggested to make a distinction between scales. There should be a point on that scale for which there is a model available which can accurately predict damage for that scale and higher scales. For the scales below that point, a second model is required to degrade the inputs of the first model such as to account for damage at these lower scales. A schematic of this idea is depicted on figure 1.2. Where the different modeling scales are depicted. The red line marks point which distinguishes between damage or degradation in this exercise.

1.2 State of the art

As has been pointed out in the previous section, fatigue is a complex phenomenon. In the present work, an attempt is made to model fatigue with a progressive damage analysis model (PDAM). This is not the first work attempting to do such. A literature study has been carried out in which PDAMs by other authors are investigated, section 1.2.1. In order to use the approach suggested by Kassapoglou [6], a damage model and a degradation model should be found. According to Philippidis and Passipoularidis [10], damage models on the micro-scale are not yet mature enough. Since then, a lot of advancements have been made in micro-scale modeling however, implementing such models in FEM is complex and time consuming. As will be shown, the currently chosen macro/meso scale already is very computationally intensive. In general, there are many failure criteria available for the macroscopic level. If one takes a macroscopic criterion and applies it on an element level, meso-scale modeling is the result. The macroscopic failure criteria considered here are of the stress-strain type, which makes

them well suitable for a finite element package, since stresses and strains are easily extracted at the element level. An investigation of such criteria is presented in section 1.2.2. Finally, the scale below macro/meso scale, for which a degradation rule has to be found will be discussed in section 1.2.3. Due to choosing stress-strain based failure criteria, the degradation rules can act on strength properties and stiffness properties of the element.

1.2.1 Progressive damage analysis models

A PDAM method aims to predict the damage state of a composite after loading. In this review, only methods which predict the state after repeated loading (fatigue) will be considered. The PDAM capabilities vary from residual strength prediction, residual stiffness prediction, life prediction, to damage propagation prediction. The reviewed PDAMs will be discussed in order of year of appearance. From the perspective of the approach to be followed (Kassapoglou [6]) the PDAM is the model that brings the damage and degradation laws together.

Shokrieh and Lessard [11, 12] presented one of the earliest papers on PDAM in fatigue. The PDAM work is an expansion on their work on modeling the multi-axial fatigue behavior using experimental data of unidirectional (UD) [13, 14]. In which they developed degradation rules and failure criteria (damage), discussed later (1.2.2 and 1.2.3). Their work is characterized by high experimental effort according to Tserpes et al. [15], ply-to-laminate approach (i.e. characterization is performed on ply level), usage of Hashin [16] type failure criteria, usage of Adams et al. [17] based degradation rules and a cycle jump which is defined by the user at the initialization phase. Their verification was extensive, and good correlation was achieved. Additionally, their model was able to capture initial strength increase of pin/bolt loaded specimens after adding additional fitting parameters to the degradation rules.

Paepegem and Degrieck [18] have performed the damage assessment using a single step which was defined as a damage growth rate theory, described in their previous work [19]. This theory combine stiffness- and strength degradation with a modified Tsai-Wu [20] failure criterion. They did use a proprietary cycle jump theory described in Paepegem et al. [21], which calculates finite elements (FE) solutions at predefined intervals and extrapolates results in between. The PDAM has its restrictions, it does not take into account delamination modeling and it can only deal with a 1 dimensional (1D) applied load. At last, the only verification was performed on a $[0]_8$ specimen in bending, where bending was said to cover multiple stress R.

Tserpes et al. [15] proposed a PDAM for rectangular CFRP. Their failure analysis was 3 dimensional (3D) and included delamination modeling. Moreover, the stress ratio (R) considered was -1, hence Tensile-Compression (T-C) regime. They tried to implement initial damage of specimens using a C-scan of the experimental specimens. The observed damage (found by the C-scan) was simulated using sudden degradation rules at initialization. Their cycle jump was created by Papanikos et al. [22]. The idea was to only do a stress analysis for the high and low stress (which are critical), and to jump cycles after applying only gradual degradation for a predefined number of cycles. Good agreement with test results were obtained especially at low loads, which was thought to be caused by the failure criteria used (mix of Hashin [16] and Ye [23]).

Lian's and Yao's [24] method was special in the way the element properties are initialized. They used a statistical distribution method to mimic material scatter. They used an imple-

mentation of Hashin and Rotem [25] failure criteria and performed simulations at a R ratio of 0. By choosing such a ratio, the risk of getting wrong experimental data is increased, since it can be possible for the specimen to go into compression due to control errors of the fatigue machine. Since composites are sensitive to compression, the results might be affected. Nevertheless, they are the only one who used a true cycle-by-cycle simulation and good results were obtained. However, the quasi-isotropic laminate test-case did not yield satisfactory results, probably because of not modeling delaminations.

Eliopoulos and Philippidis [26, 27] were the ones who did include a more sophisticated failure criterion. It was based on Puck et al. [28]. The model implements non-linear theory and is based to a greater extent on physical phenomena. Delamination modeling however was not included but cycle-mix effects were taken into account. The cycle jump was implemented on the basis of user input. Finally, decent correlation was obtained to a large experimental campaign of various loads, stress ratios and laminate stacking sequences. As with other methods, results for lower maximum stresses (σ_{max}) tended to improve.

Nikishkov et al. [8] tried a different approach too. They used a cycle jump method which tried to predict the number of cycles till failure of an element. Then, a predefined number of elements with the lowest cycles to failure were failed and the cycle counter advanced with the largest cycles to failure of the failed elements. To predict the cycles to failure, a combination of Miner's rule and failure criteria of Hashin [16] and LaRC03 [29] were used. The method was verified on a 88-ply thick specimen and a 16-ply Open-Hole (OH) specimen. Predictions were of varying quality.

Naderi and Maligno [30] extended the PDAM of Shokrieh and Lessard [11] by including the effects of material scatter. They did this by using a Gaussian distribution to assign engineering constant (EC) to the elements. Moreover, they excluded delamination modeling i.e. they only considered 2 dimensional (2D) stresses. A cycle jump method was implemented which judged the amount of cycles to be jumped on available fatigue data. Good predictions were obtained for residual strength, residual stiffness and fatigue life. Results tended to become worse for increased loads. It was thought that the increased error was caused due to not taking into account delaminations in the model.

Final remarks on current PDMs The reviewed PDA methods show little correlation in their usage of failure criteria and degradation rules, from which can be concluded that there is no generally accepted way in which fatigue can be modeled for a general case using PDA. In cases where delaminations are neglected, no clear reasoning or restriction is given based on physical phenomena, except in the work of Degrieck and Paepegem [18]. The biggest similarities were found in the cycle jump implementation, where the method of determining the cycle jump by user input was most used and is not based on any physical meaning. This method is clearly not a sophisticated one. Improvements in accuracy and efficiency might be obtained if a more advanced algorithm is developed. The reason for using cycle jumping is because in general, modeling a cycle takes longer than it take to apply such a cycle experimentally. Hence, if a model is to be feasible, cycle jumping will have to be applied. For example, in the present work, one cycle can take at least 30 seconds to be modeled. Whereas in an experimental way, 10 cycles can be applied every second (10Hz).

1.2.2 Macroscopic failure criteria

The failure criteria predict if failure occurs (damage) at the macroscopic scale and above of that. For increased performance of the PDAM, the failure criterion should also predict the mode of failure and the failure plane angle. This is such that a proper (sudden) degradation rule can be applied. The (sudden) degradation rule here is different from the degradation rule mentioned in 1.1. The (sudden) degradation is used depending on the judgment of the failure criterion, whereas the degradation rule mentioned in section 1.1 is used on the inputs of the failure criterion A large amount of failure criteria exist. As has already been said, only stress-strain based criteria are reviewed. Here, only four criteria are discussed which were chosen due to them being recommended for the load cases considered in the present work. The recommendations come from the world-wide failure exercise (WWFE)-I by Soden et. al. [31] and the WWFE-II of Kaddour and Hinton [32].

Hashin [16] developed the most simple failure criterion of the four criteria reviewed here. The criterion is quadratic, the reason for this was that it yielded good results (no physical meaning). No increased accuracy was obtained for higher order models, compared to the additional complexity induced. Four failure modes can be predicted: Fiber tensile or compression failure and matrix tensile or compression failure. The performance of the criterion drastically decreases when used in the compression regime. The criterion is not able to predict the fracture plane angle.

Puck and Schürmann [28] presented a failure criterion which distinguishes between two modes: Fiber Failure (FF) and Inter-Fiber Failure (IFF). Both modes can happen in tensile and compression. The model is based on brittle fracture mechanics and makes use of Mohr's theory. Moreover, it uses the aforementioned fracture plane angle. The criterion shows improved compression failure prediction compared to the previously discussed Hashin criterion. The criterion was made for static situations. However, Eliopoulos and Philippidis [26] successfully implemented the criterion in fatigue.

LaRC04, Pinho et al. [33] criterion is increasingly based on physical phenomena (compared to Puck and Schürmann [28]) as they tried to model in-situ strengths and fiber kinking. Six failure modes can be predicted, using 3D stress states. The criterion's characteristics are that it includes non-linear matrix shearing, in-situ strengths and the modeling of fiber kinking. In-situ strengths are strengths based on nearby ply interaction. The criterion does however need energy release rates to be determined experimentally (where usually only stiffnesses and strengths are required). The performance seems to be comparable to the criterion of Puck and Schürmann [28], they both show increased compression prediction performance compared to Hashin. The criterion was verified using data from the WWFE.

LaRC05, Pinho et al. [34] was introduced as part of the second WWFE. The criteria include non-linear modeling of shear, transverse and through-the-thickness response of the material. Mohr-Coulomb was used as the basis for the matrix failure. Although it did not seem to be the best theory according to the original authors, it was required for prediction of the fracture plane angle which is an important parameter. Additionally, the model relies on some numerical calculations to find angles. This may slow down the process if applied on a large scale (many elements). Notable is that for tensile fiber failure the maximum stress criterion was used.

Final remarks failure criteria The amount of existing failure criteria is very large. In this review a small subset is discussed based on results of WWFE-I and WWFE-II. In total about 30 different failure criteria were tested in the WWFEs. What has been found is that until today there is no criterion which is best at everything (generality). Instead, a user of failure criteria should carefully make a choice depending on the application. Where important factors are loading conditions (low/high, compression/tension, mix etc.) and material such as UD and multi-directional (MD).

The criteria presented in this review, are the ones which were the best all-round performers, in terms of different test cases, except for the criterion of Hashin, which was chosen for its simplicity. The differences in the reviewed criteria lie in their theoretical background and usage. The Hashin criterion is the only one which does not have a physical basis. The theory of the LaRC criteria are both quite similar. Moreover, LaRC criteria require more than only strength parameters as input. Numerical searching procedures are required for all criteria except the criterion of Hashin. For plane stress cases, the criterion by Puck can also be used without numerical search of the fracture plane angle. Finally, all theories proposed to use the maximum stress criterion to predict fiber tensile failure.

1.2.3 Degradation rules

The degradation rules modify the material's EC due to failure or cyclic loading. There are two types of rules. Sudden degradation rules act if failure is predicted by the failure criteria. Notice that failure does not necessarily mean final failure of an element, it can also be partial failure. The second type, gradual degradation rules, are a function of cycles and are used in order to account for damage which cannot be captured by the macroscopic failure criteria reviewed in the previous section. The gradual degradation rules cannot distinguish between damage modes, instead, they act on specific types of ECs used by the macroscopic failure criteria.

Sudden degradation rules

As has been said, sudden rules act on the failure mode predicted by a failure criterion. Hence, the sudden rules should be adapted to the failure modes of the used failure criterion. Typically, the sudden degradation rules are developed as the PDAM is built. Examples of these can be found in sources [8, 11, 15, 24, 26] which have already been discussed in the previous section. The most notable characteristics of these rules are that they typically distinguish between fiber and matrix, and between compression or tension failure. In some cases the rules act on the basis of the fracture plane angle.

The sudden degradation rules presented in the references previously mentioned have two main characteristics in common. Fiber failures always causes catastrophic failure and reduce all ECs on the element on which the failure happens to zero (or near zero due to numerical considerations). Second characteristic is that failures related to the matrix always cause a partial loss of transverse stiffness. The amount of loss varies between theories, although Liu and Tsai [35] argued that the exact amount is not that important since the predictions of failures is already not exact. Moreover, by decreasing the element on which the failure acts, the importance of the degradation value is reduced even more. Finally, the sudden rules do

not depend on experimental data and the the degradation values of matrix failures are often not well substantiated.

Gradual degradation rules

Gradual degradation rules act as a function of cyclic loading. Requirement is that there is no catastrophic failure (on element or ply) predicted by the failure criteria. The rules may then act on the basis of one cycle, or can be modified to capture more cycles at once. In the present review, two types of gradual degradation rules are considered, gradual stiffness degradation and gradual strength degradation. Gradual stiffness degradation should be modeled as to track stress redistributions. Stress redistributions will influence the accuracy of the stress field. Since the stress magnitude is the main driver for both gradual degradation rules considered here, an accurate stress solution is desired. Gradual strength degradation is required to properly fail elements and to eventually predict the residual strength.

Strength degradation rules were reviewed in Philippidis and Passipoularidis [10], they compared various theories, and concluded that there is no rule that is capable of performing well in all cases (material, loading, geometry etc.). Moreover, they found that simple rules did perform better than more complex rules, this is if you take into account the increased experimental effort required for the complex rules. The gradual degradation rules found will now be discussed in order of year of appearance.

Broutman and Sahu [36] proposed a linear strength degradation rule. It is a simple equation and requires as only inputs the initial static strength and the parameter N which is the fatigue life and in general is obtained from S-N curves. Modifications to the original equation were made by Philippidis and Passipoularidis [10] to include the cumulative density function (CDF) and by Eliopoulos and Philippidis [26] to include the ability to predict under compression loads. The equation can be applied on element, ply and laminate level. All works mentioned in this paragraph tried to verify the equation. Good correlation was obtained between predictions and experimental results. Again, lower stresses yielded better predictions. At last, this theory was one of the recommendations made by Philippidis and Passipoularidis [10] due to the low experimental effort required.

Adams et al. [17] proposed an interaction model of stress ratio and cycle ratio. These two ratios may be combined using two additional experimental fitting parameters. Advantage of the theory is that after characterization it may be used for various R ratios and that it is able to adopt to wear-out and sudden behavior. Elaborating on this, wear-out means more gradual final degradation and this behavior is noticed on low-level stress. Whereas sudden behavior has a more sudden final degradation and happens in general at high-stress levels. The theory was used in the work of Shokrieh and Lessard [11]. Although, they did modify the equations in two ways, one of which was including an additional term which should be able to catch the initial strength increase in pin/bolt loaded specimens. The modification required an additional three experimental parameters. Moreover, they translated the theory in a way that it could be used as stiffness degradation. Both the modified strength degradation and stiffness degradation of Shokrieh and Lessard [11] were adopted in the work of Naderi and Maligno [30]. Implemented in their PDAM methods the theory was verified by Shokrieh and Lessard [12] and by Naderi and Maligno [30] and it provided good predictions. Again, the high-level stresses proved to be more difficult to predict.

Paepegem and Degrieck [19] introduced a hybrid method to track damage growth. The equation incorporates stiffness degradation, strength degradation and failure criteria theories. The idea was to catch the stiffness degradation as it physically seems to occur. Hence, initial degradation, then slow degradation and at last rapid degradation. This was achieved by implementing a damage variable D acting on stiffness and strength. The residual strength was incorporated in the failure criterion of Tsai-Wu [20]. The failure criterion is then used to predict the reserve factor. Finally, the theory seemed to predict reasonably, especially at lower stress levels. As has been mentioned, the theory however has its restrictions. It can only be applied on 1D loading and is not capable of modeling delaminations.

Tserpes et al. [15] used experimental fits to predict property degradation. For stiffness degradation a linear relation was used and for the strength degradation a second order polynomial fit was used to be able to catch the steep final degradation. The rules were applied on element level.

Kassapoglou's [37] model looks similar to that of Broutman and Sahu [36], however it is non-linear. It does only require N (fatigue life) and the static strength as inputs. In previous work, Kassapoglou [38] established a method to derive the S-N curve from statistics of static strength tests only. The theory is based on his proposed residual strength equation (although it can be used with other residual strength equations too). In Kassapoglou [6] the models of Broutman and Sahu [36] and Kassapoglou [37] were compared and verified against experimental data. There was not a single equation which did perform best. Discrepancies of maximum 10% were found for the model of Kassapoglou [37] and 8% for the model of Broutman and Sahu [36].

Lian and Yao [24] thought that stiffness and strength could be related to each other since they happen due to the same accumulated damage. Hence they related the two with a single exponential parameter. Four experimental parameters are required (for every longitudinal, transverse and shearing direction) for modeling both residual strength and stiffness, although one parameter can be approximated. The theory was used in a PDAM and showed good predictions except for quasi-isotropic laminate. However, it was said that this happened due to neglecting delamination modeling.

Eliopoulos and Philippidis [26] used a non-linear regression fit on experimental data to predict stiffness degradation, where tension and compression modes required different experimental parameters. Their implementation in PDAM yielded slightly optimistic results for residual stiffness.

Concluding remarks gradual degradation rules The presented theories are quite different. They do not show any remarkable similarities in terms of modeling principle. What they do have in common is that they all require N as input. This is a problem since the determination of S-N curves is not well understood and requires a large experimental effort. One promising method to obtain the S-N curve is the method proposed by Kassapoglou [38], however it must be determined if this method is applicable. There is no clear 'winner' among the proposed gradual degradation methods, the recommended method has to be assessed on a case-by-case basis. One thing that was remarkable, but can not be admitted per-se to the degradation rules is that in general increase of $\sigma_{max}/\sigma_{ult}$ or $\sigma_{min}/\sigma_{ult}$ yielded worse predictions compared to predictions at lower load ratios.

1.3 Outline

In what follows, the structure of the present work is established based on the reviewed literature and the guidelines proposed in chapter 6 of Kassapoglou [6] for the modeling of fatigue, as has already been mentioned. It can be noted that the same approach was used by the previously reviewed PDAMs. From the background, a main research question can be derived:

How can fatigue be modeled using PDA in combination with FE?

Additionally, some sub-questions can be formulated from the conclusion drawn in the literature review (section 1.2):

How should the macroscopic damage law be implemented?

What type of degradation theories should be applied?

Can an algorithm for cycle-jumping be developed relating damage and degradation to find the amount of cycles to be jumped?

How should such a cycle-jumping be implemented in a fatigue modeling framework?

The research questions will be addressed in this thesis. To realize this, various topics will be discussed in this work. The subjects are shown below:

- Build a model which judges failure at the macroscopic level by building a PDA model for quasi-static determination of strength (chapter 2).
- Develop a sophisticated cycle-jumping algorithm which is based on the relations between the damage and the degradation model (chapter 4).
- Carry out an experimental campaign to obtain input and validate the models (chapter 3).
- Implement a fatigue degradation theory to track damage created below the macroscopic scale (chapter 4).

The model will be developed for OHT specimens. There were three reasons to choose such a geometry. First reason is that not much research is known to the author on open hole specimens regarding fatigue (except maybe for the work of Shokrieh and Lessard), hence it is interesting to investigate behavior of such a geometry in order to investigate effects of the hole on fatigue. Second reason is the interesting stress distribution around the hole, which will cause various values of σ_{max} throughout the specimen. Finally, the stress concentration will ensure that failure will occur around the hole, eliminating the need to take into consideration modeling the effect of tabs. The use of tabs in general is required in order to reduce the stress concentrations caused by the machine clamps. The proper selection of tabs however is more an art than a science according to American Society for Testing Materials (ASTM)

standard [39]. Experimental specimens failed near the clamps should be disregarded, which especially for fatigue can increase the duration of the experimental campaign.

The developed model should be able to complete within 24 hours, this is a requirement by the project initiators. Some constraints are induced due to the length of this project (9-months). The experimental campaign should be limited as much as possible. The selection of a failure criterion and degradation theory will be influenced by this since these two parts depend to a large extent to experimental input. However, the model developed in this work is built in a way such that the user may use any type of failure or degradation laws (subjected to some limitations which will be discussed later). In this way, depending on the experimental data available to the user, proper laws can be selected.

Chapter 2

Quasi-static progressive damage model

In this chapter, a quasi-static progressive damage model will be developed. The model is used to predict the (residual) strength in the modeled specimen by making use of macroscopic failure theory which predicts damage based on the stress state. The stress state is evaluated by finite element (FE) theory. These two parts of the model (stress solution and macroscopic failure analysis) will be built upon in the upcoming fatigue model, chapter 4. The model is static in the sense that the stress analysis is based solely on static theory, but quasi-static since multiple load increments are analyzed.

The model will be presented by first looking at the flow chart which describes the methodology of the model (section 2.1). The FE model will provide stress analysis and its setup is described in section 2.2. The macroscopic failure theory used to predict damage propagation is based on the original failure criterion by Puck and Schürmann [28] and its implementation is described in section 2.3. Finally, in section 2.4 the model parameters are identified such that an efficient model is built which is validated and converged.

2.1 Flow-chart

The flow-chart diagram of the model is presented in figure 2.1. The flow-chart represents the methodology of the PDA. This section is divided into sub-sections according to the blocks of the flow-chart.

2.1.1 Initialize FE model

The PDA is performed on a 3D model of the specimen. The model creation is automated using a Python script which instructs ABAQUS commercial code how the model should be built. Every element is assigned a unique material, such that property degradation can be performed on the element level. The detailed description of the model can be found in section 2.2 where modeling parameters are discussed. The objective is to make the finite

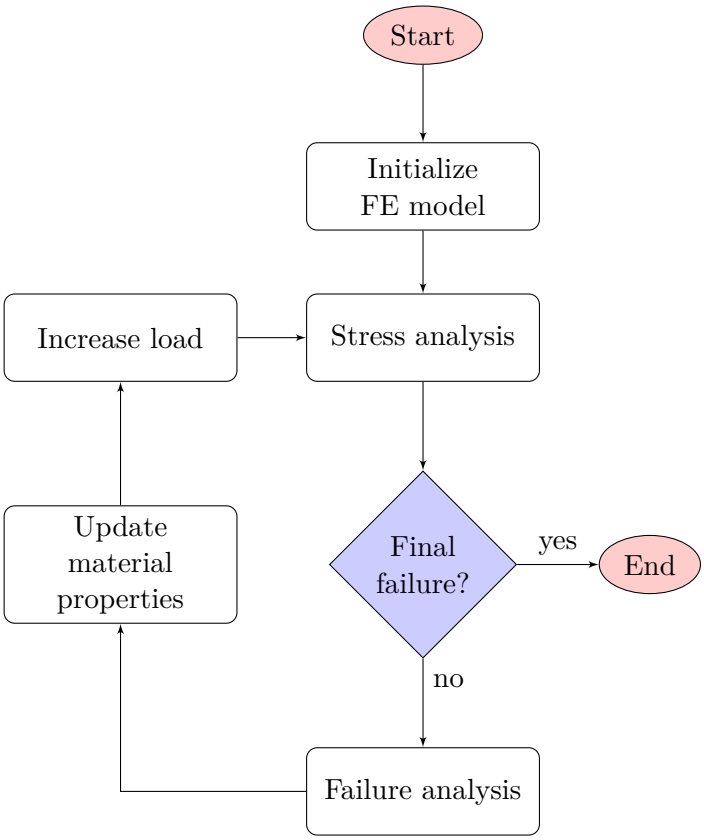

Figure 2.1: Flow-chart diagram of the quasi-static PD model

element model simulate the experimental setup as accurate as possible (regarding, boundary conditions, mesh refinement, damage pattern, etc) so as to obtain a stress solution being close to the real stress state, while keeping computational effort as low as possible (i.e. within the required 24 hours).

- Output is the finite element model including BC's and mesh parameters.

2.1.2 Stress analysis

Stress analysis is performed based on FE theory using the solver of ABAQUS commercial code. The input model for the stress analysis changes every iteration due to the load increase (section 2.1.6) and material property degradation (section 2.1.5). The stress solutions are required as input for the failure analysis and final failure criterion. The details are discussed in section 2.2 and section 2.4. It has to be emphasized that FE are solely used for the determination of the stress state, all other procedures are performed in Python.

- Output is the stress solution at every element (average of integration points).

2.1.3 Final failure?

The final failure decision is included such that the iteration ends. The final failure criterion (or global criterion) should correctly predict if a crack is present which causes fracture in in a plane perpendicular to the load and parallel to the width. Hence, failure is defined as the moment where the specimen is unable to carry load. It should be noted here, that for the FE model, there will not be a moment where the specimen is not able to carry load. This is due to not being able to degrade properties to zero for numerical reasons. Moreover, it is assumed that there is no deflection limit. The details of the global failure criterion are described in section 2.3.

- Output is the decision to continue or stop the analysis.

2.1.4 Failure analysis

The failure analysis uses the stress solution to predict failure on the element level. Additionally, the failure criterion used is able to distinguish between modes of failure and the failure plane angle. This output is needed for proper material degradation. An elaborate discussion on the failure analysis and its theory is given in section 2.3. The element failure state is passed on to the material property updater for further processing.

- Output are/is the location(s) of failure(s), type of failure(s) and the fracture plane angle(s) (if applicable).

2.1.5 Update material properties

Using the results of the failure analysis as input, the material properties are updated. The approach used is to degrade certain stiffnesses. Which stiffnesses are degraded depends on the failure mode. The method of determining which stiffnesses are to be degraded are based on physical reasoning. The details are discussed in 2.3.

- Output is updated engineering constants on the element level.

2.1.6 Increase load

Finally, the specimen load is increased. This direct increase of load requires an assumption. Since the failure of elements will cause a stress redistribution, one could argue that the load should not be increased until no more failures happen (requiring multiple stress analysis at the same load level). However, here it is assumed that failure is a dynamic process and can not happen instantaneous (which involves viscoelastic effects, beyond the scope of this research). Thus, as long as the load increment is chosen small enough the model will be able to simulate the failure process properly. The size of this increment is to be determined in the convergence study, section 2.4.

- Output is an increased load/displacement.

2.2 Finite element modeling

The FE model is used to provide stress solutions/states. These stress solutions are to be used for failure prediction and sudden property degradation of each element. The choice was made to perform the PDA implementation outside of the ABAQUS environment utilizing the Python programming language. The reasons were two. The model generation can be automated using the same Python script. Moreover, to implement such routines inside ABAQUS would require the use of FORTRAN, which is not further pursued in this work. Drawback of this decision was that analysis time will probably increase. More on the automation and model creation is described in section 2.2.1.

Due to the geometry of the tested specimen, it is expected that out-of-plane stresses will occur. These out-of-plane stresses arise due to edge effects (Kassapoglou [40]). Since edges occur at the critical location (hole) it was thought to be good practice to create a model which is capable of providing out-of-plane stresses, resulting in the choice of brick elements. The element choice is further discussed in section 2.2.2. Non-linear behavior has been observed on shear elastic properties. According to Lagace [41], non-linear effects should be accounted for when modeling parts with stress raisers (such as OHT specimens). Thus, a constituent model is written to include the non-linear shearing effect, section 2.2.3. The boundary conditions for the model were chosen with two things in mind, proper simulation of the real world environment and increase of computational efficiency. The boundary conditions are described in section 2.2.4. Finally, the load introduction is described in section 2.2.5.

2.2.1 Automatic model generation

A script file, written in Python was created to automate the FEM and PDA process. The Python scripts pursues a routine similar to the flow-chart presented in the previous section (figure 2.1). Before running the script, the user has to provide geometry, lay-up, displacement step and meshing parameters. The script then creates a 3D deformable body. What is important in particular, is that every element gets assigned a distinct material. This is required such that during the progressive damage (PD) analysis properties can be updated per element. The distinct material per element will also be exploited in the fatigue analysis. Other important aspects of the model creation are described in the subsequent sections. When the model has been set-up, the model is submitted for analysis by the same script. After analysis completion, the script calls the failure analysis (section 2.3), updates the material properties accordingly and increases the load by the given displacement step if final failure has not occurred.

2.2.2 Element choice

Element selection was based on the ABAQUS user documentation, Dassault Systemes [42]. A large library of elements is available in ABAQUS, applicability depends on the case studied. In general, composites are modeled with shell or continuum elements. Shell elements are used in 2D situations where only in-plane stresses are expected, continuum elements extend the stress spectrum to 3D and are used on more complex stress states. The area of interest in this thesis is mainly the hole, since damage is expected to start there due to the stress concentrations, Lekhnitskii [43]. The edges of the hole will cause out-of-plane stresses and hence, the choice was made for continuum elements since these elements are advised (by the documentation) when out-of-plane stresses occur. The shape of the element is chosen as brick (hexahedral) since it is advised by the documentation for better accuracy and efficiency [42]. Shear and volumetric locking were not expected since no bending is applied and the material is compressible (i.e. poisson's ratio smaller than 1). Therefore, it is possible to use full integrated elements. Reduced integration was also considered but these elements could suffer from hour glassing. Due to the implementation of non-linear shear stress it is a tedious task to implement hour glass control since updating the hour glass stiffness is not as straight forward as updating the other stiffnesses. Therefore reduced integration elements are omitted.

Two element strategies were considered. The first method results in a single element through the thickness of the model with output at various section points, one for every ply. The various plies are added by using a composite layup section. This method reduces computational cost and model complexity. However, the aspect ratio of the elements near the hole increase and therefore it was thought not to be good practice to use this strategy. The second method was giving every ply its own element through the thickness. It was thought that this method would give better stress predictions due to the increased amount of nodes. Second geometrical order elements were also considered since they are advised for problems with stress concentrations. Analysis time however increased in a way that the 24 hour requirement could not be met. The reason for this is probably the mesh refinement. In general, second order elements require less mesh refinement. However, for the progressive damage analysis, small elements are favored since they can give a higher resolution picture of the damage development. The reason for

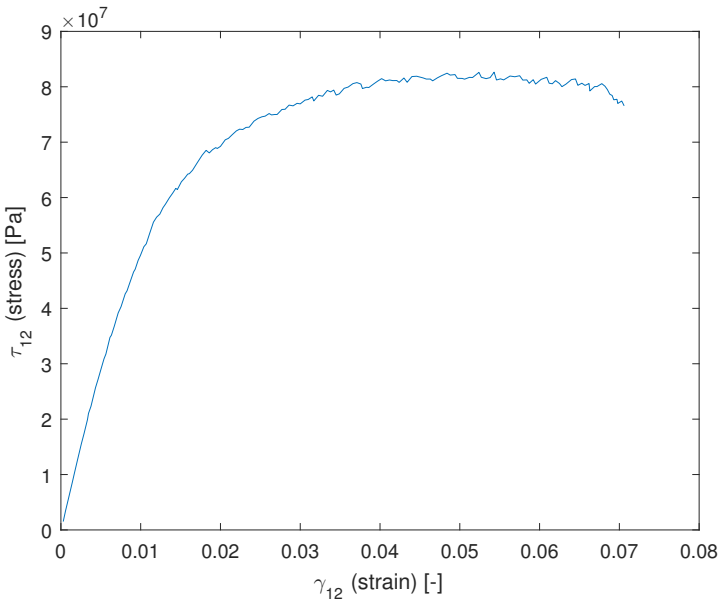

Figure 2.2: Example shear stress strain curve of AS4/8552 material

this is that failure is judged element wise, and hence if an element is smaller, the pattern obtains an higher resolution.

2.2.3 Non-linear shear behavior

According to Lagace [41], non-linear behavior happens in two modes. Stiffening due to longitudinal tension in the ply (in a ply oriented axis, so longitudinal is parallel to the fibers) and softening due to shearing. The largest non-linearity is that of shearing, with a modulus change of 105% versus 13% effect on longitudinal tension according to the source. Puck and Schürmann [28] suggest an additional non-linearity is present in the transverse compression stiffness. Only shear stress is accounted for in this thesis, the transverse compression mainly happens outside of the critical area and will thus be neglected. An example shear stress-strain curve is shown on figure 2.2. The data-points are obtained by DIC and are truncated just before final failure. As Lagace [41] states, just before final failure the tangential modulus turns negative. It could be argued that the shown non-linearity is caused by partial or total ply failures. In that case however, large discontinuities should be visible.

A plot such as shown on figure 2.2 is typically obtained from an in-plane shear test such as ASTM D3518. Before using the data in finite element analysis (FEA), it has to be pre-processed. To obtain a smooth function, a polynomial interpolation is performed. The order of interpolation depends on the data and the required accuracy (R^2). In general, a fourth order polynomial is accurate enough (i.e. $R^2 \approx 1$). Finally, to ensure that the failure criterion is able to catch the failure, the shear-stress is not allowed to go bellow the failure stress after the strain has passed the point of maximum shear stress. Implementation of this material behavior was achieved through a UMAT subroutine utilizing FORTRAN. Although it has been previously mentioned that using FORTRAN was avoided, for the the implementation of material non-linearity the use of FORTRAN was straight forward and hence it was favored.

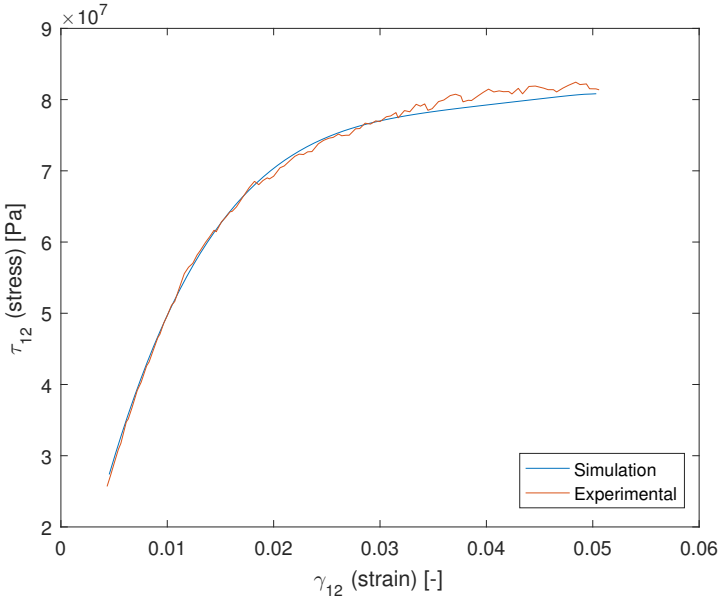

Figure 2.3: Comparison between simulated and experimental shear stress-strain data of an ASTM D3518 experiment (in-plane shear)

In this subroutine, the tangential in-plane shear modulus is calculated by equation 2.1.

$$G_{12}^{T} = \frac{\tau_{j,12} - \tau_{i,12}}{\gamma_{j,12} - \gamma_{i,12}} \tag{2.1}$$

Where the shear stresses are calculated using the polynomial fit of the data points as explained earlier. As input, the respective strain (i,j) is inserted in the fit. The strains are provided by ABAQUS. In case of $\tau_{i,12}$ being zero, equation 2.1 gives the secant modulus. Using the secant modulus yields better results according to Puck and Schürmann [28]. Therefore, the maximum step in ABAQUS is set to 1 (from zero load to maximum load in one increment) such that, if possible, the secant modulus method is used with multiple iterations instead of using the various smaller increments in combination with the tangent modulus. The choice of method is determined by ABAQUS solely.

To validate the implementation, the ASTM D3518 test was simulated in ABAQUS using the FORTRAN subroutine. Results were compared to the actual experiment, shown in figure 2.3. For the simulated model, a model was made with 3600 elements, a geometry according to ASTM and clamped at the short edges. Figure 2.3 shows that this first simple model for non-linear approximation yields reasonable results. However, as Puck and Schürmann [28] suggest, there will arise interactions if different stress states are applied by the other non-linear modes (transverse compression and parallel tensile stress). These effects are not captured in this model but are considered to be outside of the scope of this research.

2.2.4 Boundary conditions

BCs are to be used for two reasons. First, BCs are essential in simulating the real world model behavior. Second, BCs can be used to reduce computational cost by taking advantage

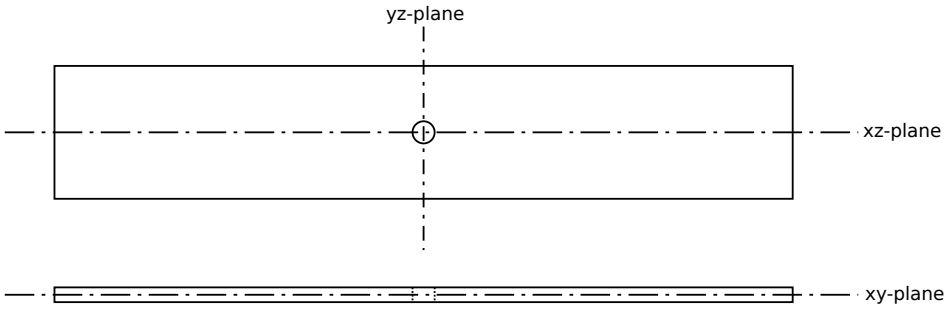

Figure 2.4: Symmetry planes in OHT specimen

of (anti-)symmetry planes. This allows modeling only a part of the model, reducing the total amount of elements required. Two boundary conditions are required to simulate real world BCs of the testing machine. These two BCs simulate the clamps of the testing machine. Since the machine uses clamps, it is logical to use the encastre conditions in Abaqus i.e. constraining all degrees of freedom.

The BCs which can be used to model only parts of the total model are now discussed. Looking at the geometry and loading conditions, three symmetry planes can be found. These planes all intersect at the center of the hole and each follow one of the three axis, x, y and z. The symmetry planes are shown on figure 2.4 and their required boundary conditions are shown in equation 2.2.

$$\begin{aligned} xy-plane; \quad & z = xr = xy = 0 \\ yz-plane; \quad & x = yr = zr = 0 \\ xz-plane; \quad & y = xr = zr = 0 \end{aligned} \tag{2.2}$$

The symmetry plane which cuts the specimen in the yz-plane, requires the applied displacement to be halved to create the same applied strain. Moreover, the usage of ± 45plies can be a problem in using all three symmetry conditions. Symmetry planes yz and xz become valid by approximation if ± 45 plies are introduced in the model. This happens due to that symmetry conditions behave like a mirror. The effect of this is shown on figure 2.5. This effect happens due symmetry implying a force equal in magnitude but opposite in direction. If we take for example the symmetry in the yz-plane, the restriction of the movement in x is what causes wrong simulation. If now 0 plies are added to the layup, the movement along x physically gets restricted compared to a case with no 0 plies. The result of such a 0 ply hence is that the error of the symmetry approximation is reduced. The same can be said for 90 plies and symmetry in the xz-plane. It can thus be concluded that the accuracy of the approximation is a function of the lay-up. Moreover, it can be expected that damage in plies surrounding the ± 45 plies (including the ± 45 plies) will cause the approximation to become less good.

To assess the accuracy and effect of the approximation, it is advised to run a full model (without symmetry boundary conditions) and compare it to the desired model with symmetry BCs every time the layup, geometry and/or material is changed. Not only the predicted failure strengths should match, but the generated failure pattern too. Engineering judgment is then required to decide if the approximation is well enough. The z-symmetry (cut through xy-plane) is always valid throughout this exercise, since only balanced and symmetric layups are used. Finally, the BCs are applied nodally.

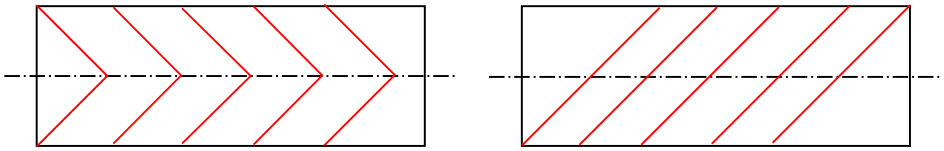

Figure 2.5: Left, symmetry boundary applied causes mirror effect on a 45 layer. Right correct representation of a 45 layer.

2.2.5 Load introduction

Load introduction happens on one of the short edges of the specimen. The load is applied as a displacement along the x-direction. This method was chosen since it simulates best a displacement controlled experiment which will be used to validate the model. The displacement increment (step) may be determined by a convergence study as is performed in section 2.4.

To reduce computational time, the first increment is automatically determined such that it does not cause damage. The automatic calculation of initial displacement happens as follows. An arbitrary load is applied on the specimen. After which the matrix FI is calculated for all elements. The maximum FI is then obtained and the initial displacement is calculated by equation 2.3.

$$u_{init} = u_{arb} \cdot \frac{1}{FI_{max}} \cdot 0.9 \tag{2.3}$$

2.3 Macroscopic failure criterion

In order to track damage progression, a failure criterion is required which can asses if elements have failed. Moreover, prediction of the damage mode helps in properly modeling behavior after damage has occurred, since damage does not always lead to final failure. There exist a lot of different failure criteria. According to Philippidis and Passipoularidis [10] they can be divided into two classes, mechanistic and phenomenological. The first class tries to model at the microscopic level. The potential of this theory lies in low experimental effort and increased applicability. Disadvantage is, that these models are not mature enough to be applied widely.

The second class is applied on the macroscopic level and is more mature. Theories often rely on inputs like stresses and strengths. To choose a proper failure criterion among the large amount of failure criteria, the WWFE I, II and III were used as starting point. The first exercise, Hinton et. al. [44] started as early as 1998 and focused on 2D stress states. The focus of the second exercise was on 3D stress states and started in 2012, Hinton and Kaddour [45]. Finally, the third exercise was launched in 2013 by Kaddour et. al. [46]. It focused on damage, matrix cracking, delaminations and stress gradients. When looking at the element level, the OHT specimen consists of various stress states, the majority of the elements can be approximated by a 2D stress state, near the hole and near the edges however, 3D stress states arise due to the edges and stress concentrations involved.

The choice was made to use a classical stress-strain based criterion. The criterion of Puck and Schürmann performed well in both 2D and 3D stress states, Kaddour and Hinton [32] and Soden et. al. [31]. It requires a fair amount of experimental input and was thus chosen as the macroscopic failure criterion. The implementation is described in section 2.3.1.

Material property degradation rules are required to define the behavior of the material after failure has been predicted by the failure criterion. The available so called sudden degradation rules are all based on physical interpretations and are further discussed in section 2.3.2.

Finally, a criterion is needed to stop the progressive damage analysis. This is discussed in section 2.3.3

2.3.1 Puck and Schürmann failure theory

The failure criterion was presented for the first time in 1998 by Puck and Schürmann [28]. Multiple papers have been published hereafter by the authors trying to improve the criterion and increase its applicability. The theory was implemented in commercial code by Puck and Schürmann [47]. Guidelines for the determination of the different variables were also presented by Puck et. al. [48]. Description of the full 3D criterion for the usage of WWFE-II was done by Deuschle and Kröplin [49]. The last known publication is the paper by Puck and Deuschle [50] which is on analytical solutions to 3D stress problems. The failure criteria distinguish between two general failure modes, fiber failure and inter-fiber failure. In this work, the work of Deuschle and Kröplin [49] is adopted as the starting point.

Fiber failure (FF) As the name implies, fiber failure mode is the mode where fibers fail. Most authors, such as Shokrieh and Lessard [11], Lian and Yao [24] and Eliopoulos and Philippidis [26] consider this as a catastrophic failure mode. This means that after fiber failure the specimen (element) is unable to carry load. The most simple form to determine fiber failure is by the maximum stress criterion, equation 2.4.

$$FI_{FF} = \frac{\sigma_{11}}{X^{t/c}} \tag{2.4}$$

Where $X^{t/c}$ is the tensile/compression strength of the material parallel to the fibers and σ_{11} the applied stress in a ply oriented axis. Finally, FI_{FF} is the failure index. If the failure index exceeds one, it means failure has occurred. For the case however, that there is multi-axial loading and stresses σ_{22} and σ_{33} are approximately the same order of magnitude as σ_{11} the FF criterion was extended by Puck and Schürmann [28] as follows. In the case of multi-axial loading, it is said that for failure, the stress in the fibers, σ_{11f}, should reach a fiber stress load identical to a case that would cause failure in an uni-axial case with only σ_{11} applied. Hence, the fiber stress is to be determined in both cases. A complete derivation will not be given here but can be found for example in Puck and Deuschle [50]. The derivation is based on the assumption that under all loading conditions the strain in the matrix and fibers will be the same. Additionally, a stress magnification will occur in the transverse direction due to the difference in stiffness, soft and stiff for respectively the matrix and fiber. This magnification factor m_{sf} is determined as 1.1 for CFRPs. The final equation then becomes equation2.5.

$$FI_{FF} = \frac{1}{X^{t/c}} \left(\sigma_{11} - \left(\nu_{21} - \nu_{21f} \frac{E_{11}}{E_{11f}} m_{sf} \right) (\sigma_{22} + \sigma_{33}) \right) \tag{2.5}$$

Where failure occurs if FF_{IF} is higher than 1, X^c is defined to be negative and the subscript f denotes fiber properties.

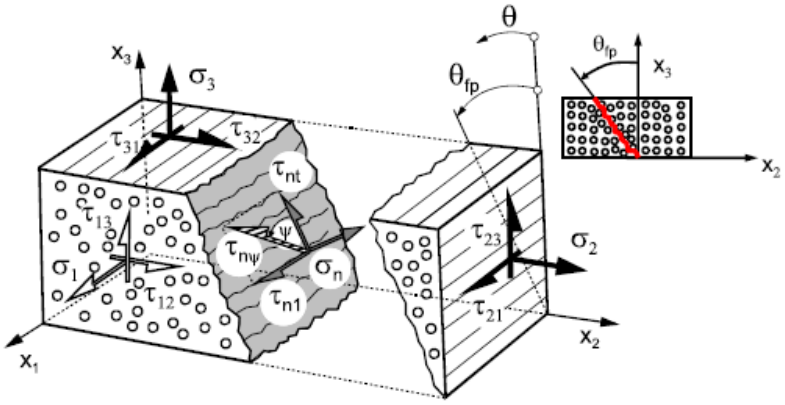

Figure 2.6: Picture showing definition of failure plane angle and related stresses (in 3D).

Inter-fiber failure (IFF) The basic idea is that IFF happens in an intrinsically brittle manner. Due to this, Mohr's fracture theory is chosen as the basis. It is then assumed that fracture happens solely due to stresses acting on the fracture plane. The key is then to find this fracture plane and the failure strengths which belong to this plane. The fracture plane is parallel to the fibers and can be inclined by a fracture plane angle θ_{fp}. The exact definition of θ_{fp} is shown on figure 2.6. To find the fracture plane angle, there exist various methods. The more general 3D case requires the usage of numerical search, a computational expensive process. Analytical solutions have been presented for the in-plane case σ_{22}, τ_{12} and a special 3D case $\sigma_{22}, \sigma_{33}, \tau_{23}$ by Puck and Schürmann [28] and Puck and Deuschle [50] respectively. 3D stress states are expected in the specimen under investigation in this thesis. Especially at the hole edges. Since fracture is expected to concentrate around the hole, the criterion will be applied in its full 3D form including all stresses $\sigma_{11}, \sigma_{22}, \sigma_{33}, \tau_{12}, \tau_{13}$ and τ_{23}. To reduce the computational cost, an extended Golden section numerical search is implemented according to Wiegand et. al. [51]. Additionally, a fiber parallel stress correction factor is applied as proposed by Deuschle and Kroplin [49]. The criterion, its required action plane strengths, the correction factor and the numerical algorithm will be discussed briefly now. For a full derivation the reader is referred to Puck and Schürmann [28], Wiegand et. al. [51], Deuschle and Kroplin [49] and Puck and Deuschle [50] respectively.

Proceeding with the statements made at the beginning of this paragraph, assumed is that the material behaves intrinsically brittle. This means that an applied normal stress perpendicular to the action plane of a material will cause fracture in the plane parallel to the action plane. To obtain the stresses on a stress action plane the transformations shown as equation 2.6 are required.

$$\begin{aligned} \sigma_n(\theta) &= \sigma_{22} \cdot cos^2\theta + \sigma_{33} \cdot sin^2\theta + 2\tau_{23} \cdot sin\theta \cdot cos\theta \\ \tau_{nt}(\theta) &= -\sigma_{22} \cdot sin\theta \cdot cos\theta + \sigma_{33} \cdot sin\theta \cdot cos\theta + \tau_{23} \cdot \left(cos^2\theta - sin^2\theta\right) \\ \tau_{n1}(\theta) &= \tau_{13} \cdot sin\theta + \tau_{12} \cdot cos\theta \end{aligned} \tag{2.6}$$

The angle θ is the inclination of the action plane. In general, this angle may vary from $-90°$ and $90°$. With the angle known, the failure index is calculated by equation 2.7 if $\sigma_n \geqslant 0$ or

by equation 2.8 for $\sigma_n < 0$.

$$FI_{IFF}(\theta) = \sqrt{\left[\left(\frac{1}{R_{\perp}^{At}} - \frac{p_{\perp\Psi}^{t}}{R_{\perp\Psi}^{A}}\right)\sigma_n(\theta)\right]^2 + \left(\frac{\tau_{nt}(\theta)}{R_{\perp\perp}^{A}}\right)^2 + \left(\frac{\tau_{n1}(\theta)}{R_{\perp\parallel}^{A}}\right)^2} + \frac{p_{\perp\Psi}^{t}}{R_{\perp\Psi}^{A}}\sigma_n(\theta) \tag{2.7}$$

$$FI_{IFF}(\theta) = \sqrt{\left(\frac{\tau_{nt}(\theta)}{R_{\perp\perp}^{A}}\right)^2 + \left(\frac{\tau_{n1}(\theta)}{R_{\perp\parallel}^{A}}\right)^2 + \left(\frac{p_{\perp\Psi}^{c}}{R_{\perp\Psi}^{A}}\sigma_n(\theta)\right)^2} + \frac{p_{\perp\Psi}^{c}}{R_{\perp\Psi}^{A}}\sigma_n(\theta) \tag{2.8}$$

Where R constants denote strengths, p constants are inclination parameters on the master fracture body and the superscripts A, t and c indicate action plane, tensile and compression respectively. Symbols $\perp$ and $\parallel$ denote transverse and parallel to the fibers. Finally, Ψ is the angle between the resultant of the shear stresses $\tau_{n\psi}$ and τ_{nt} (shown on figure 2.6. The parameters for equations 2.7 and 2.8 can be determined after the action plane related strengths are known. The action plane tensile strength is the same as the transverse tensile strength of the ply (equation 2.9).

$$R_{\perp}^{At} = Y_t \tag{2.9}$$

The shear stress strength of the action plane is the same as the shear stress strength of the ply (equation 2.10).

$$R_{\perp\parallel}^{A} = S_{21} = S_{12} \tag{2.10}$$

Finally, the action plane strength denoted as $R_{\perp\perp}^{A}$ can not be related to any standard material strengths. Also it is difficult to obtain by experiment according to Deuschle and Kroplin [49]. Instead, it is reconstructed by equation 2.11.

$$R_{\perp\perp}^{A} = \frac{Y_c}{2(1 + p_{\perp\perp}^{c})} \tag{2.11}$$

Recommended values for the inclination parameter $p_{\perp\perp}^{c}$ are given in the sources mentioned earlier and vary between 0.25 and 0.30 for CFRP's. Changing this value does not change the FI at the critical fracture angle and thus a value may be arbitrarily chosen because this thesis will only utilize the FI at the critical fracture angles. The unknowns of equations 2.7 and 2.8 can now be found by using equations 2.12, 2.13 and 2.14.

$$cos^2\Psi = \frac{\tau_{nt}^2}{\tau_{nt}^2 + \tau_{n1}^2} \tag{2.12}$$

$$sin^2\Psi = \frac{\tau_{n1}^2}{\tau_{nt}^2 + \tau_{n1}^2} \tag{2.13}$$

$$\frac{p_{\perp\Psi}^{t,c}}{R_{\perp\Psi}^{A}} = \frac{p_{\perp\perp}^{t,c}}{R_{\perp\perp}^{A}}cos^2\Psi + \frac{p_{\perp\parallel}^{t,c}}{R_{\perp\parallel}^{A}}sin^2\Psi \tag{2.14}$$

With all parameters determined, the only thing that remains to be done is to determine the fracture angle (θ_{fp}) i.e. the angle at which FI is maximized. A standard procedure would be to examine FI at all possible angles between and including $-90°$ and $90°$ and selecting the angle θ which causes the largest FI. Depending on the required resolution this could take for

example 180 evaluations of FI for a precision of 1 degree. If this method is to be applied on a large element set, the computational cost rapidly increases, especially since the calculations are done using an interpreted language. Therefore, instead of a numerical search, a numerical method known as the extended Golden-section search is applied as proposed by Wiegand et. al. [51]. The method starts with a normal Golden-section search which has obtained its name from the golden ratio it uses which is defined as equation 2.15.

$$\phi = \frac{1+\sqrt{5}}{2} \tag{2.15}$$

The golden ratio defines two intervals a and b which together form the analyzed interval. In this case, the starting interval is $-90°$ and $90°$. The ratio that should hold between these two intervals a and b is found by equation 2.16.

$$\frac{b}{a} = \phi \tag{2.16}$$

A third interval is determined by using the relation 2.17.

$$\frac{b}{a} = \frac{a}{c} \tag{2.17}$$

The endpoints of these three intervals are defined by four angles θ as shown by equations 2.18.

$$\begin{aligned} a &= [\theta_1, \theta_3] \\ b &= [\theta_3, \theta_2] \\ a+b &= [\theta_1, \theta_2] \\ c &= [\theta_3, \theta_4] \end{aligned} \tag{2.18}$$

Where θ_1 and θ_2 are the boundary angles, which for the first step are $-90°$ and $90°$ respectively. The failure index is then evaluated for angles θ_3 and θ_4. If now $FI_{IFF}(\theta_4) \geqslant FI_{IFF}(\theta_3)$ the process is repeated for boundary angles θ_3 and θ_4. In case of using a legacy Gold-section search, the process is repeated until the interval θ_1 and θ_2 is sufficiently small. The extended method as proposed by Wiegand et.al. [51] however uses an interpolation method to reduce the amount of iterations required for the Golden-section search. The interpolation method is called an Inverse Parabolic Interpolation and assumes that FI_{IFF} is locally a parabola as a function of θ. The fracture plane angle θ_{fp} can then be calculated by equation 2.19 at the cost of two extra evaluations of FI_{IFF}.

$$\theta_{fp} \approx \theta_2 - \frac{1}{2}\frac{(\theta_2-\theta_1)^2(FI_{IFF}(\theta_2)-FI_{IFF}(\theta_3)) - (\theta_2-\theta_3)^2(FI_{IFF}(\theta_2)-FI_{IFF}(\theta_1))}{(\theta_2-\theta_1)(FI_{IFF}(\theta_2)-FI_{IFF}(\theta_3)) - (\theta_2-\theta_3)(FI_{IFF}(\theta_2)-FI_{IFF}(\theta_1))} \tag{2.19}$$

With the now determined θ_{fp}, the failure index can be determined by calculating $FI_{IFF}(\theta_{fp})$.

At last the correction factor due to stresses parallel to the fibers is discussed. The correction is applied on the basis of the following arguments. The theory of Mohr does not include any effects due to stresses parallel to the fiber. However, experiments have shown that there should be some interaction. The idea is that before the FF mode, some fibers will have already failed. This can be supported by statistical laws according to Deuschle and Kroplin [49]. Hence, some fiber-matrix debonding will have occurred, which influences the action plane related strengths. For simplicity it is assumed now that these influences are independent of θ. The weakening

factor then tries to approximate the transition of IFF to FF and vica versa by an ellipse. For a general load case the weakening factor is then defined as equation 2.20 with m and s being 0.5 since no experimental data is available.

$$\eta_{w1}\left(\frac{FI_{IFF}(\theta_{fp})}{FI_{FF}}\right) = \frac{c\left(a\sqrt{c^2(a^2-s^2)+1}+s\right)}{(ca)^2+1} \qquad c = \frac{FI_{IFF}(\theta_{fp})}{FI_{FF}} \tag{2.20}$$

And is valid as long as $\frac{1}{s} \geqslant \frac{FI_{IFF}(\theta_{fp})}{FI_{FF}} \geqslant m$. The final FI is then calculated by 2.21.

$$FI_{IFF,\eta_{w1}}(\theta_{fp}) = \frac{FI_{IFF}(\theta_{fp})}{\eta_{w1}} \tag{2.21}$$

2.3.2 Sudden material property degradation

There do not exist complex theories on how to degrade material properties. Instead, in general, logical reasoning based on physical effects are used. The theory applied here is the theory introduced by Deuschle and Kroplin [49]. The theory seems applicable since it was developed especially for the failure criteria used. Moreover, Perillo et. al. [52] suggest that there is no large difference between various sudden degradation theories. For fiber failure, all ECs are multiplied by $(1-d)$ i.e. drop to almost zero [1]. The value of d is determined later in this paragraph. For matrix failure, the theory is that in principle a crack will cause a stiffness loss perpendicular to its own plane. Deuschle and Kroplin [49] suggest that the stiffness drop of shear moduli should be smaller than the drop of normal-stiffness moduli, the difference is a factor 0.6. No clear explanation is given for this value, rather than that it is based on preliminary considerations. Despite this, the value is adopted in this report on the assumption that exact values are not that important. This claim is supported by Liu and Tsai [35] which suggest that the exact degradation is not that important since the determination of failure is already just a prediction. In case now of an IFF event, the plane can have an inclination towards the stiffness properties. The angle of the crack plane then governs the stiffness degradation by equations 2.22.

$$\begin{aligned} E_2^{sd} &= E_2\left(1-d\cdot cos(\theta_{fp})\right) \\ E_3^{sd} &= E_3\left(1-d\cdot sin(\theta_{fp})\right) \\ G_{12}^{sd} &= G_{12}\left(1-d\cdot 0.6\cdot cos(\theta_{fp})\right) \\ G_{13}^{sd} &= G_{13}\left(1-d\cdot 0.6\cdot sin(\theta_{fp})\right) \\ G_{23}^{sd} &= G_{23}\left(1-d\cdot 0.6\right)\right) \end{aligned} \tag{2.22}$$

Where d is the degradation factor and the superscript sd means sudden degraded value. The degradation factor is required since the FE software does not allow stiffnesses of 0. Hence the stiffness has to be dropped to a very small quantity. A value of 0.99 for d is the most commonly used value (for example in Perillo et. al. [52]). Finally, it has to be noted that in the original paper by Deuschle and Kroplin [49] the degradation is not sudden, but instead, d is chosen sch that a constant FI is maintained. This approach is however not pursued here since it would increase the complexity, especially for the to be developed fatigue model.

[1] Dropping EC's to zero is not possible for numerical reasons.

2.3.3 Final failure criterion

A final failure criterion is required in order to stop the analysis. Before doing that, a definition for final failure has to be determined. Throughout this thesis, final failure will be defined as the moment where the specimen is unable to carry any more load, i.e. the specimen becomes two distinct parts. The failure strength however, is defined as the maximum strength the specimen reaches before the final failure event. For the real world model, this failure is not difficult to asses. In FEA, separation of the specimen into two parts is not possible in the current model. A way to asses final failure would be to analyze if the failed elements can connect two edges of the specimen in the xy-plane and through the thickness. This proved to be difficult since the failure pattern can not be predicted exactly. Hence, it is difficult to write a script which stops the analysis based on this behavior. Instead, a method similar to the one presented in Song and Rose [53] has been used, where the analysis stops if the reaction force drops with 5%. The value of 5% is not always suitable. In some cases it causes the analysis to stop before final failure has happened according to the failure pattern, or it causes the analysis to run for too long. In these cases, the value of 5% has to be adjusted manually by trial-and-error and the analysis resubmitted.

2.4 Convergence study and validation

A convergence study is required to identify model parameters such as mesh refinement and displacement incrementation (section 2.1.6). The steps and results (output) of the convergence study are discussed in 2.4. With the parameters known, the model can be validated against experimental results in section 2.4.2. The predictions are validated against results available in the literature and by an experimental campaign. Finally, the model parameters are summarized in section 2.4.3.

2.4.1 Convergence study

Convergence of the model is based on the convergence of predicted failure stress and on the failure pattern. Before going into this type of convergence however, the finite element model may be judged on stress solution convergence. This way is favorable since a single stress solution takes only minutes, and a full Quasi-static progressive damage analysis (QSPDA) can take up to hours depending on the various parameters. Hence, by doing the stress solution convergence first, an initial idea can be obtained about the mesh parameters. Moreover, the stress convergence may be used to predict usable symmetry boundary conditions by studying the effect of symmetry boundary conditions on the stress solution.

With initial mesh parameters identified by the stress convergence study, the first thing to check then is the effect of displacement incrementation step on the QSPDA. The displacement incrementation step which converges the QSPDA is then hold equal and mesh refinement is checked for convergence. If convergence is not achieved within the first two steps, displacement convergence has to be done with the last converged mesh. This iteration loops until convergence is found for both within one step. Until now it is assumed that the boundary

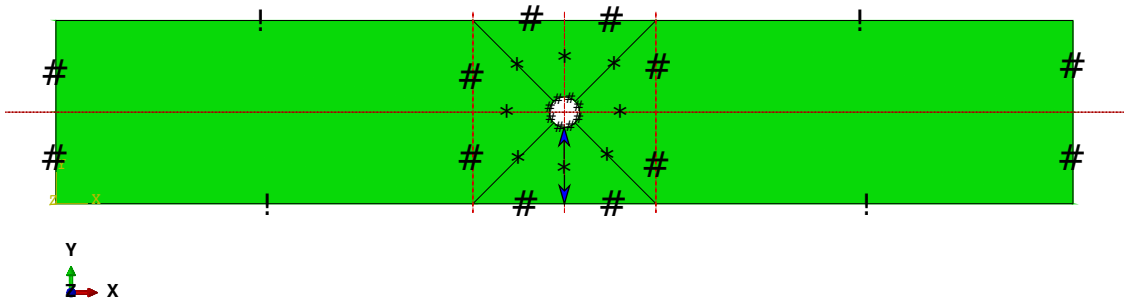

Figure 2.7: Partitioning of the model for structured meshing. Symbols denote mesh parameters.

conditions do not affect the result. A full scale PDA has to be run to check for failure pattern and failure strength equivalence of the symmetrical model. If equivalence is not found, symmetry boundary conditions must be re-evaluated.

The convergence study is performed on ASTM D5766-11 [54] specimens. The geometry of these specimens should be 36mm width, length of 200-300mm and hole diameter of 6mm. The length is chosen as 200mm to conform to the experimental campaign performed in this thesis.

Stress solution convergence

Finding stress solution convergence is a complex process. The problem is that convergence is desired around the hole, since this is the area where damage is expected, but it is difficult to judge convergence there with no experimental input. Hence, the choice was made to judge convergence against the amount of stress redistribution inside the stress concentration area. This area is defined as the area around the circle cut-out with a distance to the hole of 2 times the hole radius (total 6mm) according to Lehknitskii [43]. To reduce the complexity, a single layer of 0 oriented UD was used for the convergence study. The mesh can be changed using three parameters. The parameters are shown on figure 2.7. Where the # will be called SE (short edges), * will be called BE (edges with bias) and ! are the LE (long edges). The longer bias edges have a bias ratio of 3 and the shorter edges a ratio of 5 to reduce element distortion around the hole. The parameters define the number of elements on the edge. Meshing is then performed using the structured mesh algorithm. The exact values of all parameters are shown in table 2.1.

For all meshes, the stress solution is obtained at the nodes from 6 o' clock in a straight line to the edge of the specimen, shown also on figure 2.7 by the blue arrows. Since the stress solutions are obtained only at the nodes, the data points will be fitted with a 2-term exponential interpolant. The results of these fits can be seen on figure 2.8. It must be noted that these fits all had an R-square higher than 0.98. In the legend of figure 2.8, the number refers to the amount of elements in the area around the hole. The plot confirms that indeed the stress concentrations have faded out at 6mm.

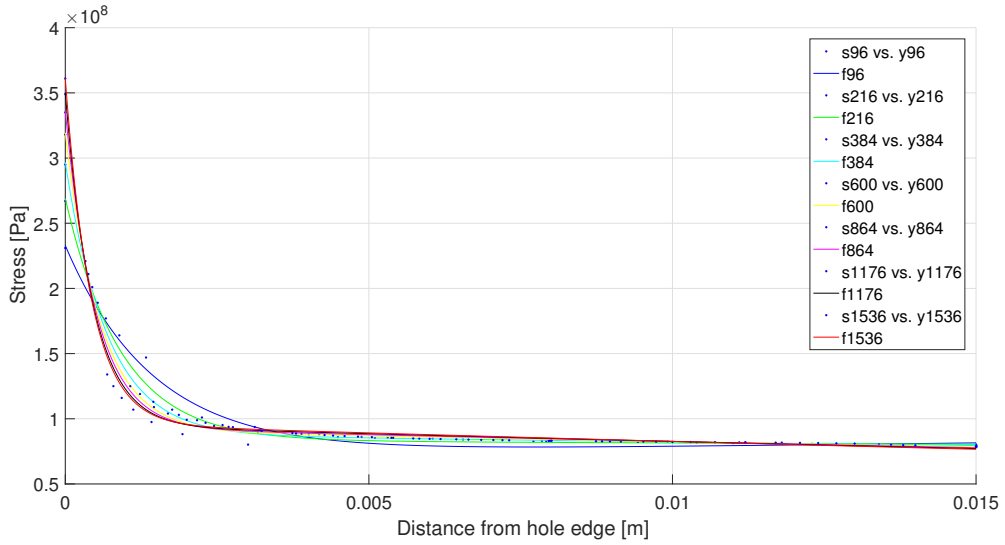

Figure 2.8: Stress solution for different meshes

Table 2.1: Parameters and results of mesh convergence study

Parameters [SE, LE, BE]	**Elements hole [total]**	ΔP $[N/m]$	**% change**
$[2, 4, 6]$	96 [128]	664395	-
$[3, 6, 9]$	216 [288]	36861	5.55
$[4, 8, 12]$	384 [512]	23497	3.54
$[5, 10, 15]$	600 [800]	16147	2.43
$[6, 12, 18]$	864 [1152]	10698	1.61
$[7, 14, 21]$	1176 [1568]	8528	1.28
$[8, 16, 24]$	1536 [2048]	6382	0.96
$[9, 18, 27]$	1944 [2592]	5060	0.76

The approach is now to determine the amount of load (in [N/mm]) which gets redistributed between to successive meshes. To do this, the equations obtained by the fitting procedure are used. Equation 2.23 can then be used to find the difference between two meshes. This difference is the amount of load which gets redistributed between the two compared meshes.

$$\Delta P = \int_{0.0}^{0.006} |f_{m,i}(x) - f_{m,j}(x)| dx \tag{2.23}$$

Where ΔP is the amount of loaded which is distributed differently between the two meshes and $f_{m,i}$ is the function obtained from the fit of the i-th nodal data points. Table 2.1 shows the results. Notice that the first mesh can not be compared to a previous mesh. Instead, as ΔP the total load in the stress concentration area is given. This load is determined by using the finest mesh, other meshes will have equal results since the total load should be equal among all meshes as the stress beyond y = 0.006 is approximately equal.

The change in load distribution can be plotted against the amount of elements. This is shown

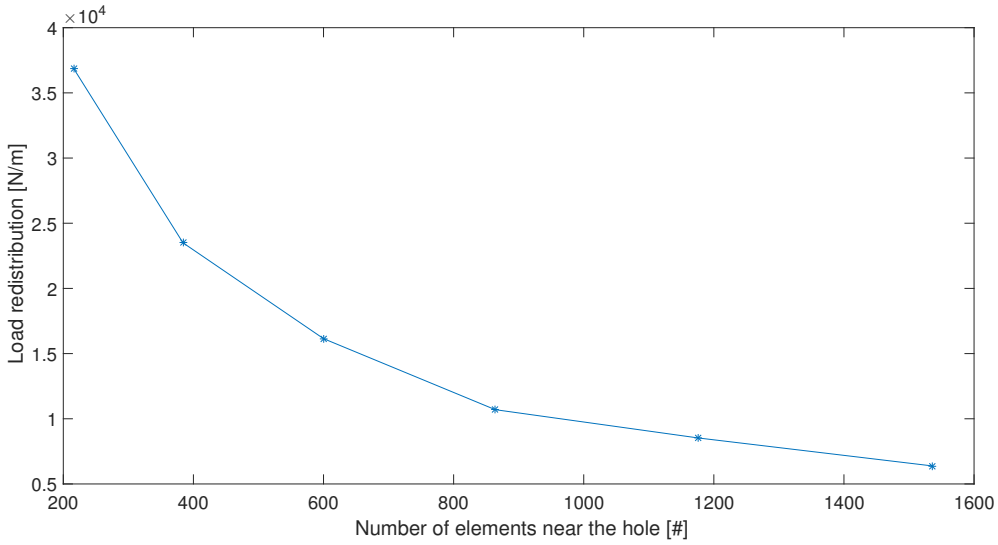

Figure 2.9: Results of stress convergence study

on figure 2.9. Although the plot does not seem very convincing as to prove convergence, there are two reasons which do support that the meshes used are sufficiently small. The first being that the percentage of the total load that gets redistributed gets as low as 0.76%. The second reason is the fact that in the convergence study of the PDA (next paragraph) the finer meshes show clear convergence. Hence, the studied meshes are sufficient for this work.

For the convergence study of the QSPDA, the model with 864 elements in the hole area seems sufficient since the overall stress solution seems to follow the same trend as the finest mesh. Moreover, a more dense mesh will have negative impact on analysis time, especially for the fatigue model to be developed.

QSPDA convergence

The QSPDA is performed on a quasi-isotropic specimen to include the different damage behavior of all ply orientations and to have a correct estimate of the required analysis time. The QSPDA is run on a model utilizing symmetry in the xy-plane and the xz-plane. Symmetry in the yz-plane seemed not to be usable. As has been mentioned earlier, first the mesh refinement is kept constant and the displacement step is varied. The results of this are presented in table 2.2.

The results show that a displacement step of 7.5E-6 is in the converged area and has a reasonable execution time. Choosing a step smaller than this results in a change of less than 2% and doubles the execution time. Mesh effects can now be checked by keeping the displacement step constant. Four additional meshes will be checked, three finer meshes and one rougher mesh. The results are shown in table 2.3. The table shows that the failure stress gradually drops, except for the 1176 mesh, there, a small increase is observed. The 864 mesh seems to be in the converged area, where the error with the finest mesh is 3.3% (which is even lower than the variation observed in experimental tests). When the additional execution time is taken into account, choosing a finer mesh than 864 does not seem logic.

Table 2.2: Results of displacement variation

Disp. Step [m]	Failure stress [MPa]	Change [%]	Execution time [h:mm]
12E-5	588	-	0:13
6E-5	513	-14.6	0:30
3E-5	468	-9.6	0:48
1.5E-5	442	-5.9	1:22
7.5E-6	435	-1.6	1:39
3.75E-6	427	-1.9	4:36
1.875E-6	426	-0.2	9:50

Table 2.3: Mesh refinement results with constant displacement step of 7.5E-6

Elements [#]	Failure stress [MPa]	Change per added element [%]	Execution time [h:mm]
600	473	-	1:19
864	435	-0.033	1:45
1176	439	0.003	2:41
1536	427	-0.008	3:27
1944	425	-0.001	4:35

Finally, failure patterns between the mesh with 864 elements near the hole and the finest mesh (1944 elements) are compared in figures 2.10 and 2.11. Not all plies will be shown here. The plies shown however do give a correct representation of the type of discrepancies found between the two meshes. In general the shape of the damaged area is identical. The coarser mesh is of course a bit more blunt (shown on figure 2.11) and in some cases the type of damage is different (shown on figure 2.11). The most common difference is that of matrix tensile failure (yellow) against no failure for the finer mesh. This might be caused by the coarser mesh not being able to have smooth stress redistributions due to damage. Due to this, additional failure can occur.

To validate the symmetry boundary conditions used, a full version of the model is also run without any symmetry BCs. The result is a failure load of 431 MPa and the damage patterns shown on figure 2.12. Comparing these results with the damage patterns of the symmetrical model shown on figures 2.10a and 2.11a the patterns seem to at least follow the same trends, the full model seems to have less damage. This might be caused by the restraining BCs causing additional stress concentrations. If the execution time of 7:51 is taken into account it seems logic to use the model with symmetry BCs.

2.4.2 Validation

Validation is performed against experimental data available in the literature and too results obtained in the experimental campaign carried out in the present work (chapter 3). The

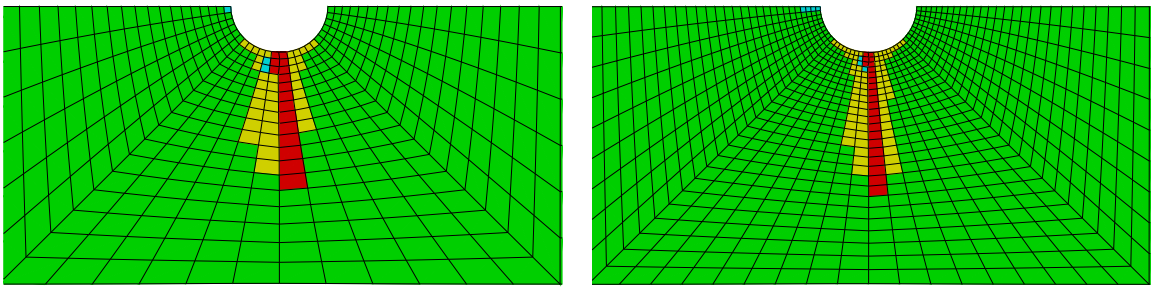

(a) 864E mesh **(b)** 1944E mesh

Figure 2.10: Damage patterns of a ply with orientation of 0° at maximum load (green=no damage, red = tensile FF, yellow = tensile MF, cyan = compression MF and blue = compression FF)

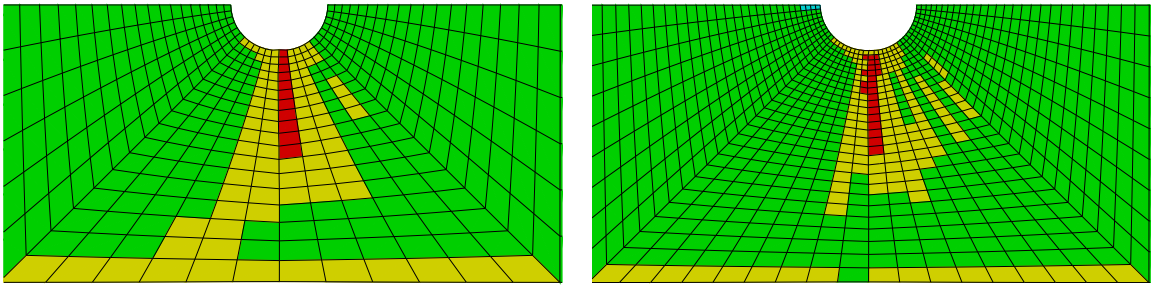

(a) 864E mesh **(b)** 1944E mesh

Figure 2.11: Damage patterns of a ply with orientation of 45° at maximum load (green=no damage, red = tensile FF, yellow = tensile MF, cyan = compression MF and blue = compression FF)

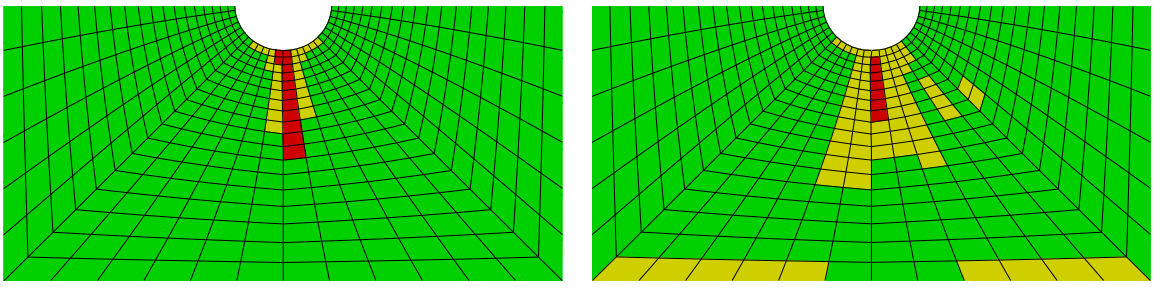

(a) 0 ply **(b)** 45 ply

Figure 2.12: Damage patterns of the model w/o symmetry BCs at maximum load. (green=no damage, red = tensile FF, yellow = tensile MF, cyan = compression MF and blue = compression FF)

Table 2.4: Comparison of IM7/8552 predictions to experimental values

Layup	Predicted strength [MPa]	Experimental mean [MPa]	Error [%]	Exp. CV [%]
QI	435	405	7.4	4.1
Soft	393	301	30.1	2.8
Hard	549	597	-8.0	5.7

validation simulations are run on specimens with geometry as specified by the ASTM standard for OHT tests [54]. Two different materials will be tested and 4 different lay-ups. The found error of residual strength predictions were in the same range as found by Perillo et. al. [52] where the same failure theory was used.

IM7/8552 The first material used in the validation is the IM7/8552 manufactured by Hexcel. Material data is obtained from the report of Marlett [55]. The report has been an effort of NIAR, NCAMP and NASA. Both material data and OHT failure strengths are provided in this report. Non-linear shear-stress strain data are obtained from Kaddour et. al. [56]. This report uses the same material, although slightly different properties were found. The final shear strengths however do coincide, therefore that curve is used without any adjustments. Three different layups were tested, a quasi-isotropic layup, a soft layup consisting of an increased amount of ±45 plies and a hard layup consisting of an increased amount of zero plies, the exact layup is presented as 2.24. The results are presented in table 2.4 where the simulated strength and experimental strength are shown, as well as the error of the prediction between these two. Moreover, the coefficient of variation (CV) observed during experimental testing is shown.

$$\begin{aligned} QI &= [45/0/-45/90]_{2S} \\ Soft &= [\pm 45/0/\pm 45/90/\pm 45/\pm 45]_S \\ Hard &= [0/45/0/90/0/-45/0/45/0/-45]_S \end{aligned} \tag{2.24}$$

In general, the predictions are within 10%, except for the soft laminate. What may be observed is that, as the amount of ±45 plies increases, the overestimation increases. The reason for this might be the factor 0.6 in the sudden degradation of the shear-elastic properties and the fact that if failure has occurred on a particular element, the element will not be checked again for the same failure mode. Due to this, it can occur that the element will carry more load than it should. Another reason for the overestimations can be that delaminations are not considered, although in some cases delaminations might even increase the static strength due to stress relaxations caused by the delaminations.

Finally, the underestimation of the 'hard' laminate might be caused by premature initiation of damage in the simulated model which happens due to the size paradox (will be discussed more in depth in the next paragraph). It has to be noted that the reasons just mentioned are not solely the cause of the discrepancies. For instance, the predicting power of Pucks criterion is already not 100% accurate for UD cases. Second, modeling a crack by dropping stiffness of a whole element will also cause errors in the stress solution.

Table 2.5: Comaprison of AS4/8552 predictions to experimental values

Simulated strength [MPa]	Experimental mean [MPa]	Error [%]	Exp CV [%]
401	384	4.4	4.3

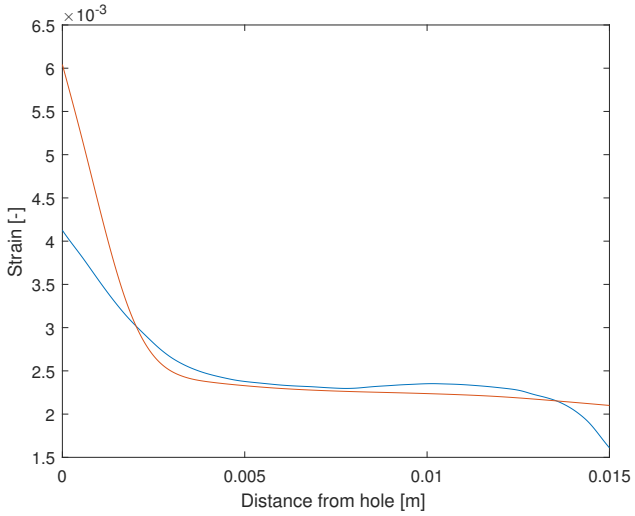

Figure 2.13: Strains observed by DIC (blue) and FEM (red) at 30% of ultimate load

AS4/8552 Validations were also performed on AS4/8552 material by Hexcel. Properties were derived from the experimental tests described in chapter 3. The properties which were not determined in the experimental campaign were taken from the report of Marlett et. al. [55] (all compression strengths). Fiber data was obtained from Kaddour et. al. [56]. Finally, ν_{23} and G_{23} were obtained from Ersoy et. al. [57]. The tested layup was $[\pm 45/0/90]_{2S}$, a quasi-isotropic layup of 16 plies in total. Very good predictions were obtained table 2.5. The same over prediction tendency was obtained as observed on the IM7/8552 material, which can probably be related to the amount of ± 45 plies.

Additionally, DIC was used to track the strain field during testing. It will be used for two types of additional validations. The first of which is comparing numerical strain values observed by the DIC and the strains calculated by the FE model. The location at which the strains are inspected for both methods is the same as the location used for the stress solution convergence and is thus depicted on figure 2.7 with the arrows. The loads at which the strains are compared are 30% and 90% of the experimental ultimate load. The strain which was inspected is ε_{xx} where x is parallel to the loading direction. Since the DIC only sees the outer 45 ply, the same ply is inspected on the FE model. Finally, the results are shown on figures 2.13 and 2.14.

First, the strains at 30% load are discussed. In general, the trend is captured well by the FE model, except near the hole. There, the discrepancies become larger. The reason for this might well be the size paradox, which states that for smaller notches, stress concentrations reduce (should be approx 2 for quasi-isotropic instead of the usual 3 at a notch diameter of 6mm). This happens due to the notch being that small, that there is not enough space for

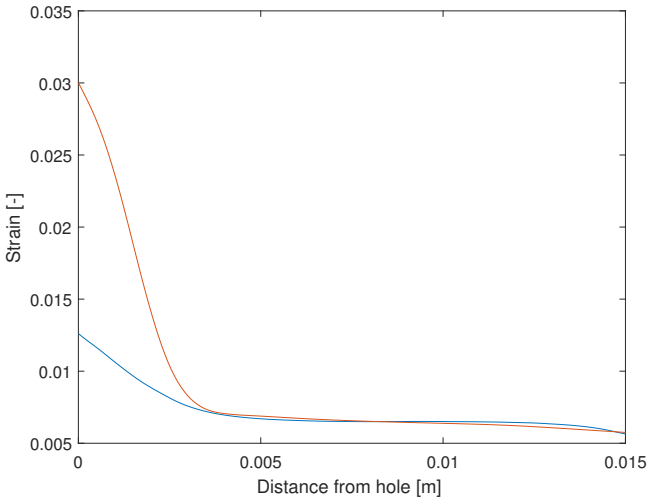

Figure 2.14: Strains at 90% of ultimate load, DIC (blue) and FEM (red)

the stress concentration to build up, the interested reader is referred to papers by Marissen et.al. [58], Waddoups et. al. [59] and Whitney and Nuismer [60] for further information about possible causes of the size paradox and how to model them. However, this effect is currently not thought to be captured (properly) by the FE model and hence a discrepancy occurs. It must be noted however, that the strains observed by the DIC will have an error too. This error may occur due to noise, due to the quality of the speckle pattern and the ability of the program to properly correlate. For instance, near the hole there is no DIC solution (approximately 0.5mm near the hole) the solution is thus extrapolated from that distance to the hole edge.

For the case of 90% load, the strains are as shown on figure 2.14. Here, again the stresses match very well outside of the hole area. This time however the discrepancy near the hole is due to a different reason. The reason is that failures will cause stiffness drops consequently, large strains occur. In the DIC specimen, this stiffness drop will occur at the crack location and will not cause the surrounding strains too increase excessively. This discrepancy is however not expected to cause errors, since the large strains in the FE model are associated to low stiffnesses. The second validation performed is on the strain field, where the observed strain fields of the DIC and the FEM are compared. The strain distribution parallel to the load (ε_{xx}) is shown on figure 2.15. Both figures use the same scale distribution. On the FEM figure, the red marked area exceeds the maximum strain observed by the DIC and the blue area is below the lowest value of the DIC. As these pictures are at a low load, it is thought that the reason for this is the size paradox.

2.4.3 Final remarks on QSPDA model

The final model is depicted on figure 2.16. It consists of 864 elements around the hole for every ply. The elements are of the type C3D8. The right edge has an encastre boundary condition which holds all displacements and rotations equal to zero. The right side has the same BC except that a displacement is applied in the x direction. This initial displacement

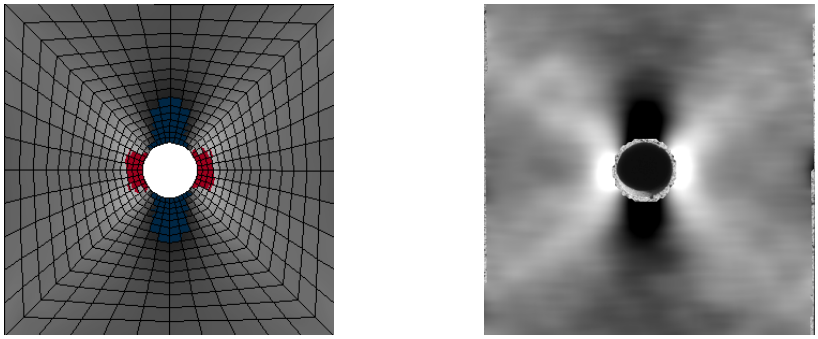

(a) FEM strain distribution **(b)** DIC strain distribution

Figure 2.15: Strain fields parallel to load

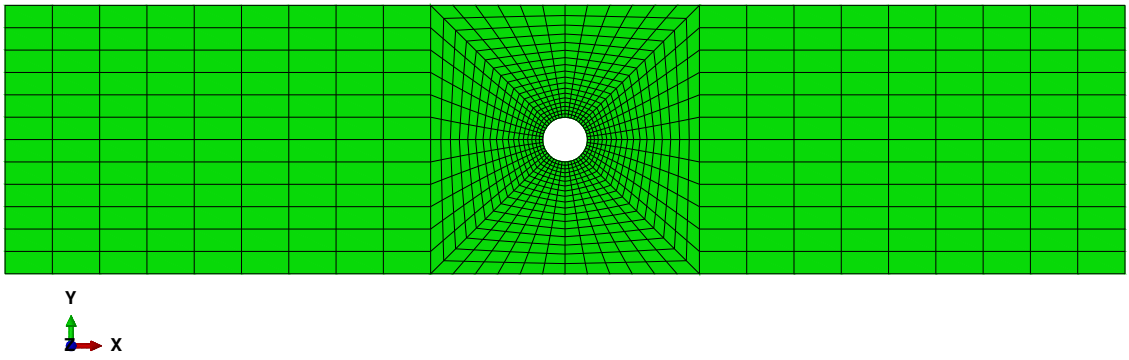

Figure 2.16: Mesh of the full QSPDM

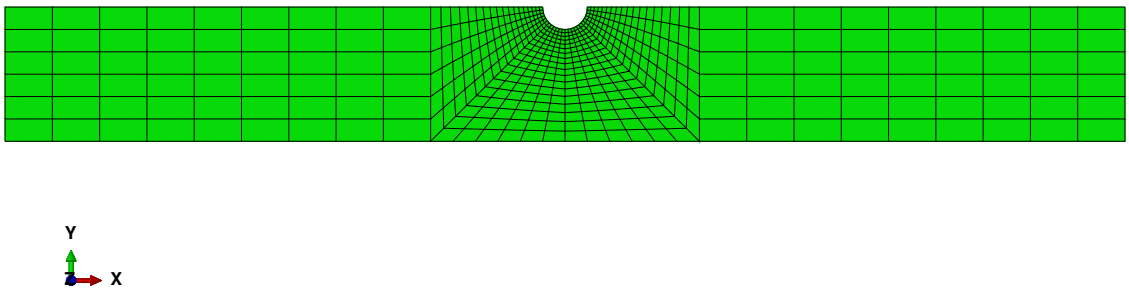

Figure 2.17: Mesh of the symmetry model

is calculated according to the method explained in section 2.2.5 and increases with -7.5E-6 m every increment. The minus sign accounts for the conventions of the FEA package. The most suitable symmetry conditions were found to be that of symmetry in the xz-plane and the xy-plane. This model looks as shown on figure 2.17 and has additional boundary conditions along the upper edge of y=zr=xr=0 and the complete lower side (xy-plane) has the boundary condition z=xr=yr=0, where the 'r' means rotation. It has to be noted that not the complete length of the specimen is modeled, 50mm is left out of the simulation since these 50mm are inside the clamp during the experiment. The encastre boundary conditions is assumed to give a correct representation of this.

As for the quality of the simulation, the stress solution seems to be reasonable when compared to DIC with some exceptions near the hole where peaks might be too high in magnitude. Which will probably cause the damage to initiate too early. The predicted failure loads seem to match quite well, with some discrepancies probably caused by not modeling delaminations, the excessive peaks, degradation rules and the ability of the failure criterion to predict.

Chapter 3

Experimental campaign

An experimental campaign has been performed to collect input data and for validation. The reason to first describe the experimental campaign and then to continue the development of the fatigue model is because the data presented in this chapter will be extensively used in the next chapter 4. Hence, it is good to have an idea where the data comes from, such that the discussions made in the next chapter are better understood. Both UD and MD specimens have been manufactured and tested. The UD specimens were made to determine the statical strengths and the non-linear behavior of the shear stress. The MD specimens are the OHT specimens which are used for fatigue experiments. Specimen geometry and usage are presented in section 3.1. Manufacturing and testing is described in sections 3.2 and 3.3. Results are presented at the end of the chapter in section 3.4.

3.1 Specimens

Four different specimens were made in total. Table 3.1 shows the relevant data of the specimens. All specimen geometries were made according to standards of the ASTM. The applicable standard is denoted below the column 'standard'. The open-hole tension specimens had a centrally located hole with a width to hole ratio of 6.

3.2 Manufacturing

Manufacturing was performed by hand lay-up and autoclave curing. The used material throughout the specimens is the same, although from different batches. Table 3.2 correlates the specimens with the batch used for manufacturing. The base material identification is Hexcel AS4/8552 RC34 AW194, where AS4 refers to the fiber type and 8552 to the resin (matrix). It must be noted that both materials were well over their expiry dates but that they appeared to have good tackiness and as such were thought to be suitable.

Table 3.1: Specimen specifications

Name	Lay-up	Geometry (L*W) [mm]	Standard	Notes
Longitudinal (SL)	$[0]_8$	250*15	D3039-14 [39]	Static
Transverse (ST)	$[90]_{16}$	150*25	D3039-14 [39]	Static
In-plane shear (SIS)	$[\pm 45]_{4S}$	200*25	D3518-13 [61]	Static
SOHT	$[\pm 45/0/90]_{2S}$	200*36	D5766-11 [54]	Static & fatigue. Hole with $d = 6$mm

Table 3.2: Material batches used

Specimen type	Roll Number
$[0]_8$	P1473205H
$[90]_{16}$	P1473205H
$[\pm 45]_{4S}$	TP3261901B
$[\pm 45/0/90]_{2S}$	TP3261901B

3.2.1 Hand lay-up

Lay-up process of the pre-preg was completely performed by hand. After removing the pre-preg form the freezer, it was put to rest for 24 hours, where-after it was cut to size in the clean room. The rest of the lay-up process was also performed in the clean room. The lay-up was build on a flat aluminum mold prepared with release agent. To align the pre-cut layers, the edges which were not cut by hand were used. To create the ±45 plies, a 0/90 ply was layed up on the cutting table with the non-stick foils still attached to the pre-preg (on the outside at least). A square was then cut-out of the 0/90 layup such that the fibers would have angle of ±45 when the rectangle edge is parallel to 0 degrees. After every 2 plies layed up on the mold, degassing was performed by covering the laminates with release foil, peel ply (for ventilation) and vacuum foil. The vacuum was then turned on for approximately 15 minutes. After the final layers were layed up, the laminates were covered with a thin aluminum backing plate covered in release foil. The mold was then covered with peel ply and breather fabric. Where after the final layer of vacuum bag was added on top.

3.2.2 Autoclave cure

The specimens were cured in the autoclave. Unfortunately the in house autoclave broke after the second batch (batch 1 = UD90, batch 2 = UD0). Therefore a different autoclave was used for the final batch (±45 and MD laminates). All batches were cured using an alternative cycle then was proposed by the manufacturer. The reason for this was such that the manufacturing process of the report by Marlett et. al. [55] was matched. This was the main source of input

Figure 3.1: Milled hole in open-hole tension specimen

data used that was not generated by the experimental campaign carried out in this project. The used cure cycle procedure can be found in Appendix A.

3.2.3 Specimen cutting

After curing, the specimens were cut to size using two cutting machines. A diamond saw with laser guidance was used to cut off the rough edges and to prepare the laminates for the second cutting machine, which was a Proth Industrial cutting tool. All tooling was liquid cooled.

3.2.4 Hole milling

For the open hole specimens, the holes were made by a qualified lab technician using the milling technique. The milling head was made from a hardened metal. Figure 3.1 shows the hole on an actual specimen. Every hole was inspected using the eye to check if no delaminations or other damage did occur due to the milling process. In general no damage was found.

3.2.5 Final preparation

The final preparation included measuring, tabbing and painting. The procedures are described in the paragraphs found below.

Measurement of the specimen width was performed at three locations, the upper part, the center and the lower part. Measuring was performed using a caliper with an accuracy of

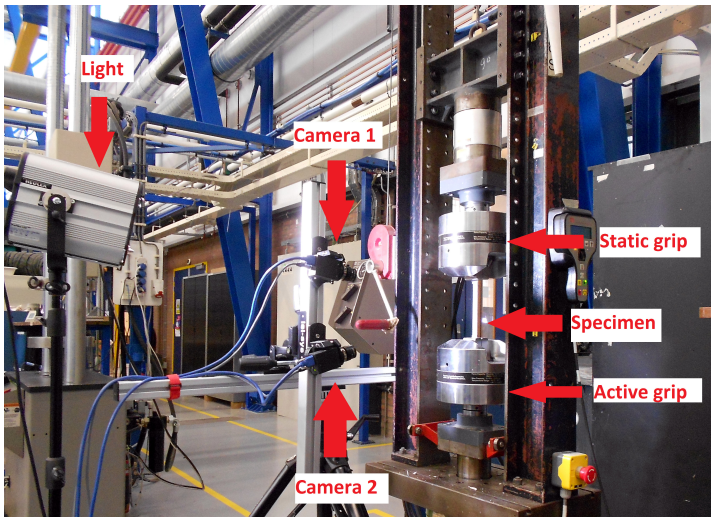

Figure 3.2: Testing setup including DIC

0.01mm. Thickness was measured at six locations. The locations coincide with the measurement of the width, except that it was measured twice, once at every edge (longer edge). Finally the length was measured with a regular ruler. The area of each specimen was calculated as the average of the thicknesses times the average of the widths. In calculating the area of the open-hole specimens, the hole was not taken into account (i.e. area calculation is the same as for rectangular specimens).

Tabs On the longitudinal and transverse specimens, tabs were attached at the clamping locations. The tab material of choice was thick paper and was bonded to the material using superglue. The other specimens did not require the usage of tabs.

Painting The specimens on which DIC was to be performed were painted, on the same day as they were tested to avoid cracks occurring in the paint. The specimens were first painted white, after which a black speckle pattern was sprayed using an airbrush.

3.3 Testing

All testing was performed using the home-made 60kN fatigue machine. The controller software was developed by MTS. The testing setup is depicted on figure 3.2. This setup includes the DIC equipment. Two cameras were used, which made it possible to view out-of-plane displacements. The force is measured at the static grip, while the force is applied at the active (moving) grip.

3.3.1 Static tests

Static testing was performed to obtain strength data (σ_{ult}). The machine was set in displacement control mode and the applied displacement was 2mm/min according to the recommendations in the standard ([39]). Two types of grips were used, type one had a flat surface, type

(a) Grip with rough surface

(b) Grip with smoother surface, arrow indicates alignment tab

Figure 3.3: Fatigue machine grips

Table 3.3: Grips and clamping pressure per specimen

Specimen type	Grip type	Grip pressure [MPa]
$[0]_8$	Flat	1500
$[90]_{16}$	Flat	500
$[\pm 45]_{4s}$	Rough	1000
$[\pm 45/0/90]_{2s}$	Rough	1000

two a rough surface. Both grips are shown on figure 3.3, proper alignment of the specimens was achieved using alignment tabs. While the alignment of the alignment tabs was performed using a specimen and a level indicator. Table 3.3 shows which type of grips were used for which specimens and the clamping pressure used.

3.3.2 Fatigue

The fatigue experiments were performed with a frequency of 10Hz. The experiments were load controlled with a proportional-integral-derivative (PID) as controller. In general, no more than 70 segments at the start of the tests did exceed the 2% error threshold set by the ASTM standard D7615/D7615M.

3.3.3 Digital image correlation

DIC was used to monitor the strains on the specimens. These strains were primarily used to obtain stiffness for the static tests, but were also used to compare against FEA solutions. The used software was the software by Correlated solutions. After calibration, a noise level of approximately 300-500 microstrain was observed. The set-up is shown on figure 3.2.

3.4 Results

From the tests various outputs were recorded. For the static tests, load (N) and strains were recorded.

Table 3.4: Static strength results

Specimen	**Mean [MPa]**	**Std**	**CV [%]**	**No. specimens [#]**
Longitudinal	2237	107	4.76	9
Transverse	70.24	3.24	4.61	11
Transverse (compression)[1]	267.8	6.11	9.47	19
Shear	92.26	1.44	1.57	11
Open-hole	383.96	16.41	4.27	6

3.4.1 Static tests

The data required from the tests were strengths, stiffness and Poisson ratii. These could not be recorded directly from the testing equipment. The testing equipment provided only loads (fatigue machine) and strains (DIC). The strength could be recovered by using equation 3.1.

$$\sigma_{ult} = \frac{F_{max}}{A} \tag{3.1}$$

Where F is the maximum load measured, and A the surface are of the specimen (w*t). For determination of the shear strength, the maximum load was taken before reaching 5% strain and the area was multiplied by 2. Stiffness determination was done using equations 3.2.

$$E = \frac{\Delta\sigma}{\Delta\varepsilon} \tag{3.2}$$

Where E is the stiffness, $\Delta\sigma$ is the change in stress between two strain points and $\Delta\varepsilon$ is the change in strain between these two points. The calculation was performed between 1000 and 3000 microstrain, as recommended by the standard. The average stiffness E_{11} was found to be 131.21 GPa. The average stiffness E_{22} was found to be 8.93 GPa. Shear stiffness was calculated by equation 3.3.

$$G = \frac{\Delta\tau_{12}}{\Delta(\varepsilon_x - \varepsilon_y)} \tag{3.3}$$

The Δ between 2000 micrsotrain and 6000 microstrain were used to calculate the shear stiffness, however in the model mostly the shear stress-strain curve is used. The average shear stiffness G_{12} was determined as 4.98 GPa. Finally, the poisson ratio can be determined by using equation 3.4. The average poisson's ratio ν_{12} was found to be 0.312.

$$\nu = \frac{-\Delta\varepsilon_x}{\Delta\varepsilon_y} \tag{3.4}$$

The obtained data after processing are presented in table 3.4. Where applicable, the testing mode was tension. Additionally the data obtained from the report of Marlett et. al. [55] is shown, since it will be also subjected in the upcoming statistical analysis.

A statistical analysis is performed on the strengths of the UD specimens (and the ±45) using the MIL-HDBK-17 [62] as reference. All assumed fits and raw data can be found in Appendix

[1] Data is obtained from literature, Marlett et. al. [55]

Table 3.5: Observed significance level and fitting coefficients

Specimen	shape α	scale β	OSL [norm/wbl]
Longitudinal	25.89	2283868000	0.2747/0.4855
Transverse	26.15	71713600	0.3364/0.4014
Transverse (compression)[1]	-	-	0.8489/0.1893
Shear	-	-	0.6451/0.6210

B. The type of distribution to fit the data was determined using the Anderson-Darling (AD) test statistic and an observed significance level calculated by using equation 3.5. The AD was calculated using the function *adtest* of Matlab commercial code. Depending on the assumed distribution, the corresponding equation for the observed significance level (OSL) should be used, where OSL is the probability of seeing the same or higher test statistic under the hypothesis that the samples come from the assumed distribution.

$$\begin{aligned} AD^* &= \left(1 + \frac{0.2}{\sqrt{n}}\right) \cdot AD \\ OSL_{wbl} &= 1/\left\{1 + exp\left[-0.1 + 1.24ln(AD^*) + 4.48AD^*\right]\right\} \\ OSL_{norm} &= 1/\left\{1 + exp\left[-0.48 + 0.78ln(AD^*) + 4.58AD^*\right]\right\} \end{aligned} \tag{3.5}$$

Results of the OSL are shown in table 3.5. Where applicable, the coefficients of the Weibull fit are shown. For the cases were the normal distribution is favored, the mean and standard deviation (std) can be read off table 3.4. According to Kassapoglou [6] the fit with the highest OSL is the preferred fitting distribution. It must be noted that when the proposed probability density functions are compared to the experimental histograms (Appendix B), the amount of tested specimens was probably too low to obtain reliable statistical data, whereas the test data of Marlett et. al. [55] whom tested 19 specimens did yield better fits.

3.4.2 Fatigue tests

A total of 18 fatigue experiments have been performed. Most of which were subject to a predefined amount of cycles and tested for residual strength thereafter. The remaining test were conducted until the fatigue life was reached. The experiments have been performed with $R = 0.1$. Constant amplitude (CA) was applied on all specimens. The maximum applied stress σ_{max} was not constant between the different specimens, the value can be read from table 3.6. This table also shows the amount of cycles the specimen has been subjected to and what the failure strength was. Finally the observed damage patterns are denoted and will be discussed now.

Damage pattern Various damage patterns have been observed throughout the fatigue experiments. In general there seemed to be a correlation between the maximum applied stress and the amount of delaminations (higher stress yields more increases delaminations). There

[1] Data is obtained from literature, Marlett et. al. [55]

Table 3.6: Fatigue data

ID **SOHT-**	$\sigma_{max}/\sigma_{ult}$	**cycles (n)**	σ_{res} [**MPa**]	**Damage pattern**
305	0.6	80,000	397	A
601	0.6	80,000	398	A
604	0.6	80,000	391	A
mean	0.6	80,000	395	A
101	0.6	150,000	367	A
502	0.6	150,000	399	A
504	0.6	150,000	398	A
mean	0.6	150,000	388	-
104	0.7	1,000,000	438	A
303	0.7	1,471,809	431	A
505	0.7	3,516,805	461	A
103	0.85	2,367,973	Fatigue life	B
503	0.85	2,337,476	Fatigue life	B
605	0.85	1,464,613	Fatigue life	C
mean	0.85	2,056,675	Fatigue life	-
603	0.9	797,063	Fatigue life	C
406	0.9	458,325	Fatigue life	A/C
202	0.9	219,367	Fatigue life	A/C
mean	0.9	419,585	Fatigue life	-
204	0.9	200,000	426	A/additional delaminations
405	0.9	200,000	444	A/additional delaminations
203	0.9	200,000	433	A/additional delaminations
mean	0.9	200,000	434	-

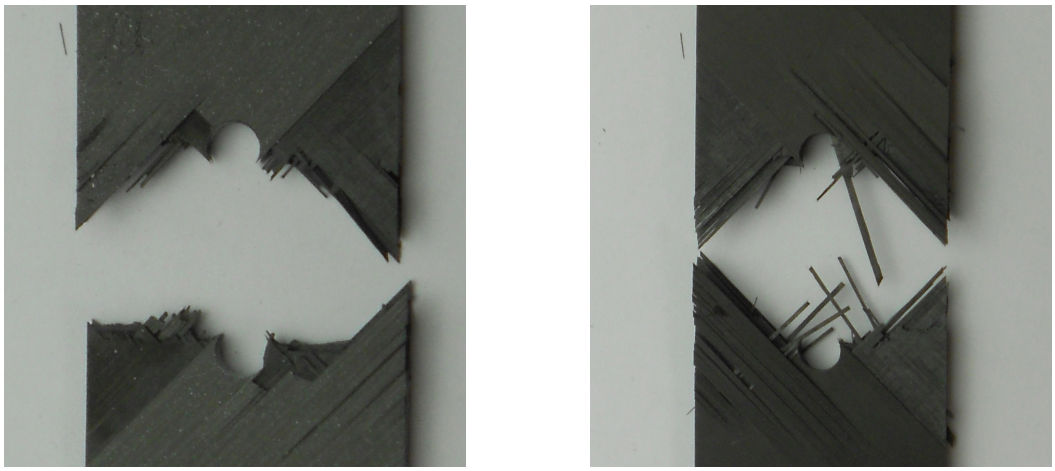

(a) Less delaminations **(b)** Increased delaminations

Figure 3.4: Damage pattern A

has also been observed a correlation between the amount of total fatigue cycles and the the damage pattern. The more cycles the specimen was subjected to, the less the damage pattern looked like the pattern of the static specimen. The damage patterns will be discussed now, in order to understand why and how the specimens failed. In general, damage observable to the naked eye, started as delaminations on the outside edges (not the hole-edges) at the 0/90 interfaces nearest to the mid-plane as soon as 25% of the fatigue life was reached. Delaminations between the 0/90 interfaces farthest from the mid-plane started as soon as 50% of the fatigue life was reached. Other forms of damage could not be observed during the fatigue test due to the motion of the specimen. They were however investigated after failure and will be discussed now.

Damage pattern **A** is the most observed damage pattern and is equal to the damage pattern observed during static testing, except that the fatigue specimens in some cases had an increased amount of delamination damage (in length). The damage pattern is depicted on figure 3.4a and the pattern with increased delaminations on figure 3.4b. The fracture plane is clearly perpendicular to the length of the specimen, although the ±45 plies did protrude. This suggests that the stress concentration has remained around the hole. Although some specimens with this damage pattern did have an increase of strength (compared to the observed mean static strength). The increase of strength might be related to increased delaminations or fiber splitting (of the zero plies) as has been observed by Lagace and Nolet [63] . These delaminations and splits may have reduced, but not diminished the effect of the stress concentration. The observed types of damage are matrix cracking near the hole for the ±45 and 90 plies. The 0 plies suffered from fiber failure. Finally, delaminations occurred at all interfaces.

Damage pattern **B** was observed on specimens which were fatigued up to the fatigue life and had the highest number of cycles of the current experimental campaign. The damage pattern is depicted on figure 3.5. The ±45 and 90 plies all failed near the hole. For the zero plies no clear fracture plane is visible. They failed at random places. This behavior was also observed on the static tests on UD specimens with a fiber orientation of zero degrees. It suggest that at the moment of failure the stress concentration was not affecting the zero plies enough to make the failure initiate at the hole. Compared to damage pattern C, the zero plies did not

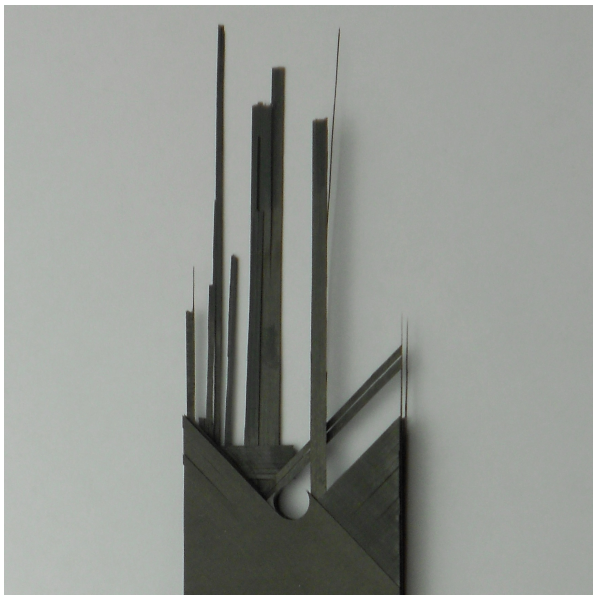

Figure 3.5: Damage pattern B

stay as properly together in pattern B. This might be an indicator that for pattern B an increased amount of delaminations surrounded the zero plies (compared to pattern C) such that the zero plies could fail more explosively. Whereas for pattern C the explosivenesses is damped due to the surrounding plies. This statement is based on observations and reasoning, no conclusions can or should be drawn by this statement.

Damage pattern **C** was observed on specimens which were fatigued up to their fatigue life but had in general lower cycles than specimens with damage pattern B. The pattern is depicted on figure 3.6, the protruding parts are mostly zero plies. The ±45 plies show matrix cracks only near the hole. The 90 plies suffered from matrix cracking along the complete length. On the locations where the zero plies did not remain in place (i.e. no zero plies were visible after failure) the amount of matrix cracks increased as can clearly be seen on the pictures made by the macro-scope. At the hole, the crack in the 90 plies went completely through the width of the specimen. The zero plies did suffer from fiber failures and splits. Interesting about this damage pattern is that the fiber failure was not only observed near the hole, which means that effectively the stress concentration has been reduced at least in some of the zero plies. This has been caused probably by a combination of splitting of zero plies and damage (mainly delaminations) around the plies which reduce the stress concentration. Delaminations occurred between the ±45, 90 interface and the ±45, 0 interface. The later did not occur on the side were the 0 plies were still in place. The cracks and delaminations can be clearly seen on the pictures made with the macro-scope.

Macro-scope investigation Damage pattern C has been investigated using a macro-scope and is shown on figure 3.7. Both sides of the specimen were investigated, the observed location is the thickness plane (i.e. the load runs parallel to the horizontal axis, and the thickness is parallel to the vertical axis). There are two differences which stand out the most. Number one is that the amount of matrix cracks is larger at the side where the 0 plies were pulled

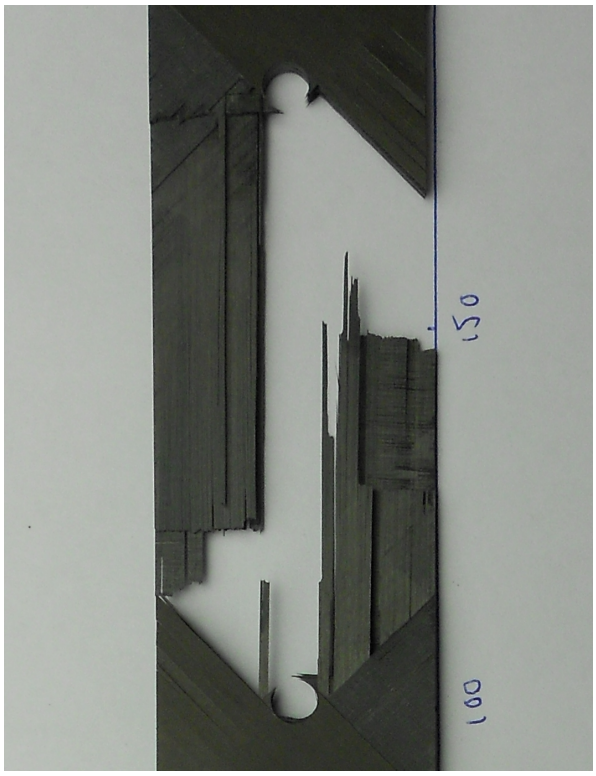

Figure 3.6: Fatigue damage pattern C

out. The second difference is that the amount of delaminations between ±45 and 0 layers is smaller in the case were the 0 plies were not pulled out. Damage modes A and B had similar failure as the ones depicted on the side with 0 plies (i.e. subfigures 3.7c and 3.7d

S-N curve approximation From the experiments at 0.85 and 0.9 load an S-N curve is approximated. According the ASTM D7615 [64] practice, constructing S-N curves for OHT specimens requires data-points for at least three different loads. The third load in this case will be the static strength. In total, between 6-12 specimens are required for constructing S-N curves for preliminary and research purposes. Here, 6 fatigue specimens are used and the mean of 6 static specimens to construct the S-N curve. The S-N curve should constructed according to ASTM standard [65]. The standard advises to use a linear to approximate the S-N curve using equation 3.6.

$$log(N) = A + B \cdot \sigma_{max} \tag{3.6}$$

After fitting using this equation and testing for the hypothesis of linearity, linearity was rejected. The standard then advises to adopt a fit using equation 3.7.

$$log(N) = A + B \cdot \sigma_{max} + C \cdot \sigma_{max}^2 \tag{3.7}$$

Matlab commercial code was used to compute the coefficients. The upper bound of coefficient C and B were restricted to 0 such that erroneous results would be avoided (if no restriction is applied the S-N curve can increase at high σ_{max}). The obtained coefficients were $A = 52.79$, $B = -1.418e-8$ and $C = -0.000347$. The result, including 95% confidence bands is depicted

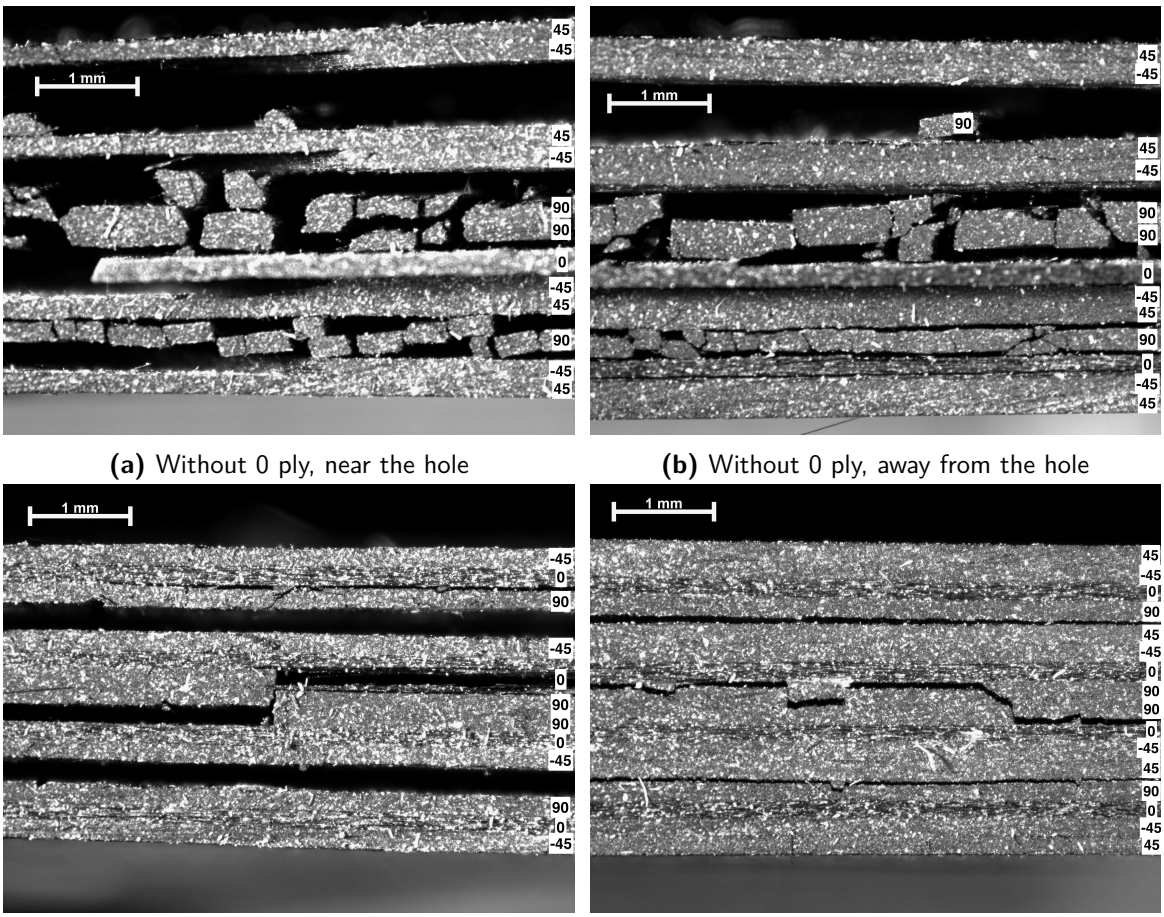

(a) Without 0 ply, near the hole

(b) Without 0 ply, away from the hole

(c) With 0 ply, near the hole

(d) With 0 ply, away from hole

Figure 3.7: Macro-scope damage patterns

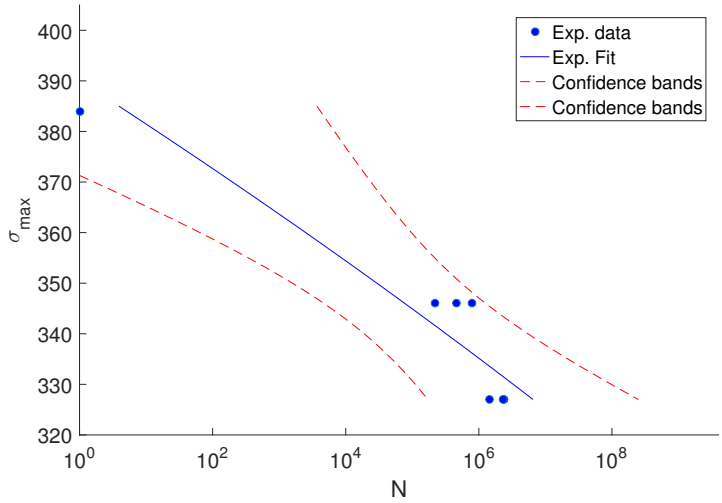

Figure 3.8: Experimental S-N curve of OHT specimen with 95% confidence bands

on figure 3.8. The fit still is almost linear. More experimental data is needed to create a better approximation.

Chapter 4

A framework to model fatigue using cycle-jumping

4.1 Introduction

In this chapter, a fatigue model is developed which can be used for simulation of tension-tension or compression-compression fatigue experiments with CA under any layup, R, σ_{max} and n. The model is based on the principle of using a macroscopic damage law and a degradation law in order to model the progression of damage. Furthermore, a stress analysis module is used in order to assess the state of the structure after failure events occur. These three parts are brought together using a newly developed cycle-jumping algorithm.

For the sake of clarity, a short summary of what is already available and what is still to be done will be presented by using a general fatigue experiment as guidance. The experiment is depicted on figure 4.1. This is a typical tension-tension experiment with $0 < R < 1$ and a quasi-static test for residual strength after n_f cycles.

In chapter 2, a QSPDA model has been build. As presented in the previously mentioned chapter, the model is able to simulate a static tensile test from zero load to the final failure load. By simple adjustments, the model will be able to determine the damage state of the specimen for a predefined load level. How to do this will be described in section 4.2. For the discussion, this new QSPDA will be called QSPDA2. Suppose now that a fatigue test is to be performed which looks like the one depicted on figure 4.1. Using QSPDA2, the damage state can be assessed up to the point of the arrow.

If now CA cycling is applied at that load, no more failures will be predicted. This behavior can be related to the fact that the macroscopic failure criterion relies on the inputs of stresses and strengths, both of which will remain constant with the model developed so far.

For this reason, a degradation model is required. The degradation model will associate damage created at scales below the macroscopic level, to parameters used by the macroscopic model (QSPDA2). By doing this failure events as depicted on figure 4.1 (with red dots) will now be predicted by the macroscopic criterion.

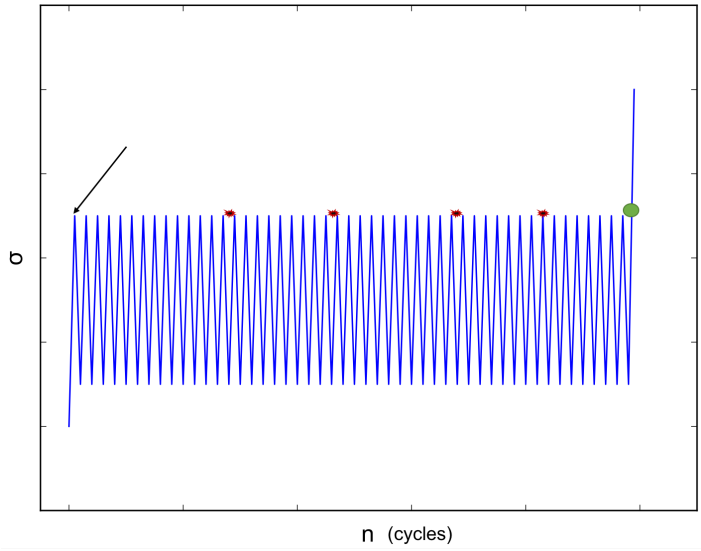

Figure 4.1: Typical fatigue experiment with determination of residual strength after fatigue loading.

In this chapter, a clear distinction will be made between damage and degradation. Damage refers to the macroscopic criterion (Puck) and degradation refers to the law which degrades the input of Puck's criterion as a function of cycles. With the currently used failure criteria (Puck) by QSPDA2, stiffness and/or strength degradation are an option. In the current work, only strength degradation is considered, because the stiffness degradation rules require additional experimental and computational effort. The degradation theory used in this work is presented in section 4.3. What has to be emphasized is that the degradation will be performed on the element level, since the degradation law implemented is a function of stresses and stresses are obtained at the element level.

What remains to be done, is to find a relation between macroscopic failure and the degradation as a function of applied cycles. In that way, a cycle-jumping algorithm can be developed. The cycle-jumping algorithm is a critical part in the fatigue model to be developed. There are two reasons for this. Firstly, cycle-jumps are required such that stress solutions (by FEM) can be omitted, this is required since a single cycle requires approximately 30 seconds to be evaluated using the current model. With the maximum of 24 hours of running time set by the project initiators, a maximum of 2880 cycles can be simulated. If one then considers that fatigue critical designs are often in the range of 1E6 cycles, the model becomes unfeasible.

The second reason for developing the new cycle-jumping algorithm, is that it will be based on some assumptions in order to find the cycles to be jumped instead of requiring the user to input an interval as is the common way for the models reviewed in chapter 1. An additional feature of the algorithm will be the use of a numerical root finding method in order to avoid the cumbersome process of applying strength degradation and macroscopic failure assessment on a cycle-by-cycle basis.

The complete fatigue model, including the cycle-jumping algorithm, will be described in section 4.2 using a flow-chart of the model as guidance. For the quasi-static parts i.e. the initial ramp and final ramp an adapted version of the model developed in chapter 2 will

be used. A new algorithm based on the relation between macroscopic damage and a cyclic degradation is developed for the model, which finds the cycles that can be omitted from the FEM analysis. By doing this, the largest possible amount of cycles that have to be analyzed with FEM equals the amount of elements that have to fail such that final failure occurs, section 4.2. The strength degradation theory and determination of S-N curves proposed by Kassapoglou [38, 66, 67] are then implemented in the model, section 4.3. The model with the implemented strength degradation theory is then compared to experimental results to find areas where the models perform well and where there is room for improvement, section 4.4.

4.2 Model development

In this section, the complete fatigue model will be developed in its most general form, including the new cycle-jumping algorithm. The only thing that will have to be done for the model to be able to run, is the implementation of the chosen degradation theory, section 4.3.6. The description of the model will follow the flow-chart of the model, figure 4.2. The variables which will be used in this section are n_f, which is the cycle up to which the specimen has to be fatigued. The variable n_j is the amount of cycles found by the cycle-jumping algorithm which can be jumped, i.e. which do not require an additional stress solution by FEM. The model will be developed on the basis of one main assumption. This assumption is that FEM stress solutions are only needed if the macroscopic failure criteria detect a failure. Stress distributions due to fatigue induced degradation of stiffness may be accounted for by the stiffness degradation law used (which in this work is not considered at all).

The description will start with the adjustment of the QSPDA to QSPDA2, section 4.2.1. Where after the different stages of the cycle-jumping algorithm are described in sections 4.2.2, 4.2.3 and 4.2.4. The fatigue life criterion is discussed in section 4.2.5 which stops the analysis if the fatigue life is reached. Finally, the residual strength determination of the specimen after fatigue is described in section 4.2.6.

4.2.1 Determine macroscopic state after loading up to peak fatigue load

In order to perform the fatigue analysis, the initial macroscopic damage state of the specimen has to be determined. This initial damage happens due to the initial ramp to the peak fatigue load (first peak on figure 4.1). It is identical to a static tensile test, except that the specimen is loaded up to a predefined load (σ_{max}) and not up to failure. Hence, the QSPDA developed in chapter 2 is used with a slight modification (QSPDA2). Just before the reaction load reaches the predefined σ_{max}, the analysis is changed to load control instead of displacement control to match the experimental setup. The analysis is then run at load σ_{max} as many times required, such that no more elements will fail due to the stress redistributions. This seems contrary to the assumption made in chapter 2, where the analysis is not repeated to account for stress redistributions. However, in this case it is assumed that the elements that fail due to stress redistributions will have failed before reaching the first fatigue cycle (i.e. first peak after the peak depicted by the arrow on figure 4.1).

The assumption may be supported by the following example. Suppose the analysis has just reached load σ_{max}. At this point some elements fail, which cause a stress redistribution. In

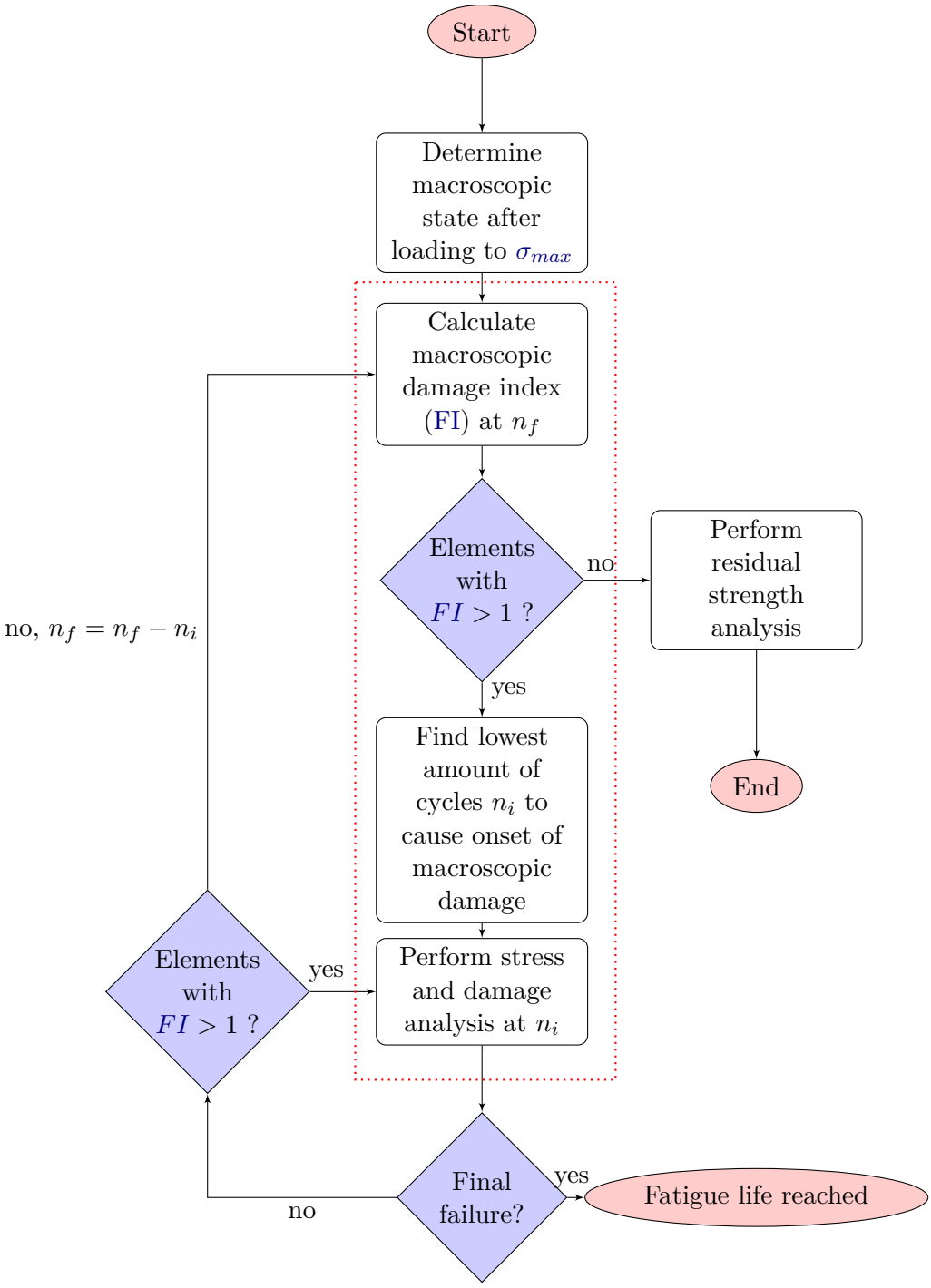

Figure 4.2: Flow-chart of fatigue model

chapter 2, the assumption was made that this stress redistribution can not happen instantaneously and thus failure due to stress distributions will not be considered before moving on. However, there are two remarks that invalidate the instantaneous nature of the experiment under investigation. Firstly, during a load controlled experiment, the applied load is regulated by a controller which can not be instantaneous. If the controller is however faster than the stress redistribution (implying not all elements have failed at the first peak), the elements will fail prior to reaching the first fatigue cycle (second peak). The reason for this is that by going from the first peak to the second peak some degradation will occur which will make the elements more critical and let them fail before reaching the peak fatigue stress. Hence, for reducing complexity it is assumed that all stress redistributions will occur at the first peak.

The output of the currently discussed block will be:

- Stress (obtained by FEM) state of every element
- ECs state of every element
- Failure state of every element

4.2.2 Calculate macroscopic damage index (FI) at cycle n_f

The cycle jumping algorithm starts at this block and includes all blocks contained by the red rectangle on the flow-chart 4.2. It has to be found now if for the requested amount of cycles, n_f, there are elements which will fail. This is done by temporarily updating the element properties with n_f cycles. This is done by utilizing the degradation model (section 4.3.1). The degradation model will be able to use the most current stress solution at the elements in order to determine the magnitude of the degradation. After that, the macroscopic damage state will be determined for every element. It has to be noted that the failure state of the element will determine to what extent the current damage analysis is conducted (if element is in MF state only FF is considered, if FF no damage analysis is performed). If now after the damage analysis no elements fail, the temporarily update properties are saved and the model state is exported to section 4.2.6. In the other case, where there are failed elements found, the elements are flagged and section 4.2.3 is triggered. The outputs of this block are concisely shown below:

- Identification number(s) of flagged element(s) (if element failures are found)
- Updated material ECs determined from degradation model (if no element failures were found)

4.2.3 Find lowest amount of cycles to cause onset of macroscopic damage

For the flagged elements of the previous analysis (block), the cycles to failure initiation will be determined. In a most simple form, this procedure can be done by simply applying the degradation followed by macroscopic damage analysis on a cycle-by-cycle basis. However this is not an efficient way. Instead, use will be made of a so called root finding algorithm. To use such an algorithm, it has to be realized that the macroscopic damage function will

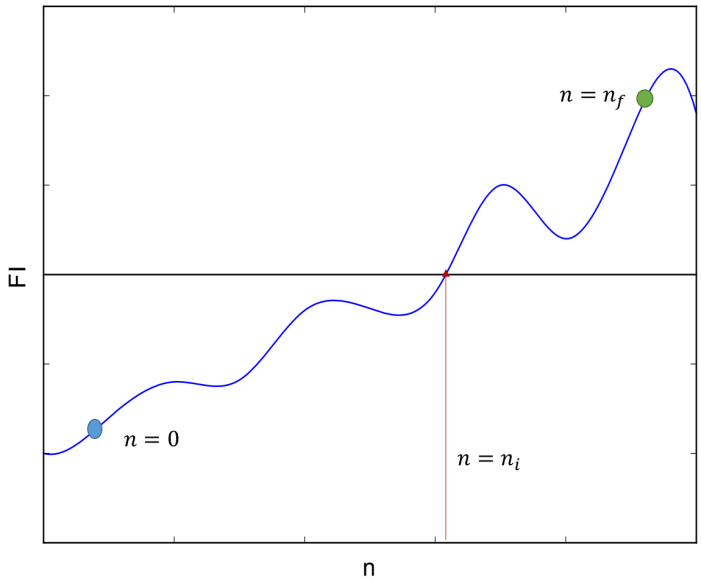

Figure 4.3: Arbitrary macroscopic damage function as a function of degradation (which is a function of n)

be a function of the degradation function and the degradation will be a function of fatigue cycles. Hence, what has to be found now is the number of fatigue cycles n which will cause macroscopic damage. In general, damage functions predict the onset of damage when the threshold of 1 is reached. Since a root finding algorithm is to be used, the damage function has to be forced to go to zero at the onset of damage (i.e. subtract 1). The user is however free to change this value if another threshold is to be used. The proposed root finding method here is the method by Brent [68]. As input, the method requires two points, one where no damage has happened and one where the threshold has been exceeded. Fortunately, these locations are already known. The lower bound is $n = 0$ and the upper bound equals $n = n_f$ and are shown on figure 4.3. By giving these two boundaries the algorithm can proceed and find the amount of cycles n_i for every flagged element which will cause failure. Output of this block is:

- The minimum of the found n_i

Brent's method Is a numerical root finding algorithm with guaranteed convergence for finding a zero given a function f on an interval [c,b] where $f(c)$ has a different sign then $f(b)$. There are no further restrictions on f for the algorithm to work. The method is a modification too Dekker's method [69]. It combines the use of inverse quadratic interpolation, secant method and regular bisection. It differs too Dekker's method because it ensures that additional bisections are performed by implementing tests on the result of the secant method before using it for the next iterate. Finally, in the current implementation, it is assumed that failure index will be only increasing or constant as a function of cycles. This is required for two reasons, the first which is that if the FI can be decreasing, it can happen that the method in section 4.2.2 will not flag the element as critical since it is possible that at cycle n_f the element FI will be below the threshold, whereas before n_f the FI could be above the

threshold. Second, if the FI can be decreasing it is also possible that the FI can have more than one zeros (if the critical threshold is forced to be the zero). Hence, it can occur that the root finding algorithm will return the wrong root (i.e. not the one with the lowest cycles). The assumption that the FI is indeed only decreasing and/or constant may be justified by the following reasoning. Since the stresses are assumed to remain constant between cycle jumps, the only variables that will change as a function of cycles are the strengths (due to degradation). These strengths are a function of cycles and will always be decreasing as a function of cycles. Hence, it is not likely to obtain lower failure indexes if the strengths decrease.

4.2.4 Stress analysis and failure analysis at damage initiation cycle

With the cycles to jump n_i determined in section 4.2.3 the analysis is continued by firstly degrading all elements with n_i cycles. The damage analysis runs and the failed elements will be degraded according to the sudden degradation rules. A stress analysis is then performed to obtain the stress redistribution due to the failed element(s). This stress analysis is performed at the cycle peak. The reason for this will be given by means of an example. Lets assume that element x is at cycle n_1. At this cycle the damage threshold has not yet been exceeded. At the next cycle however ($n_2 = n_1 + 1$) the element has exceeded the damage threshold. This implies that the failure happens at a lower stress than the peak stress of that cycle (n_2) since the damage threshold was calculated at the peak stress. It could be argued then that the stress analysis has to be performed at a stress lower than the cycle peak. However the cycle will not have been completed at this lower stress and thus, it can not be said if the strength will have been degraded enough, such that failure occurs before the cycle peak. By the failure of the fatigued elements, the stress redistribution may cause other elements to fail too. The stress and failure analysis is repeated until no more failure occurs under the same assumption as in section 4.2.1, where the elements would have to be failed before reaching the new cycle. Outputs of this block will be:

- Updated stress solution at every element
- Updated element state
- Updated ECs i.e. degraded up to cycle n_i

4.2.5 Fatigue life criterion

In order to stop the analysis if the fatigue life has been reached, a check has been built in. This check compares the initial displacement (at the first fatigue cycle) to the current displacement. If the ratio $\frac{u_i}{u_c}$ exceeds 0.75 the analysis is stopped. The ratio of 0.75 will not always be correct, especially for very high fatigue loads it may be too small. In general however the ratio yielded satisfactory results. Changing the ratio should be performed by trial and error in order to judge correctly if the fatigue life has been reached. The correctness of the ratio can be verified by looking at the damage pattern. Output of this block will be:

- Fatigue life (N)

4.2.6 Perform residual strength analysis

When the amount of cycles n_f has been reached, a normal QSPDA is performed according to the procedure described in chapter 2, except that the first increment will be the displacement of the most current iterate. Moreover, the most recent element state will be adopted (such that the damage due to fatigue is captured) and degradation of the macroscopic damage parameters up to cycle n_f. Final output will be:

- Residual strength after cyclic loading up to cycle n_f

4.2.7 Remarks on cycle jumping algorithm

The description of the fatigue modeling process and its cycle jumping have now been completed. Some remarks should be made such that one can asses if it is a feasible to use the proposed approach. The advantage of the model lies in the reduction of FEM stress solutions by assuming that no FEM stress solutions will be required in between macroscopic failure events. Nevertheless, the user is free to make the degradation procedure call some additional FEM stress solutions if required. The second advantage is the way in which it can find the cycles to be jumped. It is built with the philosophy of reducing damage and degradation function evaluations. There are some limitations however in the choice of damage and degradation laws. The first limitation is that the combination of damage and degradation law should produce only one root in between cycle jumps such that Brent's method is guaranteed to find the correct root. Second limitation is that degradation has to be calculable in one function evaluation for any amount of cycles n. If this is not possible, it is not efficient to perform the operations of section 4.2.2 because n_f function evaluations will be required for every element.

If one of the two limitations is not met, the calculation of n_i should be done on a cycle-by-cycle basis.

4.3 Implementation of a degradation theory

As has been mentioned already, in the present work only strength degradation will be considered explicitly. The assumption of only using strength degradation might be justified with the following reasoning. In general, loss of stiffness is the cause of damage. It is now postulated that this damage will occur as fiber failure (FF) or matrix failure (MF) solely. Any other types of damages will be assumed to not cause stiffness loss. Then, if the discretization is sufficiently small, the loss of stiffness will be captured implicitly by the sudden degradation rules presented in chapter **??**. What is sufficient will have to be determined using experimental or numerical simulations. In the present work the convergence study performed in chapter 2 and is assumed to cover the numerical part.

The strength degradation theory of choice is the theory by Kassapoglou presented originally in his PhD thesis [5]. It is comparable to the strength degradation theory by Broutman and Sahu [36] which is one of the recommended theories by Philippidis and Passipoularidis [10], especially if low experimental effort is required. It has to be noted here, that the strength

degradation theory by Kassapoglou was not yet developed at the time of publication of the paper by Philippidis and Passipoularidis [10] and thus was not taken into account by them. Both strength degradation theories require as input the fatigue life (N). Since the fatigue life determination from Kassapoglou is used, it seemed logical to use his strength degradation theory. This section will start with the description of the strength degradation theory 4.3.1.

Due to stress distributions, the element will feel a variable amplitude loading. Therefore a theory proposed by Kassapoglou [66] will be used to account for this in section 4.3.2.

Two methods will be presented by which the required S-N curves can be obtained. The methods are described in section 4.3.3, 4.3.5. An attempt is also made to find a way to transform the obtained S-N curves such that they can be used for different R-ratios in section 4.3.4. Finally, the implementation considerations are discussed in section 4.3.6.

4.3.1 Non-linear strength degradation theory

A short summary will be given here which covers the assumptions made for the determination of the strength degradation theory. For the full derivation, the reader is referred to the PhD thesis of Kassapoglou [5] (chapter 2). The theory is based on the relation 4.1.

$$\Delta\sigma_{res} = (A\sigma_{res} + B)\,\Delta n \tag{4.1}$$

This equation states that the change of residual strength ($\Delta\sigma_{res}$) after an amount of cycles (Δn) with constant amplitude loading will be a function of some constant (B) and another constant (A) times the state of the structure (current residual strength σ_{res}) before cycling. To solve this equation for the residual strength (σ_{res}), three boundary conditions are required, such that three unknowns can be solved for. The third unknown occurs in the process of solving the derivatives. These assumptions are that at $n = 0$ the strength will equal the pristine strength (σ_{fs}). One cycle before reaching the fatigue life ($n = N$) the residual strength will equal the applied stress (σ). Since the applied stress should exceed the residual strength at N because the structure will have to fail at the N-th cycle. The last assumption will be that the structure has an endurance limit (σ_E). A stress below the endurance limit will never lead to failure. This endurance limit however will be set to zero after the solution has been found. The equation for residual strength then becomes equation 4.2.

$$\sigma_{res} = \sigma^{\frac{n}{N-1}} \sigma_{fs}^{\frac{N-n-1}{N-1}} \tag{4.2}$$

4.3.2 Accounting for spectrum loading

In between a cycle jump, the cyclic load will be of CA, this will also hold on the element level. However, due to to progressing damage, at the element level the cyclic loading will be of variable amplitude (VA) between cycle jump*s*. Notice the subtle difference of CA *in between* a cycle *jump* and VA *between* cycle *jumps*. The cause of this variable amplitude is progressing damage causing stress redistributions, which will change the stress at every element from cycle jump to cycle jump.

The approach to account for VA relies on a slightly modified version of the residual strength equation previously presented, equation 4.3.

$$\sigma_{rm} = \sigma_m^{\frac{n_m+N_{mu}}{N_m-1}} \sigma_{fs}^{\frac{N_m-(N_{mu}-n_m)-1}{N_m-1}} \tag{4.3}$$

Where the subscript m refers to variables of the current investigated loading (block). The newly introduced variable N_{mu} is the cycles required at the current loading to reach the residual strength of the previous block. To find this new value equation 4.4 is used. For the complete derivation, the user is referred to Kassapoglou [66].

$$N_{mu} = \frac{(N_m - 1)}{ln(N_m)} \left[\sum_{i=1}^{m-1} \frac{n_i}{N_i - 1} ln(N_i) \right] \tag{4.4}$$

4.3.3 S-N curve determination by statistical strength distribution

To use the equation presented in the previous section (4.3.1), a value has to be found for the fatigue life (N). In this report, S-N curves will be constructed for every strength, and will be a function of stress ratio only. If a conventional approach is to be used to determine these S-N curves, the ASTM suggest 12 fatigue test to be conducted for all required S-N curves (i.e. 60 fatigue experiments in total). Therefore, instead an approach proposed by Kassapoglou [5] is used in this exercise in which the S-N curves can be constructed by making use of the statistical strength distribution and the residual strength equation derived in the previous section. For the complete derivation, the reader is referred to the actual PhD thesis [5].

Here, a concise derivation will be given such that the basic approach, its assumptions and implications will be understood. For the current work, where the R ratio of 0.1 is used, it suffices to assume that the static strength distribution will be a two parameter Weibull distribution (see section 4.3.4). If in equation 4.2 now σ_{fs} is a two parameter Weibull distribution, it can be shown (see ref. [5]) that the residual strength will be also a two parameter Weibull distribution with new shape and scale parameters. It can be shown however, that if one would like to obtain the CDF of this new distribution, it will be given by equation 4.5 with the shape and scale parameters of the original static strength distribution (derivation in [5]).

$$p = 1 - e^{-\left(\frac{\sigma}{\beta}\right)^{\alpha}} \tag{4.5}$$

This equation gives for an applied load σ the probability that the strength is lower or equal to this applied load (i.e. probability of failure). For constant p, the probability of failure between 1 and n cycles is then given by equation 4.6.

$$P = np(1-p)^{n-1} \tag{4.6}$$

Taking the derivative of equation 4.6, setting it equal to zero and solving for n gives the cycles at which the probability will be the largest that the structure will have failed (equation 4.7). This n will be used as the fatigue life N.

$$N = -\frac{1}{ln(1-p)} \tag{4.7}$$

If now equation 4.5 is substituted into equation 4.7, simplified and rearranged, a closed form expression is obtained which can be used to draw a S-N curve, equation 4.8.

$$\sigma = \frac{\beta}{N^{\frac{1}{\alpha}}} \tag{4.8}$$

This equation gives the S-N curve for $R = 0$. For different R-ratios, new shape and scale parameters have to be derived according to the methodology described in 4.3.4

4.3.4 Considerations for different R-ratios

The aforementioned equations in section 4.3.3 are derived assuming that the applied ratio is either ∞ or 0. This is however difficult to apply in an experimental setup since it is possible for the machine to go into compression for some cycles due to the accuracy of the control equipment. For this reason, but also for generality, introduction of the R-ratio effects are required. To do such a transformation, first the requirements have to be understood. The equations derived up to here require the statistical distribution of some test starting from 0 up to the failure strength. In order to include the effect of non-zero R ratio, a statistical distribution should be obtained for the 'imaginary' test case where the test is started at a load $\sigma_{ult} \cdot R$ and ended at the load σ_{ult}, which is the failure load for this particular test. Two problems arise (which is the reason for calling it 'imaginary'), a test cannot be conducted from some non-zero load ($\sigma_{ult} \cdot R$), without first applying a load from zero up to that non-zero load $\sigma_{ult} \cdot R$. Second, you cannot a priori determine the true failure load σ_{ult} of the specimen such that you can determine at what load to start. Hence, a way has to be found to create such data.

To do this, the original obtained distribution from the static tests will be changed according to the following methodology and assumptions. Starting by assuming that the 99th percentile will remain constant after the transformation i.e. the point after which 1 percent of the strongest specimens are contained remains the same. The reason for this will be that since these specimens are the strongest they will be assumed to be near perfect. Perfect means that there will be no flaws caused in the manufacturing process (voids, resin rich, resin poor etc) or during the specimen insertion into the testing machine (delaminations caused by impact, scratches etc). Testing errors will be neglected for now (i.e. misalignments, measuring errors etc). Hence, their failure load will be constant and cannot change due to starting from a non-zero load. One can argue that the strongest specimens might also be due to flaws, however a flaw in a simple rectangular specimen will always cause some type of stress gradient, reducing the failure load. It seems therefore unlikely that there will be a specimen which is stronger than the specimen which has no imperfections. Specimens below this 99th percentile will have defects. Where the influence (on ultimate strength) of defects increases up to the 1st percentile and below the 1st percentile the effects are expected to be constant due to the severity of the defects. For the purposes of this work, the damaging effect of the defects contained between the 1st and 99th percentile, will be assumed to be translatable at the 1st percentile such that the 1st percentile might be moved to a new location $x_1 + R(x_2 - x_1)$ the procedure is depicted on figure 4.4. Implicitly, the effect of R-ratio reduces with increasing strength. This transformation is not based on any physical principle, but rather is a first approximation since there is no further information available.

The assumption might be justified by remembering that the effects of this transformation apply on the scale for which no physical models are available (at least for the scales considered in this work), hence such first order assumptions seem reasonable for this case. In order to compute now the new distributions, the 1st and 99th percentile values have to be calculated which will be represented by x_1 and x_2 respectively. The new x_1 will be denoted as x_1^n and is obtained by equation 4.9.

$$x_1^n = x_1 + R \cdot (x_2 - x_1) \tag{4.9}$$

No matter what the type of the starting distribution is, the newly to be found distribution will be a two parameter Weibull distribution, since for example for a normal distribution

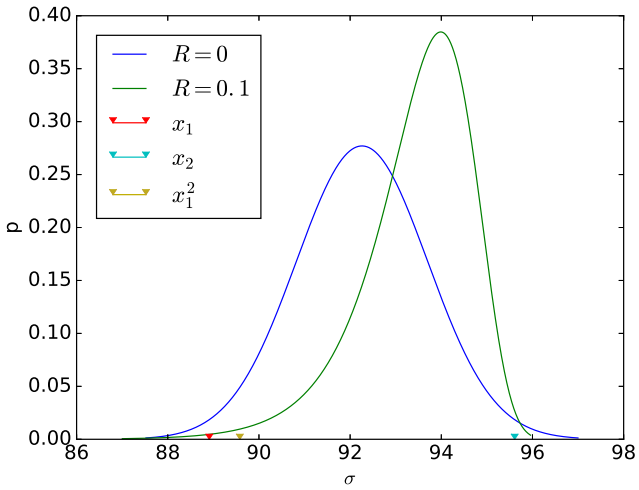

Figure 4.4: Calculation of new 1st percentile location

Table 4.1: Distribution transformations for $R = 0.1$

Strength	α [-]	β[Pa]	**Mean [MPa]**
X_t	29.1283603358	2298920873.34	2255.96
Y_t	29.4189891578	72181003.79	70.84
Y_c	64.3790965593	275490609.813	273.09
S	98.2918365726	93997652.7531	93.46

it is impossible to change x_1 and keep x_2 constant. Moreover, the MIL handbook advises to use a Weibull distribution due to being better compatible with the brittle fracture of composites [62]. The parameters are found by using equations 4.10

$$\begin{aligned} Q &= \frac{log(-log(0.99))}{log(-log((0.01))} \\ \beta^n &= \left[\frac{x_1^n}{x_2^Q}\right]^{\frac{1}{1-Q}} \\ \alpha^n &= \frac{log(-log(0.99))}{log(x_1^n/\beta^n)} \end{aligned} \tag{4.10}$$

It must be mentioned here that the transformations applied here are strongly inspired by the methods presented by Kassapoglou with subtle changes in the determination of x_1. The change was performed such that the reasoning just discussed can be applicable. Applying these transformations to the experimental data presented in chapter 3 for $R = 0.1$, two parameter Weibull distributions are obtained with the shape (α) and scale (β) parameters as shown in table 4.1. With the determination of the new distributions, new mean values are derived, which, if used, will introduce a small error at low cycles. However, since the simulations run in this work are mostly high cycles, the choice was made to use the new mean values for the residual strength determination. Finally the S-N curve determination of section 4.3.3 and the R-transformation of this section is applied on the statical strength data

of Marlett [55] for which the mean strength is comparable to that of Justo et. al. [70]. Both sources used the same 'AS4/8552' material. The two obtained S-N curves coincide very well, which suggest that the described method can be usable, at least as a first approximation. The results are depicted on figure 4.5. It has to be noted here that it was not possible to validate

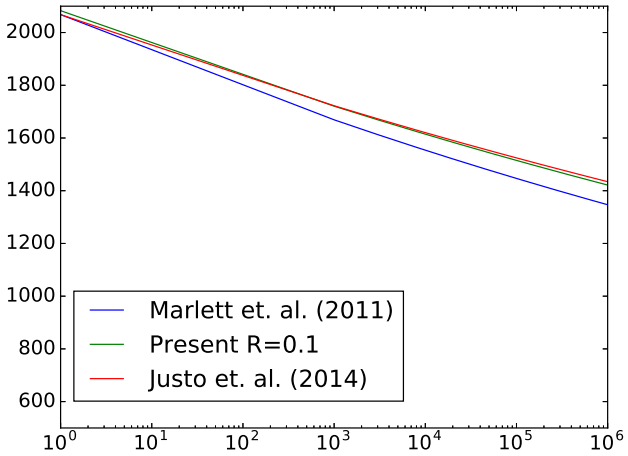

Figure 4.5: Comparison between transformed S-N curve and experimental S-N curve

the S-N curves obtained using the experimental campaign of this project. The reason for this is that no S-N curves were available in literature to compare the obtained S-N curves too. The only found S-N curve was the curve of Justo et.al. [70], however the static strength did not coincide with the current experimental campaign (error of approx 13%) and the amount of tests conducted in their effort was low.

4.3.5 S-N curve determination by fitting experiments

The S-N curves determined with the method presented in section 4.3.3 did not yield satisfying results when implemented in the current model, this will be shown in section 4.4. By stating this, it is not implied that the method is wrong. What is meant, is that in the current implementation, the S-N curves determined by the previous section are not useful for assessing the behavior of the fatigue model developed. Three reasons which are thought to be the cause of this will be discussed now. The first of which is that the experimental campaign was probably not large enough in order to provide good estimates for the statistic distribution of the static properties. This may be supported by the fact that the histograms and the plots as shown in Appendix B are not convincing.

Second reason is that improper stress solutions are causing too fast degradation of strengths. These improper stress solutions can be caused by the size paradox as mentioned earlier and by not modeling delaminations. Delaminations were clearly available during fatigue testing as has been mentioned in chapter 3 and delaminations can have orders of magnitude impact on the fatigue life according to experimental data of Nixon-Pearson and Hallet [71].

The third reason is that the S-N curves can probably not be applied on a single element without any adjustments. There are two reasons for this. It can be that there is a size effect

Table 4.2: Results for inclination parameter B after fitting to experimental data

Name of fit	$\frac{\sigma_{max}}{\sigma_{ult}}$	**Mean experimental N**	**Simulated N**	**Parameter B**
NL	0.85	2,056,675	2,092,213	69
NH	0.9	419,585	425,793	107.5

which might cause the statistical distribution for a single element to be different than for a specimen, such size effects are described for example in Okabe and Takeda [72]. The second reason is that as there are in-situ strengths (Pinho et. al [33]), it can be that there is also some in-situ fatigue life. To this end, in this section an alternative method will be used to determine S-N curves. The method will be used in order to account for the errors introduced by the previous mentioned reasons. It is assumed here that the previously mentioned reasons will have an increasing effect on the fatigue life of the properties on the element level. Hence, to account for this, the fatigue lifes of the elements will be increased by an experimental fitting parameter. The increase of fatigue life is achieved by changing the inclination parameter of the S-N curve. For keeping the new S-N curves as close as possible to the S-N curves of section 4.3.3 (for comparison reasons) the same base equation 4.11 is adopted.

$$\sigma = \frac{A}{N^{\frac{1}{B}}} \tag{4.11}$$

Here, A will be the initial static strength as determined in table 4.1 and B will be the inclination parameter. The B parameter will be chosen such that simulation gives a predefined amount of fatigue cycles for the fatigue limit at a specified load. In the present exercise, two load levels are chosen, namely the loads at which fatigue life values were obtained in the experimental campaign. This yielded the values shown on table 4.2. A graph showing the sensitivity of the model to the inclination parameter (B) is shown in appendix C. Two remarks are in place for the table. The simulated and experimental values still do not match exactly. The reason for this is that the fit was performed by trial-and-error. Since a complete analysis takes approximately 10 hours, it was not feasible to reduce the error even more.

The second thing to notice, is that fit 'NL' did coincide closely with the value obtained from the experimental S-N curve as it was derived in chapter 3. Finally, it has to be noted that the same inclination parameter was applied on all the required S-N curves according to the theory of Kawai [73]. Where it is stated that S-N curves for arbitrary fiber orientation angle will coincide if the S-N curve is divided by the static strength. This method does only work for tensile loads and is here assumed to be applicable also for the shear-elastic properties. Therefore, and because compression failures seemed not that likely, the S-N curves for compression loads remained the same as derived in section 4.3.3. Figure 4.6 shows the normalized S-N curves for the found inclination parameters of section 4.3.3 in combination with 4.3.4 and the inclinations found in the current section. For completeness, the inclination parameter found by using the S-N curve of Justo et.al. [70] is also shown.

It must be stressed here that it is not believed that the 'fitted' inclination parameters will reconstruct the correct S-N curves. Rather, the fits try to account for the effects described at the start of this section in an non-physical way.

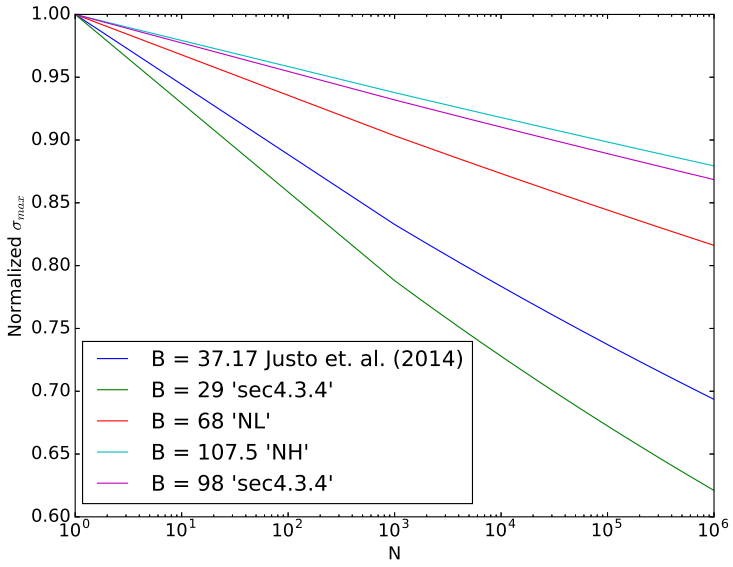

Figure 4.6: Comparison of the effect of inclination parameter B on the S-N curve

4.3.6 Implementation considerations

As has already been mentioned, the stress solution is obtained at the element level. From the residual strength equation 4.2 it is clear that degradation is based on the applied stress. Hence it seems logical to apply the degradation on the element level. In general, every element has five strengths (equation 4.12) for which the strength degradation has to be assessed (at least in the case of using the theory of Puck and Schürmann to predict failure).

$$\begin{aligned} X_t &= \text{tensile strength parallel to fibers} \\ X_c &= \text{compression strength parallel to fibers} \\ Y_t &= \text{tensile strength transverse to fibers} \\ Y_c &= \text{compression strength transverse to fibers} \\ S_a &= \text{in-plane shear strength} \end{aligned} \tag{4.12}$$

This immediately raises a problem, since six different stresses can act on an element and in general the strength degradation theories associate one stress with one strength. In this work, stresses and strengths will be associated one to one, which means that the effect of multi-axial loading on the strengths is neglected. Multi-axial loading is however considered by the failure criterion. Hence the effects do get, at least partially, captured at the macroscopic level. To associate stresses with strengths for the degradation, the assumption has to be made that every strength will have its own damage.

To assign stresses to strengths, the following reasoning will be used. In principle stresses that act parallel to the strength direction will be associated to each other. Tension stresses are associated to tension strengths, the same holds for compression. The remaining three stresses are out-of-plane stresses (σ_{33}, τ_{13}, τ_{23} and according to the PhD thesis by Bhat [74] these stresses cause delaminations, which are not covered throughout this exercise. Hence, their

effect on the strengths is neglected. Moreover, the elements will feel a VA loading, despite the fact that the specimen is loaded in CA. This happens due to the damage propagating and as a consequence of this propagation, the stress distribution changes. This may even mean, that at some cycle, the element will have a tension-tension cycle, whereas at a different cycle it might be compression-compression. The effects of these changes can not be tracked by the current model. Experimental results of Philippidis and Assimakopoulou [75] suggest that at least, for a pristine structure, loading in c-c fatigue, the transverse tensile strength remains unaffected. This argument tries not to be conclusive but rather tries to show that the assumption made might be not that limiting.

4.4 Comparison to experimental results

Three characteristics of the model will be investigated. At first, the stiffness of the specimen will be investigated in section 4.4.1. The results will be used to asses the models ability to predict the behavior of the specimen during cyclic loading. The model is then compared to its ability to predict the fatigue life of a specimen subjected to constant amplitude loading. An S-N curve will be constructed using the simulated data and compared to the S-N curve obtained from the fatigue experiment, section 4.4.2. Finally, the ability of the model to predict the residual strength after cyclic loading will be judged in section 4.4.3. Simulation results shown here will be based on inputs of the S-N curve determination in section 4.3.3 and section 4.3.5. For convenience, the model of section 4.3.3 will be called 'Kassapoglou'. The model based on the high experimental load will be called 'NH'. Finally, the model based on the low experimental load 'NL'. Not all models will be used in every section.

4.4.1 Stiffness behavior during cyclic loading

Modeling the stiffness behavior can be useful in applications where deflection limits are critical. Moreover, monitoring the stiffness can be used in order to asses at what point the specimen is in its fatigue life without breaking the specimen. Stiffness behavior will not be compared to experimental results since no experimental data was available (displacement output of the machine was not considered since it is not reliable according to the lab technicians). In this section, only the trend of behavior will be examined. Three load cases are tested and only 2 of the S-N curve models. The obtained stiffness predictions are shown in figure 4.7. Clearly, the higher loads show a more sudden behavior, this is expected and was also shown in the book by Vassilopoulos [3]. The initial stiffness loss is mainly caused by the initial ramp to σ_{max} but also due to the first fatigue cycles.

4.4.2 S-N curve determination

In this section all three input models, Kassapoglou, NH and NL will be considered. The fatigue model will be used to create S-N curves for the OHT specimen. The same approach is used as for the determination of the experimental S-N curves. The model was run at the exact same loads as the experimental tests in order to keep parameters constant. The obtained data points (produced by the fatigue model) and the fits are shown on figure 4.8.

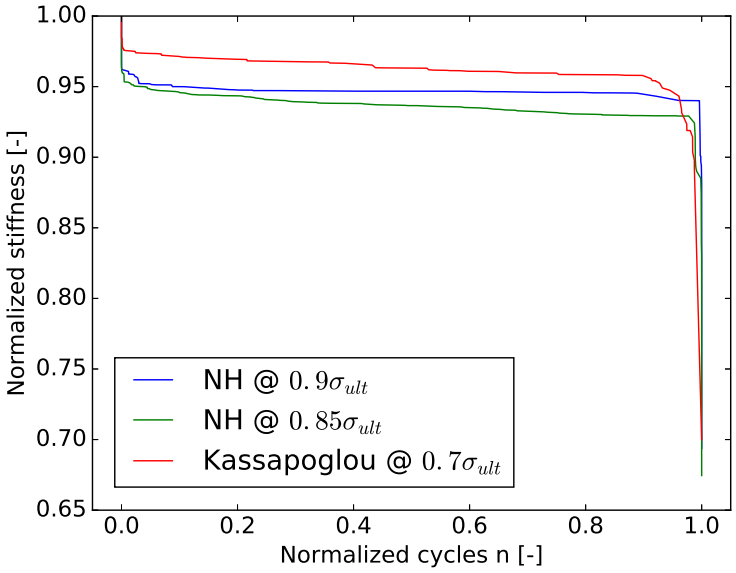

Figure 4.7: Residual stiffness as a function of cycles

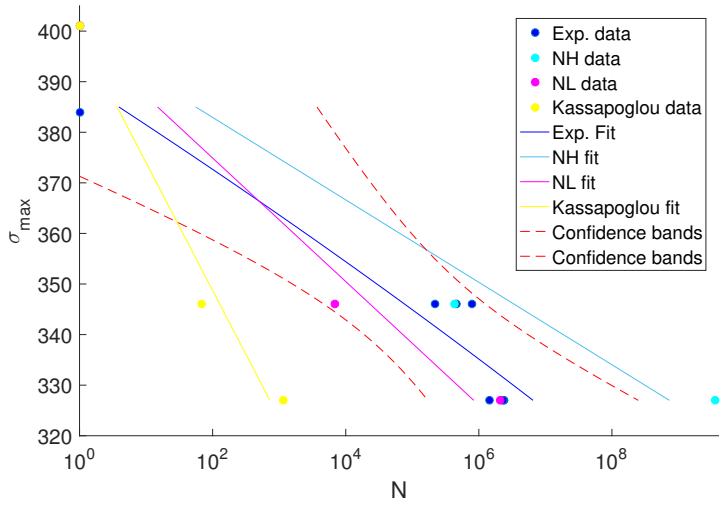

Figure 4.8: Predicted S-N curves by the different models

Table 4.3: Residual strength after 80,000 cycles at 0.6 of static strength

Method	**Residual strength [MPa]**	**Error σ_{res} [%]**	$\frac{\sigma_r}{\sigma_{ult}}$	**Error** $\frac{\sigma_{res}}{\sigma_{ult}}[-]$ **[%]**
Experimental	395	-	1.03	-
Kassapoglou	386	-2.3	0.96	-6.8
NL	381	-3.5	0.95	-7.8
NH	404	2.3	1.01	-1.9

Table 4.4: Residual strength after 150,000 cycles at 0.6 of static strength

Method	**Residual strength [MPa]**	**Error σ_{res} [%]**	$\frac{\sigma_r}{\sigma_{ult}}$	**Error** $\frac{\sigma_{res}}{\sigma_{ult}}[-]$ **[%]**
Experimental	388	-	1.01	-
Kassapoglou	386	0.5	0.96	-5.0
NL	404	4.12	1.01	0
NH	404	4.12	1.01	0

As can be seen, the model by Kassapoglou did not yield satisfactory results. It must be stressed that it can not be concluded thus that the model by Kassapoglou is incorrect, since the obtained predictions were comparable to S-N curves found in literature (Justo et. al. [70]). Possible reasons for obtaining incorrect results with the model by Kassapoglou might be the amount of static tests conducted as was mentioned in chapter 3 and/or not modeling delaminations. Since delaminations were observed during almost $\frac{3}{4}$ of the fatigue life. The 'NL' model seems to predict the S-N curve quite accurately and is within the experimental 95% confidence bands. The 'NH' model over-predicted the S-N curve. This is not surprising, as in chapter 1 it was already mentioned that at higher loads predictions get worse in general. Hence, by performing a fit at a high load, it seems logical that the predictions at lower loads will suffer.

4.4.3 Predicting residual strength

Residual strength predictions are assessed for three different cases. Two cases were performed at a σ_{max} of 0.6 of the static strength. The third case was performed at 0.9 of the static strength. Tables 4.3, 4.4 and 4.5 show the results obtained with the different input models. The amount of cycles the specimens were subjected to is shown in the table caption.

The tables show that, if the applied cycles are not higher than the fatigue limit predicted by the model, the models are able to predict the residual strength fairly correctly. In some cases, even the correct trend is predicted. The usage however of these predictions becomes questionable if the applied cycles are near the predicted fatigue limit by the model. On the other hand, it shows that in general the fatigue model has potential if adjustments are made

Table 4.5: Residual strength after 200,000 cycles at 0.9 of static strength

Method	**Residual strength [MPa]**	**Error σ_{res} [%]**	$\frac{\sigma_r}{\sigma_{ult}}$	**Error** $\frac{\sigma_{res}}{\sigma_{ult}}[-]$ **[%]**
Experimental	434	-	1.13	-
Kassapoglou	FLR[1]	-	-	-
NL	FLR[1]	-	-	-
NH	387	-10.8	0.97	-14.2

such that correct fatigue lifes are predicted. Due to limited time, the amount of performed experimental residual strength tests was kept low. Moreover, due to the material being fairly insensitive to fatigue, but having quite large scatter, it was not possible to perform tests in the region where the residual strength drops. Therefore, the steepness of the final strength drop can not be compared to experimental results. As was stated in chapter 1 in general the strength is expected to remain constant up to just before the point of failure, where the residual strength will drop drastically. From the experimental campaign however, a strength increase is observed in the early stages of fatigue. This is not an unknown phenomenon and was also observed by Shokrieh and Lessard [11] and by Lagace [76]. The increase is thought to be the cause of damage which results in stress redistributions, which lower the initial stress gradient of the hole.

From the simulated results, only models NL and NH were able to capture some slight strength increase. From which it can be concluded that the model at least is able to predict stress increases. However, the amount of stress increase predicted might be limited by the used inputs i.e. the S-N curves, the degradation of properties on the element level and the lack of modeling delaminations. For the sake of completeness, a residual strength curve predicted by the fatigue model will be presented now, figure 4.9. The plot shows that the model is able to capture some strength increases, although the magnitude and location of strength increases can not be verified due to the lack of experimental data. Finally, the final steep drop of strength is captured. Although it does look very steep, one should not forget that the applied load is near the final failure load (0.85) and the plot is on a semi-log scale. Figures 4.10 show the damage progression of due to fatigue. The ply shown is the outer 0 ply.

4.5 Concluding remarks fatigue model

In this chapter, a framework is presented for a fatigue model which can be applied on general cases after proper adjustments. In its current form it was developed for OHT specimens. The model can be used to predict stiffness, strengths and fatigue lifes. It is based on the assumption that below the macroscopic level only strength degradation occurs due to cyclic loading. The model was able to predict the trend in all these tests. The model was unable however to predict correctly the magnitudes and locations of these trends. Recommendations will be given in chapter 5 in order to improve the model.

[1]FLR=Fatigue limit reached before reaching requested cycle

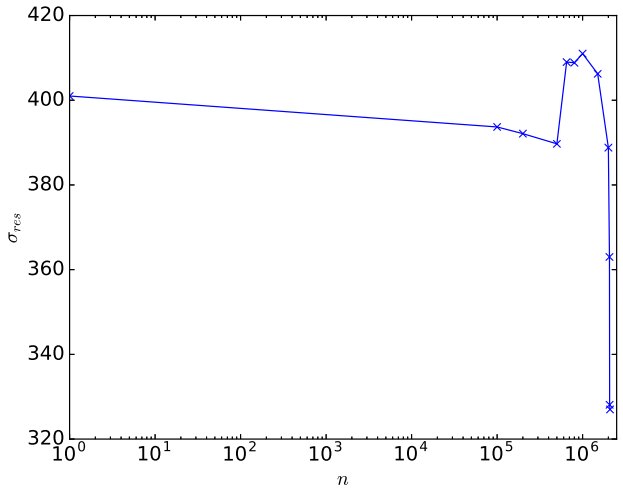

Figure 4.9: Residual strength as a function of cycles predicted by 'NL' at $0.85\sigma_{ult}$

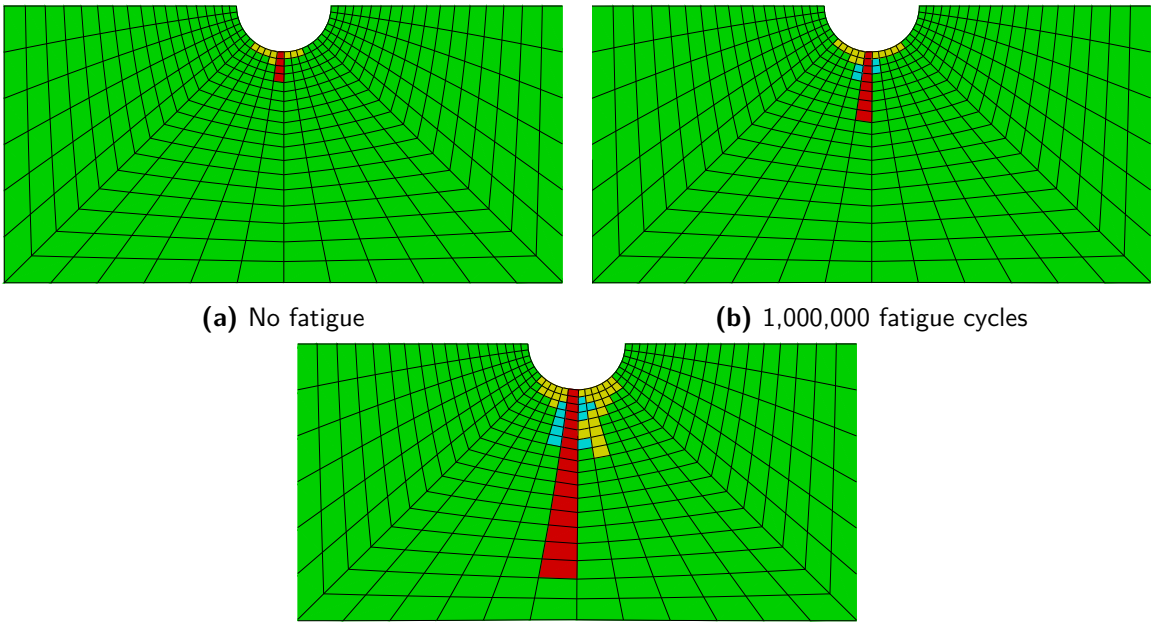

(a) No fatigue

(b) 1,000,000 fatigue cycles

(c) 2,070,000 fatigue cycles

Figure 4.10: Damage patter of a zero ply for different fatigue cycles at constant σ_{max} of 327MPa

Chapter 5

Discussion and recommendations

In the present exercise, a progressive damage analysis model has been built for modeling the effect of quasi-static and cyclic loading. It can be used to predict stiffness behavior, residual strength and fatigue life. The model has been developed around an open hole specimen with a quasi-isotropic layup, in that way, the complexity of stress gradients and complex damage states are considered. Inputs are only required in the form of engineering constants and S-N curves. The S-N curves are also acquired at the engineering constant level. By doing this, the model can be applied on any structure and layup. This does not mean however that the model will make good predictions on any tape of layup and/or structure. In fact, as the model is at its infancy (this work is the initiation of the current model) it can currently only be used to make trend estimates of stiffness and strength. For the prediction of S-N curves additional experimental input was required in order to get predictions to within the experimentally observed 95% confidence bands. In this final chapter, the different parts of the model will be discussed in section 5.1, if, how and to what extend the research questions are answered will be reviewed in section 5.2 and finally recommendations for the further development of the model will be made in section 5.3

5.1 Discussion

The model developed in this exercise is built using three parts. Two of the three parts contain the theoretical laws which are used for the progressive damage analysis. The first of which is the macroscopic damage law, in the current model usage is made of the criterion by Puck and Schürmann [28], the discussion of this part is held in section 5.1.1. The second part are the laws which act on the properties of part one. Currently, a theory by Kassapoglou [5] is utilized (which shows close similarities to the theory of Broutman and Sahu [36]). It is implemented using a method for determining S-N curves also proposed by Kassapoglou [5], the second part is discussed in section 5.1.2. The third part brings together the laws and applies them on a structure using FEM and a proprietary cycle jumping algorithm. This part was developed in the present work and is discussed in 5.1.3

5.1.1 Macroscopic

In the current model, macroscopic failure of two failure modes can be captured by the model. These modes are fiber failure (either tensile or compression), and inter-fiber failure caused by tensile or compression forces. As the predictions of the quasi-static model are mostly close to the experimental observed values, it is thought that these failure modes are well modeled. However, no compression tests have been done as validation and hence the compression part is not sufficiently validated. In the static model, the largest discrepancies were probably due to the sudden degradation mechanisms. The effect of this was most notable for the soft (± 45 rich) specimens.

Two characteristics of the currently implemented sudden degradation theories are incorrectly representing physical events. The first is the degradation of element properties, where in the physical small cracks occur, the simulated model creates lump 'cracks' which are as large as one element. Although for the static model the lump modeling seems to be sufficient, it will be the cause of wrong stress redistributions, especially in the fatigue case where stress redistributions are increasingly important due to the large sequence of events. The second incorrect physical representation of sudden degradation rules is the degradation of the shear-elastic properties. From the results it is clear that the model has difficulty providing good predictions when the influence of the shear-elastic properties increases (i.e. increased ± 45 plies).

Finally, delamination modeling has to be included if fatigue is to be modeled correctly. Delaminations start as early as $\frac{1}{4}$ of the fatigue life (at least as can be observed by the naked eye) and will cause stress redistributions which will affect the degradation of macroscopic properties.

5.1.2 Degradation of macroscopic properties

In the current implementation, the degradation of macroscopic properties is achieved by a simple (near-) linear line. The slope of this line is solely based on the fatigue life of the applied load. This seems reasonable for a first approximation. However, using the fatigue life (N) obtained from large UD specimens in this approximation may be on the conservative side. Three effects are thought to be the cause of this, for clearness, the effects to be discussed are thought to happen below the macroscopic level. First, scaling might be needed. Okabe and Takeda [72] actually observed such scaling effects on CFRP's caused by impurities on the microscopic level. As the reason of fatigue is thought to be the cause of these impurities, it might not be correct to use S-N curves derived from UD specimens on the element level without any scaling parameters.

A second effect which does affect the degradation but is not related to it directly is the size paradox. This concept was already introduced in chapter 2. The formation of cracks will cause additional stress raisers, but due to their small size will probably be susceptible to the size paradox too.

Finally, there might be comparable effects as the in-situ strengths (Pinho et. al. [33]. These effects can be for example adjacent plies acting as crack inhibitors if the adjacent plies have fibers perpendicular to the (to be formed) crack-plane.

5.1.3 Framework

In the present exercise an effort has been made to create a framework by bringing together three distinct parts. These parts are the stress solution, macroscopic damage laws and degradation of macroscopic properties. The fourth part is the framework itself, which brings these parts together with the goal to make an efficient model. In the present exercise this is done by assuming that there is no stiffness degradation at the element level and by using a numerical root finding algorithm in order to reduce the required amount of function evaluations of the macroscopic damage laws and the degradation routines.

In the current implementation, the model uses mean values and will always give the same solutions as the inputs are kept constant. As is known however, fatigue of composites is subjected to scatter. This scatter has also been observed in the performed experimental campaign. In order to obtain useful predictions, the model should predict scatter too. Finally, the combination of Python and Abaqus commercial code is not that efficient. The reason is that due to this combination, for every increment (stress solution) the input file has to go through the pre-processor of Abaqus, where it spends a lot of time without actually performing any finite element calculations.

5.2 Reflecting on research questions

The research questions will be treated one by one in this section. Starting with the sub-questions. The main research question will be treated as last.

How should the macroscopic damage law be implemented?

The implementation of a macroscopic damage law is discussed in chapter 2. A stress-strain based approach was used and the assessment of damage was performed at the element level. Two failure modes were modeled, fiber failure and matrix failure. For prediction of static strengths this model seemed to be sufficient (at least if the amount of ± 45 plies does not dominate the lay-up). For modeling fatigue not taking into account delaminations is unacceptable.

What type of degradation theories should be applied?

In general, the types of degradation laws that can be considered depend on the used macroscopic damage criterion. In the present study, two types of degradation theories were considered (due to the used damage criterion). Stiffness- and strength-degradation. Eventually, only strength degradation has been built-in explicitly using an approximation as proposed by Kassapoglou [5]. Stiffness degradation is accounted for implicitly. As the model apparently is able to capture some residual strength increases, which are caused by stress redistributions, it is thought that the way of implicitly accounting for stiffness loss might not be that limiting.

Can an algorithm for cycle-jumping be developed relating damage and degradation to find the amount of cycles to be jumped?

In the present case this relation was found by assuming that in between the cycle jumps the stress will remain constant. By making this assumption, the damage criterion becomes a function of strengths only. Since the strengths are a function of cycles only, the to be jumped cycles will be calculated using Brent's method to minimize the number of function evaluations. With this method, the cycle to be jumped can be found on the element level.

How should such a cycle-jumping be implemented in a fatigue modeling framework?

The cycle jumping algorithm has been implemented in a fatigue framework according to the flow-chart presented in chapter 4. It is implemented such that the amount of elements which have to be checked for critical cycles is reduced.

How can fatigue be modeled using PDA in combination with FE?

Modeling fatigue using PDA may be achieved by a model which should consist of four distinct parts. Part one will have to provide stress solutions for various (damage) states of the structure. A second part should assess damage initiation with as input the stress solution. Another part will be used to track for degradation of properties due to cyclic loading. Finally, the fourth part is the framework which lets the other three parts collaborate in an efficient way. In this exercise it is called the cycle jumping algorithm but can also be seen as the 'framework', because it will ensure that all other parts will work together.

5.3 Recommendations

The recommendations made in this section are predominantly connected to the observations made in the previous discussion. Here, the recommendations will be discussed in order of increasing complexity. Although, it is not exactly known how complex every recommendation will be and as such an engineering estimate is applied.

- Increase specimen size and hole size.

This recommendation is most easily implemented and shall be performed in order to reduce discrepancies caused by the aforementioned size paradox. For quasi-isotropic lay-ups, a hole diameter of approximately 12mm (instead of 6mm) will reduce the effects up to negligible values if the approach of Marissen et. al. [58] is to be believed. Simultaneously, the width shall be increased according to ASTM practice [64] such that edge effects are reduced.

- Implementation of an auto-correcting displacement incrementation algorithm

In the current implementation the displacement controlled simulations have a constant step. This is both inefficient and inaccurate, therefore, it is recommended to use an algorithm which can predict (approximately) how much the displacement should be increased such that a minimal amount of failures occurs. This algorithm can be based on the failure index as is the load introduction described in chapter 2.

- Allocate engineering constants on the element level according to statistical distribution of the engineering constants.

In principle this is can be a straight forward process and has already been done by other authors such as Naderi and Maligno [30]. Aspects to consider if such an approach is to be used are the association of strengths and stiffnesses and the association of strengths to fatigue life. The advantage of such a method is that now confidence bands can be created (at the cost of additional computational effort). This seems an important aspect if the results are to have some statistical meaning. Especially due to the high scatter, it might be needed to have such confidence bands in order for the results to be of any use.

- Include modeling of delaminations

Including modeling of delaminations seems to be a requirement for a proper fatigue model. Although the effects of delaminations in the current observed case can not be easily quantified, literature (Nixon-Pearson and Hallett [71]) suggests that delaminations can have orders of magnitudes difference in fatigue life. Approaches on modeling fatigue life are already available in literature. It might however be more difficult to find a method on how to degrade properties due to cyclic loading associated with delaminations.

- Investigate the validity of applying S-N curves obtained from specimens to the element level.

It will have to be investigated if a one-to-one relation can be used. Or that for instance size or in-situ effects occur, which may require some scaling properties. Possible ways to determine these effects might be the investigation of specimens of variable size, and testing MD specimens.

- Use eXtended Finite Elements (XFEM) to model cracks

In order to get better stress solutions it might be necessary to use XFEM. Although XFEM is already commercially available, it might be a tedious task to combine it with the currently proposed model.

5.4 Final remarks

The present project is the first step towards a general fatigue model. The topics treated are mainly horizontally related. By doing this, the potential of the model is shown. Successors of the current project should focus more on topics vertically related to the topics addressed in this work (i.e. going more in depth). With as guidelines the just made recommendations.

References

[1] William M Swan and Nicole Adler. Aircraft trip cost parameters : A function of stage length and seat capacity. 42:105–115, 2006.

[2] P. F. Liu and J. Y. Zheng. Recent developments on damage modeling and finite element analysis for composite laminates: A review. *Materials and Design*, 31(8):3825–3834, 2010.

[3] Anastasios P. Vassilopoulos. *Fatigue of Fiber-reinforced Composites*. 2011.

[4] George Marsh. Airbus A350 XWB. *Reinforced Plastics*, 54(6):20–24, 2010.

[5] Christos Kassapoglou. *Predicting the Structural Performance of Composite Structures Under Cycling Loading*. PhD thesis, Delft University of Technology, 2012.

[6] Christos Kassapoglou. *Modeling the Effect of Damage in Composite Structures*. Wiley, 2015.

[7] Anastasios P Vassilopoulos. *Fatigue life prediction of composites and composite structures*. Elsevier, 2010.

[8] Yuri Nikishkov, Andrew Makeev, and Guillaume Seon. Progressive fatigue damage simulation method for composites. *International Journal of Fatigue*, 48:266–279, 2013.

[9] Joris Degrieck and Wim Van Paepegem. Fatigue damage modeling of fibre-reinforced composite materials: Review. *Appl. Mech. Rev.*, 54(4):279, 2001.

[10] T. P. Philippidis and V. A. Passipoularidis. Residual strength after fatigue in composites: Theory vs. experiment. *International Journal of Fatigue*, 29(12):2104–2116, 2007.

[11] M M Shokrieh and L B Lessard. Progressive fatigue damage modeling of composite materials, Part I: Modeling. *J. Compos. Mater.*, 34(13):1056–1080, 2000.

[12] M. M. Shokrieh and Larry B Lessard. Progressive Fatigue Damage Modeling of Composite Materials, Part II: Material Characterization and Model Verification. *Journal of Composite Materials*, 34:1081–1116, 2000.

[13] Mahmood M Shokrieh and Larry B Lessard. Multiaxial fatigue behaviour of unidirectional plies based on uniaxial fatigue experimentsâĂŤI. Modelling. *Int. J. Fatigue*, 19(3):201–207, 1997.

[14] Mahmood M Shokrieh and Larry B Lessard. Multiaxial fatigue behaviour of unidirectional plies based on uniaxial fatigue experimentsâĂŤII. Experimental evaluation. *Int. J. Fatigue*, 19(3):209–217, 1997.

[15] K. I. Tserpes, P. Papanikos, G. Labeas, and Sp Pantelakis. Fatigue damage accumulation and residual strength assessment of CFRP laminates. *Composite Structures*, 63(2):219–230, 2004.

[16] Z Hashin. Failure Criteria for Unidirectional FibreComposites. *Journal of Applied Mechanics*, 47(June):329–334, 1980.

[17] T. Adam, R. F. Dickson, C. J. Jones, H. Reiter, and B. Harris. A Power Law Fatigue Damage Model for Fibre-Reinforced Plastic Laminates. *Proceedings of the Institution of Mechanical Engineers, Part C: Journal of Mechanical Engineering Science*, 200(3):155–166, 1986.

[18] W Van Paepegem and J Degrieck. Coupled residual stiffness and strength model for fatigue of fibre-reinforced composite materials. *Composites Science and Technology*, 62:687–696, 2002.

[19] W. Van Paepegem and J. Degrieck. A new coupled approach of residual stiffness and strength for fatigue of fibre-reinforced composites. *International Journal of Fatigue*, 24(7):747–762, 2002.

[20] S. W. Tsai and E. M. Wu. A General Theory of Strength for Anisotropic Materials. *Journal of Composite Materials*, 5(1):58–80, 1971.

[21] W. Van Paepegem, J. Degrieck, and P. De Baets. Finite element approach for modelling fatigue damage in fibre-reinforced composite materials. *Journal of Chemical Information and Modeling*, 53:1689–1699, 2001.

[22] P. Papanikos, K. I. Tserpes, and Sp Pantelakis. Modelling of fatigue damage progression and life of CFRP laminates. *Fatigue and Fracture of Engineering Materials and Structures*, 26(1):37–47, 2003.

[23] Lin Ye. Role of matrix resin in delamination onset and growth in composite laminates. *Composites Science and Technology*, 33(4):257–277, 1988.

[24] Wei Lian and Weixing Yao. Fatigue life prediction of composite laminates by FEA simulation method. *International Journal of Fatigue*, 32(1):123–133, 2010.

[25] Z. Hashin and A. Rotem. A Fatigue Failure Criterion for Fiber Reinforced Materials. *Journal of Composite Materials*, 7(4):448–464, 1973.

[26] Elias N. Eliopoulos and Theodore P. Philippidis. A progressive damage simulation algorithm for GFRP composites under cyclic loading. Part I: Material constitutive model. *Composites Science and Technology*, 71(5):742–749, 2011.

[27] Elias N. Eliopoulos and Theodore P. Philippidis. A progressive damage simulation algorithm for GFRP composites under cyclic loading. Part II: FE implementation and model validation. *Composites Science and Technology*, 71(5):750–757, 2011.

[28] A. Puck and H. Schürmann. Failure analysis of FRP laminates by means of physically based phenomenological models. *Composites Science and Technology*, 58(7):1045–1067, 1998.

[29] P. Camanho and C.G. Davila. Mixed-Mode Decohesion Finite Elements in for the Simulation Composite of Delamination Materials. *Nasa*, TM-2002-21(June):1–37, 2002.

[30] M. Naderi and A. Maligno. Finite element simulation of fatigue life prediction in carbon/epoxy laminates. *Journal of Composite Materials*, 47(4):475–484, 2012.

[31] P. D. Soden, A. S. Kaddour, and M. J. Hinton. Recommendations for designers and researchers resulting from the world-wide failure exercise. *Failure Criteria in Fibre-Reinforced-Polymer Composites*, 64:1223–1251, 2004.

[32] A. S. Kaddour and M. J. Hinton. Maturity of 3D failure criteria for fibre-reinforced composites: Comparison between theories and experiments: Part B of WWFE-II. *Journal of Composite Materials*, 47(6-7):925–966, 2013.

[33] S. T. Pinho, C. G. Dávila, P. P. Camanho, L. Iannucci, and P. Robinson. Failure Models and Criteria for FRP Under In-Plane or Three-Dimensional Stress States Including Shear Non-linearity. *Nasa/Tm-2005-213530*, (February):68, 2005.

[34] S. T. Pinho, R. Darvizeh, P. Robinson, C. Schuecker, and P. Camanho. Material and structural response of polymer-matrix fibre-reinforced composites. *Journal of Composite Materials*, 46:2313–2341, 2012.

[35] Kuo Shih Liu and Stephen W. Tsai. A progressive quadratic failure criterion for a laminate. *Composites Science and Technology*, 58(7):1023–1032, 1998.

[36] Lj Broutman and S Sahu. A new theory to predict cumulative fatigue damage in fiberglass reinforced plastics. *Composite materials: testing and design (2nd Conference)*, pages 170 – 88, 1972.

[37] Christos Kassapoglou and Myriam Kaminski. Modeling damage and load redistribution in composites under tension-tension fatigue loading. *Composites Part A: Applied Science and Manufacturing*, 42(11):1783–1792, 2011.

[38] C. Kassapoglou. Fatigue Life Prediction of Composite Structures Under Constant Amplitude Loading. *Journal of Composite Materials*, 41(22):2737–2754, 2007.

[39] ASTM International. Standard Test Method for Tensile Properties of Polymer Matrix Composite Materials. *ASTM Standard D3039/D3039M*, pages 1–13, 2014.

[40] Christos Kassapoglou. *Design and analysis of composite structures: with applications to aerospace structures*. John Wiley & Sons, 2013.

[41] Paul A Lagace. Nonlinear Stress-Strain Behavior of Graphite/Epoxy Laminates. 23(10):1583–1589, 1985.

[42] Dassault Systemès. ABAQUS Version 6.14, user documentation. *Dassault Systemes, Providence, RI*, 2014.

[43] S G LekhnitskiÄŋ. *Theory of elasticity of an anisotropic elastic body*. Holden-day, 1963.

[44] MJ Hinton, AS Kaddour, and P. D. Soden. The World-Wide Failure Exercise: its origin, concept and content. *Failure Criteria in Fibre Reinforced Polymer Composites: The World-Wide Failure Exercise*, pages 2–40, 2004.

[45] M. J. Hinton and A. S. Kaddour. The background to the Second World-Wide Failure Exercise. *Journal of Composite Materials*, 46(19-20):2283–2294, 2012.

[46] AS Kaddour, MJ Hinton, and PA Smith. The background to the third world-wide failure exercise. *Journal of Composite*, 2013.

[47] A. Puck and H. Schürmann. Failure Analysis of Frp Laminates By Means of Physically Based Phenomenological Models. *Composites Science and Technology*, 2002.

[48] A. Puck, J. Kopp, and M. Knops. Guidelines for the determination of the parameters in Puck's action plane strength criterion. *Composites Science and Technology*, 62(3):371–378, 2002.

[49] H. Matthias Deuschle and B.-H. Kroplin. Finite element implementation of Puck's failure theory for fibre-reinforced composites under three-dimensional stress. *Journal of Composite Materials*, 46(19-20):2485–2513, 2012.

[50] A. Puck and H. M. Deuschle. Progress in the Puck Failure Theory for Fibre Reinforced Composites : Analytical solutions for 3D-stress. *www.alfredpuck.de*, 2012.

[51] J. Wiegand, N. Petrinic, and B. Elliott. An algorithm for determination of the fracture angle for the three-dimensional Puck matrix failure criterion for UD composites. *Composites Science and Technology*, 68(12):2511–2517, 2008.

[52] Giovanni Perillo. Numerical application of three-dimensional failure criteria for laminated composite materials. *SIMULIA Community ...*, pages 1–15, 2011.

[53] Kyonchan Song, Yingyong Li, and Cheryl a. Rose. Continuum Damage Mechanics Models for the Analysis of Progressive Failure in Open-Hole Tension Laminates. *Aiaa*, pages 1–18, 2011.

[54] ASTM International. Standard Test Method for Open-Hole Tensile Strength of Polymer Matrix Composite Laminates. *ASTM Standard D5766/D5766M*, pages 1–7, 2011.

[55] Kristin Marlett, Yeow Ng, and John Tomblin. Hexcel 8552 AS4 Unidirectional Prepreg at 190 gsm & 35 % RC Qualification Material Property Data Report. *Niar*, 2011.

[56] A. S. Kaddour, M. J. Hinton, P. A. Smith, and S. Li. Mechanical properties and details of composite laminates for the test cases used in the third world-wide failure exercise. *Journal of Composite Materials*, 47(20-21):2427–2442, 2013.

[57] Nuri Ersoy, Tomasz Garstka, Kevin Potter, Michael R. Wisnom, David Porter, Martin Clegg, and Graeme Stringer. Development of the properties of a carbon fibre reinforced thermosetting composite through cure. *Composites Part A: Applied Science and Manufacturing*, 41(3):401–409, 2010.

[58] R Marissen, H R Brouwer, and J Linsen. Notched Strength of Thermoplastic Woven Fabric Composites, 1995.

[59] M.E. Waddoups, J.R. Eisenmann, and B.E. Kaminski. Macroscopic Fracture Mechanics of Advanced Composite Materials. *Journal of Composite Materials*, 5(October):6, 1971.

[60] J.M. Whitney and R.J. Nuismer. Stress Fracture Criteria for Laminated Composites Containing Stress Concentrations. *Journal of Composite Materials*, 8, 1974.

[61] ASTM International. Standard Test Method for In-Plane Shear Response of Polymer Matrix Composite Materials by Tensile Test of a 45 ° Laminate 1. *ASTM Standard D3518/D3518M*, pages 1–7, 2013.

[62] USA Department of Defense. Handbook Composite Materials Handbook Volume 1 . Polymer Matrix Composites Guidelines for Characterization. 1(June), 2002.

[63] Paul A Lagace and Stephen C Nolet. Effect of ply thickness on longitudinal splitting and delamination in graphite/epoxy under compressive cyclic load. *Composite Materials: Fatigue and Fracture*, pages 335–360, 1986.

[64] ASTM International. Standard Practice for Open-Hole Fatigue Response of Polymer Matrix Composite. *ASTM Practice D7615/D7615M*, (February 2011):1–8, 2011.

[65] ASTM. Standard Practice for Statistical Analysis of Linear or Linearized Stress-Life (S-N) and Strain-Life (Ât -N) Fatigue Data 1. *Annual Book of ASTM Standards*, i(Reapproved):1–7, 2012.

[66] Christos Kassapoglou. Fatigue of composite materials under spectrum loading. *Composites Part A: Applied Science and Manufacturing*, 41(5):663–669, 2010.

[67] C. Kassapoglou. Fatigue Model for Composites Based on the Cycle-by-cycle Probability of Failure: Implications and Applications. *Journal of Composite Materials*, 45(3):261–277, 2011.

[68] R. P. Brent. *Algorithms for minimization without derivatives*. Dover Publications, 2013.

[69] T J Dekker. Finding a zero by means of successive linear interpolation. *Constructive aspects of the fundamental theorem of algebra*, pages 37–51, 1969.

[70] J Justo, J C Marin, F París, and J Cañas. Graphite-Epoxy Composites. (June):22–26, 2014.

[71] S R Hallett and O.J. NIxon-Pearson. An investigation into the damage development and residual strengths of open-hole specimens in fatigue. *COMPOSITES PART A*, 69:266–278, 2015.

[72] T Okabe and N Takeda. Size effect on tensile strength of unidirectional CFRP compositesâĂŤexperiment and simulation. *Composites science and technology*, 62(15):2053–2064, 2002.

[73] M. Kawai. A phenomenological model for off-axis fatigue behavior of unidirectional polymer matrix composites under different stress ratios. *Composites Part A: Applied Science and Manufacturing*, 35(7-8):955–963, 2004.

[74] Narendra Venugopal Bhat. *Delamination growth in graphite/epoxy composite laminates under tensile loading*. PhD thesis, Massachusetts Institute of Technology, 1993.

[75] Theodore P. Philippidis and Theoni T. Assimakopoulou. Strength degradation due to fatigue-induced matrix cracking in FRP composites: An acoustic emission predictive model. *Composites Science and Technology*, 68(15-16):3272–3277, 2008.

[76] Paul A Lagace and Stephen C Nolet. Effect of ply thickness on longitudinal splitting and delamination in graphite/epoxy under compressive cyclic load. *Composite Materials: Fatigue and Fracture*, pages 335–360, 1986.

Appendix A

Baseline/Medium cure cycle (M)

All temperatures are thermocouple temperatures of the part. Apply upper limit of 180±5°C on autoclave temperature to avoid overshoot.

a Pull vacuum (min 22 in Hg) (min -0.75 bar)

b Heat at 0.55 to 4.4°C/min (2.5°C/min nominal) to 180 ± 5°C and ramp autoclave pressure to 7bar gauge (i.e. with atmospheric pressure defined as 0) (or100 psig).

c Before temperature reaches 60°C and when autoclave pressure is 1.38 ± 0.6 bar gauge (or 20 ± 10 psig), vent vacuum bag to atmosphere

d From 163°C to 180 ± 5°C a minimum heat-up rate of 0.17°C/min is acceptable.

e Hold 180 ± 5°C for 150min

f Cool down rates from cure temperature to 66°C shall be no more than 5.55°C/minute.

g Release autoclave pressure when thermocouple is below 66°C or minimum 1 hour into cool down, whichever occurs sooner. h. Remove from autoclave when autoclave temperature is less than 49°C

The cure cycle parameters are depicted on figure A.1.

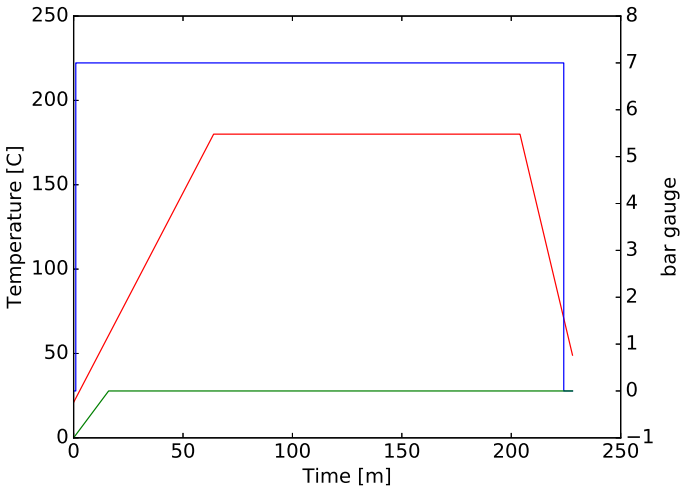

Figure A.1: Cure cycle parameters

Appendix B

Static strength statistics

In this appendix the assumed fits can be found. The fits were obtained using the software package R with library 'fitdistrplus'. The fits were created using command *fit(x, 'norm'* or 'weib' for normal or Weibull fit respectively.

The first fit is for the longitudinal tensile strength. In chapter 3 it was found that a Weibull distribution was the best fit. It is shown on figure B.1.

Second data to be tested is the transverse tensile strength. Again, a Weibull fit was determined to be the best fit according to the procedures in chapter 3. The results of the fit are depicted on figure B.2.

The transverse compression strengths were obtained from the report of Marlett et. al. [55]. The same analysis was carried out as for the other strengths. A Normal fit was found to be the best choice here. The fit is shown on figure B.3.

Finally, the shear-elastic properties or shear strength was best fitted by a Normal distribution. The fit is depicted on figure B.4. The raw data strength data is shown in table B.1. Specimens not shown in this table were not tested.

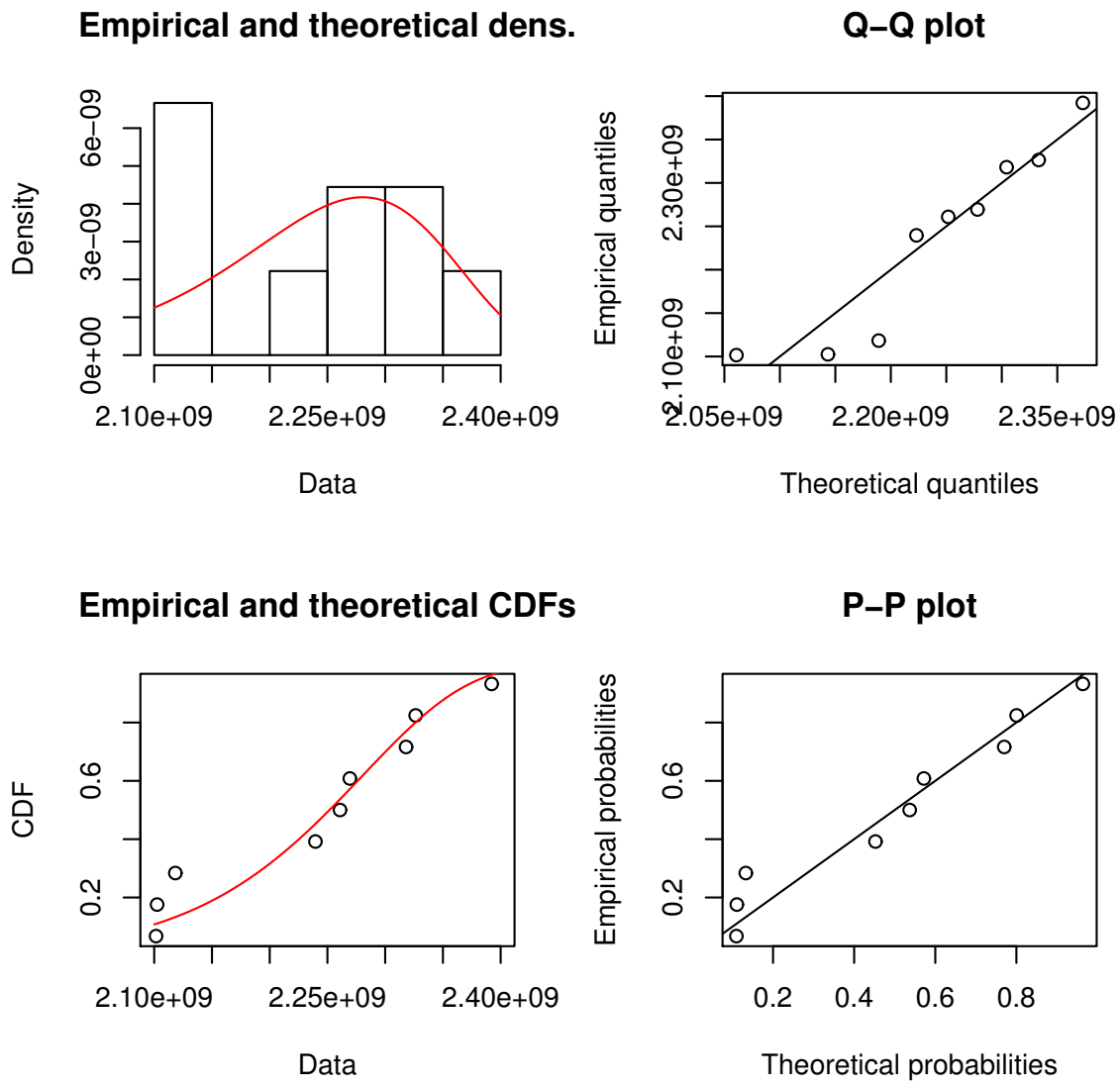

Figure B.1: Weibull fit of longitudinal tensile strength data

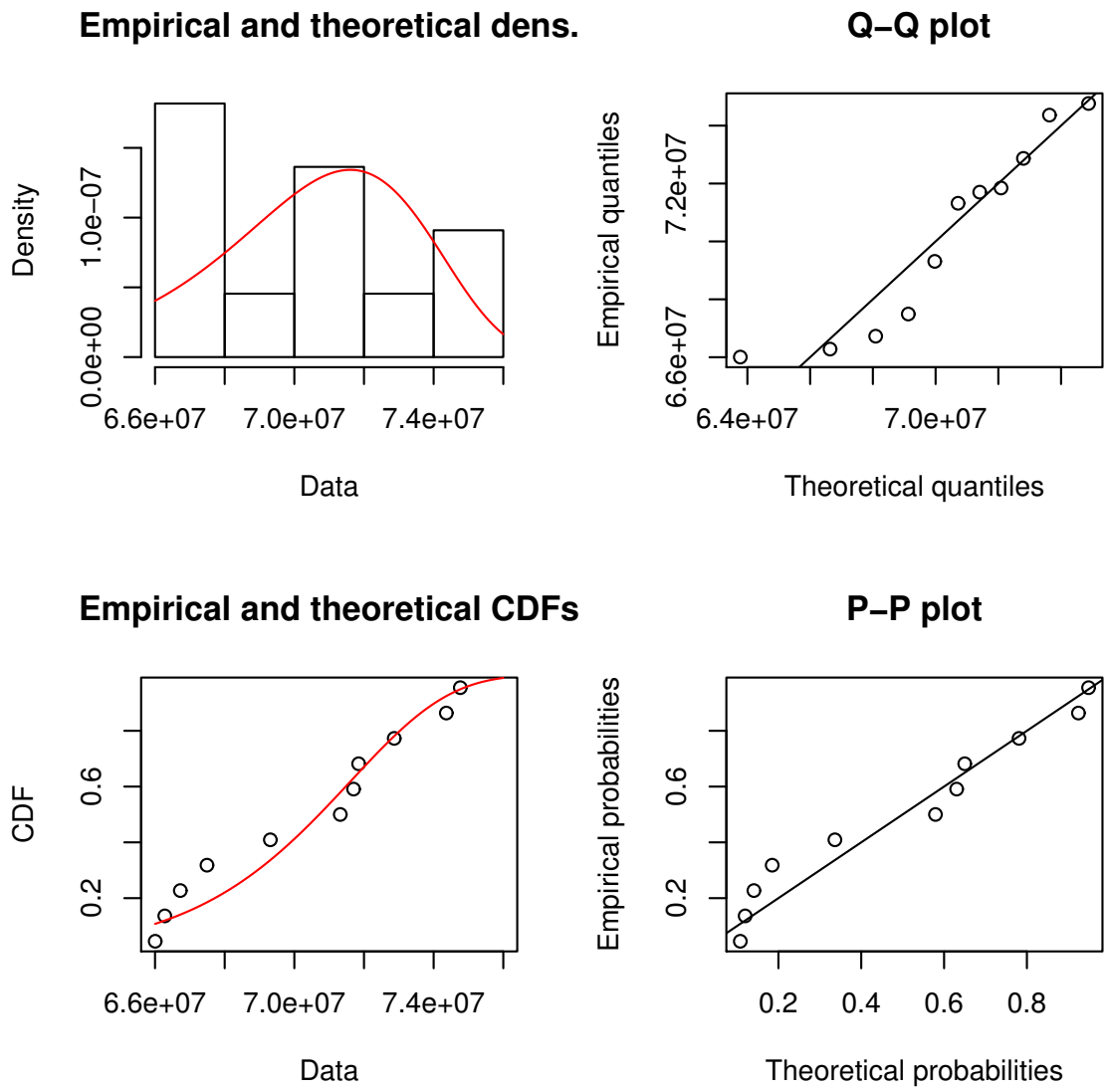

Figure B.2: Weibull fit of transverse tensile strength data

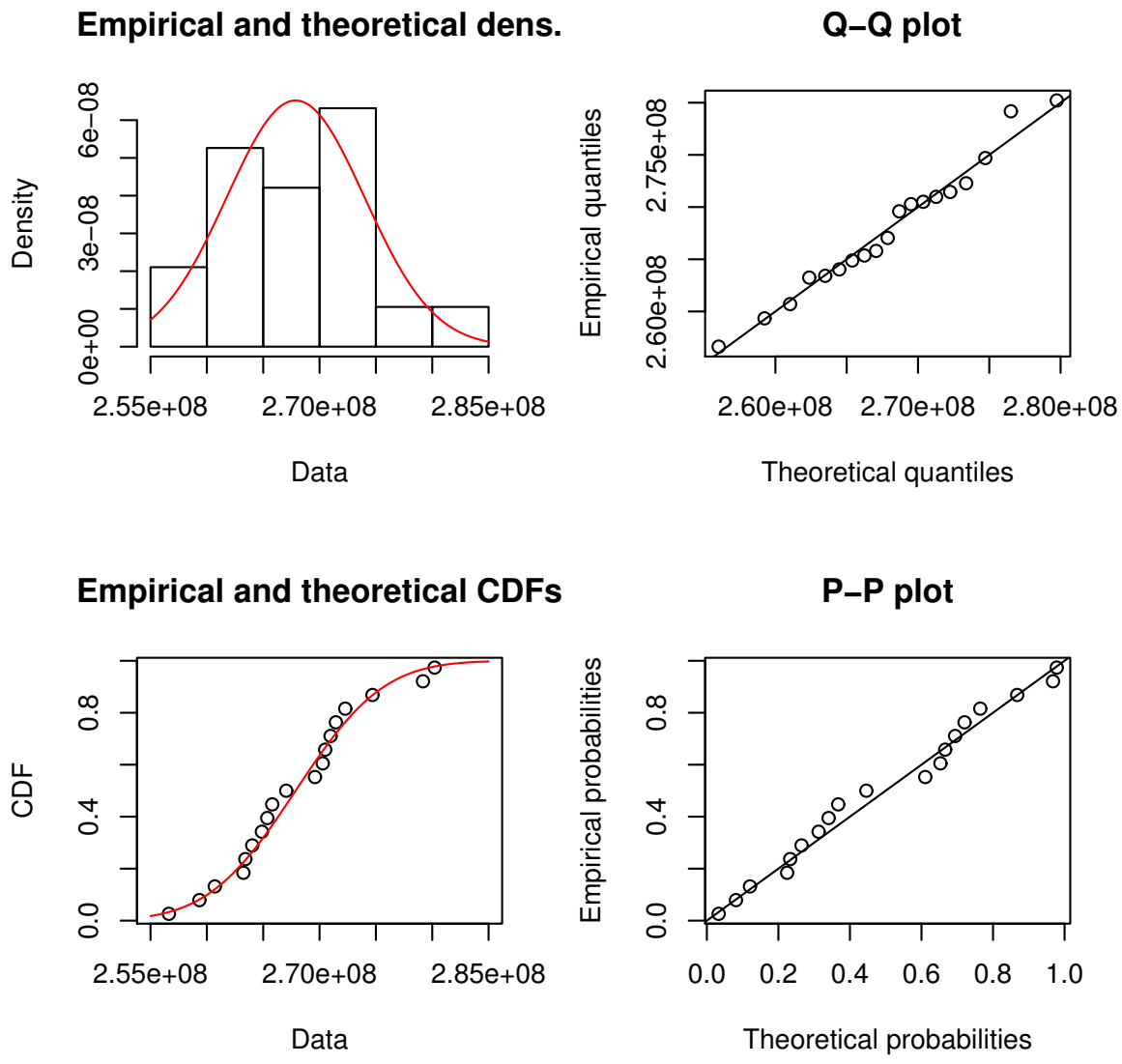

Figure B.3: Normal fit of transverse compression strength data

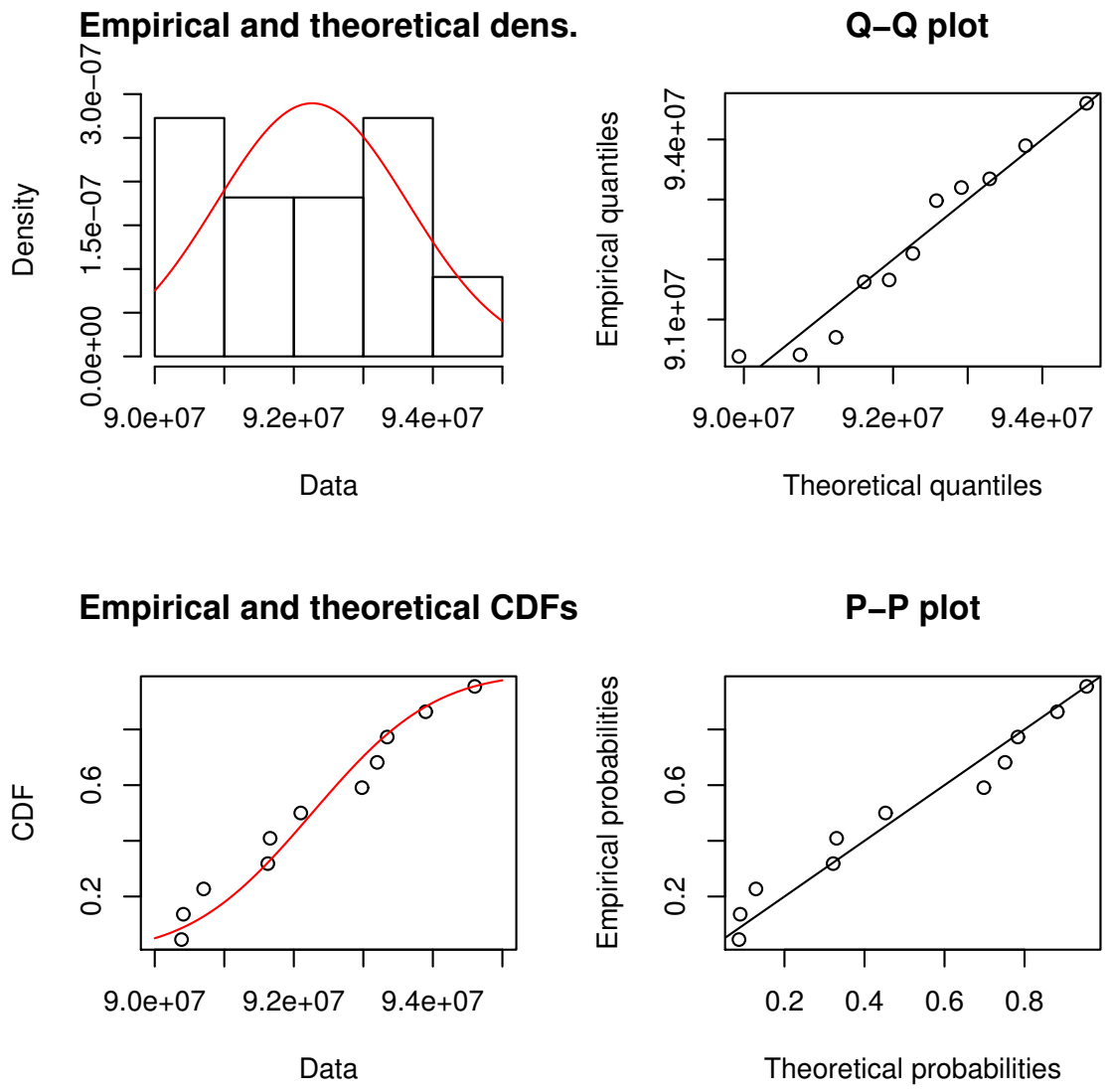

Figure B.4: Normal fit of shear strength data

Table B.1: Raw static test-data

Specimen	Strength [MPa]	Comment
SL201	1555	slip
SL202	1694	residual in clamp
SL203	2269	
SL204	2239	
SL205	2102	
SL206	2261	
SL207	2118	
SL208	2102	
SL209	2326	
SL210	2392	
SL211	2318	
SL212	1737	residual in clamp
ST201	72	
ST202	0	Failed before test
ST203	75	
ST204	55	Grip Failure
ST205	32	Grip Failure
ST206	74	
ST207	67	Grip failure
ST208	73	
ST209	64	Grip failure
ST101	61	Grip failure
ST102	72	
ST103	71	
ST104	67	
ST105	66	
ST106	67	
ST107	45	Grip failure
ST108	69	
ST109	66	
SIS109	93	
SIS208	92	
SIS104	93	
SIS105	95	
SIS205	91	
SIS207	90	
SIS203	92	
SIS204	90	
SIS206	92	
SIS103	93	
SIS102	94	

Appendix C

Sensitivity of the fatigue model to inclination parameter B

The effect of inclination parameter B is plotted against the obtained predicted fatigue limit (N) on figure C.1. The sensitivity study was carried out at $\sigma_{max} = 0.9\sigma_{ult}$. On a semi-log plot, it can be seen that the fatigue life behaves linearly as a function of inclination parameter B.

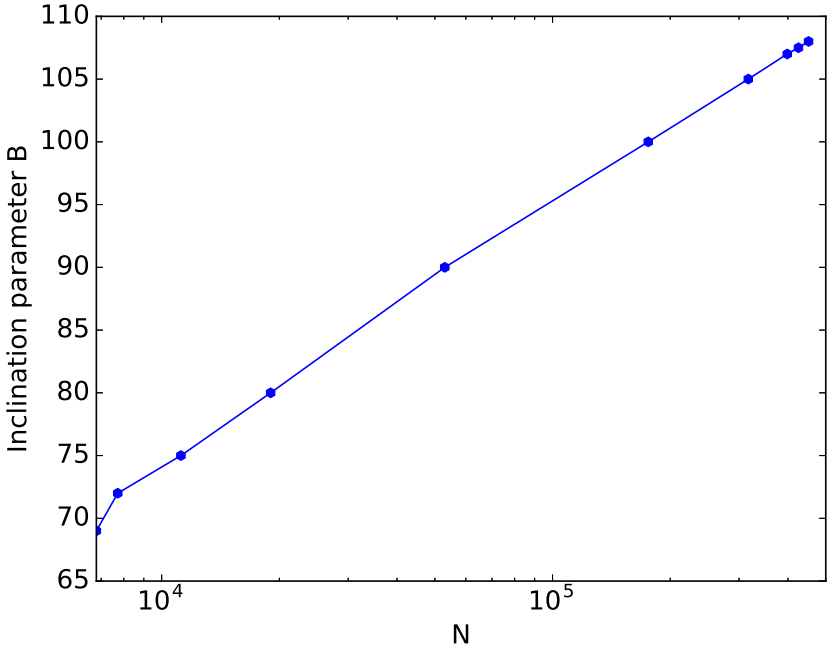

Figure C.1: Effect of inclination parameter B on predicted fatigue life